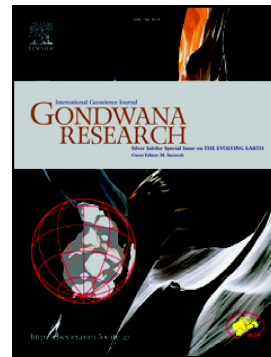


Accepted Manuscript

Oceanic accretionary belt in the West Qinling Orogen: Links between the Qinling and Qilian orogens, China

Liming Yang, Shuguang Song, Mark B. Allen, Li Su, Jinlong Dong, Chao Wang



PII: S1342-937X(18)30223-5
DOI: [doi:10.1016/j.gr.2018.06.009](https://doi.org/10.1016/j.gr.2018.06.009)
Reference: GR 2012

To appear in: *Gondwana Research*

Received date: 7 November 2017
Revised date: 18 May 2018
Accepted date: 20 June 2018

Please cite this article as: Liming Yang, Shuguang Song, Mark B. Allen, Li Su, Jinlong Dong, Chao Wang , Oceanic accretionary belt in the West Qinling Orogen: Links between the Qinling and Qilian orogens, China. Gr (2018), doi:[10.1016/j.gr.2018.06.009](https://doi.org/10.1016/j.gr.2018.06.009)

This is a PDF file of an unedited manuscript that has been accepted for publication. As a service to our customers we are providing this early version of the manuscript. The manuscript will undergo copyediting, typesetting, and review of the resulting proof before it is published in its final form. Please note that during the production process errors may be discovered which could affect the content, and all legal disclaimers that apply to the journal pertain.

Oceanic accretionary belt in the West Qinling Orogen: links between the Qinling and Qilian orogens, China

Liming Yang¹, Shuguang Song^{1*}, Mark B. Allen², Li Su³, Jinlong Dong¹, Chao Wang¹

¹ MOE Key Laboratory of Orogenic Belt and Crustal Evolution, School of Earth and Space Sciences, Peking University, Beijing 100871, China

² Department of Earth Sciences, Durham University, Durham DH1 3LE, UK

³ Institute of Earth Science and State Key Laboratory of Geological Processes and Mineral Resources, Chinese University of Geosciences, Beijing 100083, China

Corresponding author:

*Shuguang Song

sgsong@pku.edu.cn

Abstract

We present an integrated study of ophiolite complexes and island arc rocks from the Tianshui-Wushan Accretionary Belt, West Qinling Orogen. The West Qinling Orogen is important because it links the Qinling orogen to the east and the Qilian and Kunlun orogens to the west. The link between these orogens is commonly assumed, but has little study in detail. Zircon U-Pb analyses from ophiolitic rocks indicate the oceanic lithosphere formed in the Cambrian (530-500 Ma). Pillow lavas in the ophiolite complex show geochemical signatures of enriched MORB, suggesting they represent remnants of an oceanic plateau or seamounts. The island arc rocks include a volcanic complex with basalt-andesite and boninite of Late Ordovician age (460-440 Ma), and a serpentinized peridotite massif. The serpentinized peridotite most likely represent a highly refractory mantle residue with subsequent melt-rock interaction at ~450 Ma, suggesting that it formed in a forearc setting. The co-occurrence of ophiolite complexes and island arc rocks indicates that Tianshui-Wushan Accretionary Belt is an oceanic suture zone caused by oceanic subduction in the Early Paleozoic. The island arc rocks most likely represent the early product of an Izu-Bonin-Mariana (IBM)-type intra-oceanic arc, developed in response to a collision between an oceanic plateau and a continental margin. Our study permits a tectonic correlation between the Tianshui-Wushan Accretionary Belt in the West Qinling Orogen and the South Qilian Accretionary Belt in the Qilian Orogen, thereby establishing the continuity between the Early Paleozoic orogenic belts along the southern margin of the North China Craton.

Keyword: Cambrian ophiolite, Ordovician intra-oceanic arc complex, Tianshui-Wushan Accretionary Belt, West Qinling Orogen, Qilian Orogen

1. Introduction

Accretionary belts in continental orogens are records of ancient oceanic subduction, with preservation of ophiolite complexes, magmatic arc complexes and high-pressure/low-temperature (HP/LT) metamorphic rocks (e.g. Cawood et al., 2009). These belts play important roles in understanding continental assembly and growth in the Earth's history. Ophiolite complexes are relics of oceanic lithosphere that commonly delineate suture zones between former oceanic or continental terranes (e.g., Dewey and Bird, 1971), but may also be fragments scraped off the downgoing oceanic plate during subduction, and accumulated in broad subduction-accretion complexes. In either case, the origin and tectonic evolution of the ophiolite complexes provide important constraints on reconstructions of orogenic belts and the evolution of ancient oceans, including the opening, closure, development of the subduction system (e.g., Dilek and Furnes, 2011; Song et al., 2013, 2015).

The West Qinling Orogen is located in the middle part of the Central China Orogenic Belt (CCOB), and has a geographical position between the Qinling Orogen to the east and Qilian and Kunlun orogens to the west (Pei et al., 2009; Dong and Santosh, 2016). The Shangdan Suture Zone in the Qinling orogenic belt consists of ophiolite fragments and arc magmatic sequences, and has been suggested to continue east of the West Qinling Orogen, as far as the eastern limit of the entire Qinling at ~117° E (e.g. Li, 2008; Pei et al., 2009; Dong and Santosh, 2016). However, previous researchers have proposed different connections between the West Qinling Orogen and orogens in the west, including the North Qilian Orogen (Zhang et al., 1994; Tseng et al., 2009), the North Qaidam UHPM Belt (Yang et al., 2003; Dong et al., 2015; Zhang et al., 2005), or the East Kunlun Orogen (Li, 2008). Dong and Santosh (2016) depicted the Shangdan

Suture as continuing west of the West Qinling Orogen, along the south side of the Central Qilian Block, which is itself a microcontinent embedded within the broader Qilian Orogen (Song et al., 2017).

Tianshui-Wushan Accretionary Belt (TWAB) in West Qinling is considered as westward extension part of Shangdan Suture Zone and consists of two parallel lithological suits, including the ophiolite complexes and the island-arc units (Dong and Santosh, 2016 and reference therein). Although extensively studied, the rock assemblages, petrogenesis, geochronology and tectonic attributions of the accretionary terranes in the TWAB remain unclear, which restricts understanding, not only of the evolution of the West Qinling Orogen, but also of the correlation with the orogens further west. In this paper, we present detailed petrological, geochemical and geochronological studies for ophiolite complexes and island arc complex of the TWAB. We try to determine the formation process of boninite lavas, and their possible genetic relationship with a collision between an oceanic plateau and a continental margin. Furthermore, we attempt to decipher its tectonic relations to Qilian Orogen in the northwest, and the evolution history of the Qinling-Qilian-Kunlun Ocean in the Early Paleozoic.

2. Geological setting

The CCOB, consisting of the Dabie, Qinling, Qilian and Kunlun orogenic belts from east to west, is located in the central part of China (Fig. 1a). Collectively, these orogenic belts record the collisions between major blocks to the north (Tarim, North China) and south (Tibetan terranes and the South China Block) (Dong and Santosh, 2016). The Qinling Orogen is bounded by the Lingbao-Lushan-Wuyang fault in the north and the Mianlue-Bashan-Xiangguang fault in the south and divided into the North and South

Qinling Belts by the Early Paleozoic Shangdan suture zone (e.g., Meng and Zhang, 1999, 2000; Dong et al., 2011a and b). The Early Paleozoic Shangdan suture zone, located at the southern margin of the North Qinling Orogenic Belt, records the existence and subduction of the Shangdan Ocean (Dong et al., 2011a). It is marked by a discontinuously-exposed tectonic mélange, consisting of ophiolite complexes and arc-related volcanic rocks (Dong et al., 2011a). The ophiolite complexes are predominantly composed of ultramafic and mafic rocks that can be proposed to be remnants of the oceanic crust of the Shangdan Ocean (e.g. Pei et al., 2004; Li, 2008; Dong et al., 2011a). Available data suggest that the Shangdan Ocean was formed at a mature N-type middle ocean ridge (MOR) setting between 534-470 Ma (Dong and Santosh, 2016).

The West Qinling Orogen is located in the Tianshui-Wushan area, at the junction between the Qilian and Kunlun orogens to the west and the Qinling Orogen to the east (Fig. 1a). From north to south, it consists of North Qinling Orogenic Belt, the TWAB and Silurian sedimentary rocks (Fig. 1b).

The North Qinling Orogenic Belt in West Qinling Orogen is bounded to the south of the Qilian Orogen by the Baoji-Tianshui (also called Xinyang-Yuanlong) strike-slip fault (Fig. 1b). It can be considered as an Andean-type active continental margin at the south side of the North China Craton and mainly comprises Precambrian basement, Early Paleozoic arc magmatic rocks, which are unconformably covered by locally occurring Carboniferous or Permian clastic sediments (Dong et al., 2011a and b). The multi-deformation and metamorphism determined that the North Qinling Orogenic Belt extend as discontinuous S-shaped, and complicated contact relations of each unit (Pei et al., 2009). The Precambrian basement outcrops as several lenticular units and predominantly consists of (1) peraluminous gneisses and orthogneiss; (2) amphibolites, which was transformed from interlayer of continental tholeiitic lavas, (3) marbles, and

(4) garnet-bearing granitic veins (Pei et al., 2009; Zhang et al., 1994; Dong et al., 2011a). The peraluminous gneisses from the Qinling Group have zircon ages of 2.27-2.17 Ga. Early-Neoproterozoic granitic gneisses were emplaced mainly between ~960 Ma and ~900 Ma, which was closely related to the assembly event during the formation of Rodinia (Lu et al., 2003; Song et al., 2012). Zircons from the Paleozoic granitoids in the North Qinling Orogenic Belt show three episodes of magmatism with peaks at ~500, ~452 and ~420 Ma generally correlated with HP-UHP metamorphism at ca. 500 Ma, retrograde granulite-facies metamorphism at ~450 Ma and amphibolite-facies metamorphism at ca. 420 Ma, respectively (Liu et al., 2013,2016; Zhang et al., 2013). The Precambrian basement was strongly overprinted by Early Paleozoic high P/T granulite-eclogite during ~ 500 Ma as a result of northward continental deep-subduction and crustal thickening (Yang et al., 2003; Su et al., 2004; Chen et al., 2004, 2011; Zhang et al., 2009; Wu and Zheng et al., 2013; Liu et al., 2013), and subsequent low-medium P/T granulite–amphibolite facies metamorphism result from widespread Barrovian-type metamorphic event (Zhang et al., 2011; Mao et al., 2017). The Early Paleozoic arc magmatic rocks are bimodal volcanic rocks consisting of tholeiitic basalt and calc-alkaline dacite-rhyolite, with the ages of 449 ~ 443 Ma; a back-arc extensional setting has been suggested (Li, 2008; He et al., 2007). A large number of arc-related gabbroic and I-type granitic intrusions, with subduction-related geochemical features of significant depletion of Nb–Ta and Ti, and enrichment of Th, Pb and Sr, widely intruded into the west North Qinling Terrane during ca. 514–420 Ma (Wang et al., 2009; Dong and Santosh, 2016; Yang et al., 2015,2016). The diorites and granites in Tianshui area respectively exhibit island-arc related and adakitic geochemical signatures with slightly enriched Sr-Nd isotopic compositions (Zhang et al., 2006). Together with the back-arc basin to the north, the Shangdan Ocean subducted toward north underneath the North

Qinling Terrane during Early Paleozoic (Wu and Zheng et al., 2013; Dong and Santosh, 2016).

The TWAB in the west Qinling Orogen is considered as the westward extension of the Shangdan Suture Zone and consists of two parallel lithological suits, including the ophiolite complexes and the island-arc unit (Dong and Santosh, 2016). Ophiolite complexes in the TWAB consist of mafic-ultramafic fragments, which were interpreted as relicts of obducted Cambrian ocean crust (e.g. Hou et al., 2006b; Pei et al., 2004, 2007a; Dong et al., 2007, 2008; Li, 2008). The mafic rocks with N- and E-MORB affinity in ophiolite complexes are characterized by depletion or slight enrichment of LREE without fractionation of HFSE and no negative Nb-Ta anomaly (Dong and Santosh, 2016). Nd-Pb isotopic compositions of mantle source in Tianshui-Wushan ophiolite complex show that there are two types of mantle component, DMM and EMII, thus proposing that ancient oceanic mantle for these Early Paleozoic ophiolite complexes are different from the normal depleted mantle source (Hou et al., 2006 a,b). The island-arc unit in the TWAB are exposed along the south side of the ophiolite complexes and predominantly consist of intermediate-mafic volcanic rocks (including boninite) and fore-arc volcanic-sedimentary series (Pei et al., 2006). Zircon U-Pb ages of 456-440 Ma for arc-type gabbroic intrusions constrain the time of subduction in Wushan Terrane (Li, 2008). Besides, intermediate and basic igneous complexes (e.g., the Baihua magmatic complex) with arc-related magma characteristics yield a magma crystallization age of ~450Ma (Pei et al., 2007b).

3. Field relations and petrography

The TWAB occurs as several discontinuous fault-bound slivers along a WNW-ESE orientation between the intercontinental basin in the south and the active continental

margin in the north in Wushan and Guanzizhen terranes (Fig. 1b). These terranes are composed of two sequences: (1) the ophiolite complexes, and (2) the island-arc series with volcanic rocks and peridotite massifs. Most rocks underwent low-grade metamorphism and are foliated. The two sequences contact in north-dipping thrust faults.

The Wushan terrane is located in the west part of the TWAB, fifteen kilometers to the west of the Guanzizhen terrane (Fig. 1b). The ophiolite complex in the Wushan terrane is distributed along several sections that is composed predominantly of the metaperidotite, metagabbro and metabasalt. Most of these blocks thrust northward onto the island-arc complex (Dong et al., 2007). The meta-peridotite show blackish-green color and imposed by serpentinization. The metabasalts mostly crop out as greenschists and mainly consist of chlorites (~30%), hornblendes (15-20%), plagioclases (30-35%) and some other minerals. It can be distinguished by some fine-grained pyroxene and plagioclase grains preserved within a matrix composed of chlorite and epidote.

The ophiolite complex in Guanzizhen terrane is located in the east part of the TWAB. It consists of minor serpentinite, meta-gabbro, plagiogranite, voluminous metabasalt with pillow structure (Fig. 2a) and a thin layer of meta-chert (Fig. 2b). The gabbro shows cumulate bands with weak deformation (Fig. 2c). The metabasalts occur as deformed pillow lavas and have experienced low-grade metamorphism with a mineral assemblage of amphibole, epidote and plagioclase. A white-colored, ~30-meter-thick marble and mica-quartz schist layer occurs on the top of the ophiolite complex (Fig. 1c and 2d), most likely a carbonate cap of a seamount.

The island-arc volcanic rocks extend parallel to the ophiolite complexes (Fig. 1b). These rocks predominantly compose of island basaltic andesite and boninite without a clear geologic boundary. The basaltic andesite are dark green in color with massive

structures (Fig. 2e) and shows phenocryst-poor intergranular textures with microlites of augite, plagioclase and quartz. The boninite samples are porphyritic, with coarse-grained phenocrysts (olivine and Cpx pseudomorphs) in a usually intersertal textured groundmass filled with plagioclase, metamorphic amphibole, chlorite and Cr-spinel (Fig. 3a and b). Mineral assemblages and structure suggest that these volcanic rocks have experienced greenschist-facies metamorphism and deformation.

The ultramafic massif occurs as a fault-bounded, lentoid, spinel peridotite massif, and occupies an area of ~25 km² in Wushan terrane. The boundaries between the ultramafic massif and its surrounding meta-mafic rocks are tectonic and are characterized by ductile deformation and mylonitization. The ultramafic massif mainly consists of serpentinized dunite and harzburgite with relict olivine, orthopyroxene and minor spinel (Fig. 3c). Chromium spinel occurs as euhedral crystals either between or within olivine and orthopyroxene grains (Fig. 3d).

4. Analytical methods

4.1. Mineral chemistry

Mineral analyses for major element oxides, including olivine and spinel, were done on a JEOL JXA-8100 Electron Probe Microanalyzer (EPMA) at Peking University. Analytical conditions were optimized for standard silicates and oxides at 15 kV accelerating voltage with a 20 nA focused beam current for all the elements. Routine analyses were obtained by counting for 30 s at peak and 10 s on background. Repeated analysis of natural and synthetic mineral standards yielded precisions better than ±2% for most elements.

4.2. Bulk-rock major and trace element analyses

Bulk rock major and trace elements analysis was done at the Geological Lab Center, CUGB. Bulk-rock major element oxides were determined using inductively coupled plasma-atomic emission spectroscopy (ICP-OES). The analytical uncertainties are generally less than 1% for most elements with the exception of TiO₂ (~1.5%) and P₂O₅ (~2.0%) based on rock standards GRS-1, and GSR-3 (national geological standard reference material of China), AGV-2, W-2 (U.S. Geological Survey: USGS). Loss on ignition (LOI) was determined by placing 1 g of samples in the furnace at 1000°C for 3 hours before being cooled in a desiccator and reweighed. Bulk rock trace elements were determined on an Agilent-7500a inductively coupled plasma-mass spectrometry (ICP-MS) at the Institute of Earth Science, CUGB. Rock standards AGV-2, W-2, and BHVO-2 (USGS) were used to monitor the analytical accuracy and precision. Analytical accuracy, as indicated by relative difference between measured and recommended values, is better than 5% for most elements, 10-13 % for Cu, Sc, Nb, Er, Th, and U, 10-15% for Ta, Tm and Gd. The detailed analytical procedures follow Song et al. (2010).

4.3. Bulk rock Sr-Nd isotope analyses

The bulk-rock Sr-Nd isotope analyses were done at MOE Key Laboratory of Orogenic Belts and Crustal Evolution, Peking University. About 300 mg of unknown sample and ~200 mg of standard sample (BCR-2) were dissolved by using HF+HNO₃ in Teflon vessels and heated at 140°C for a week in order to be completely dissolved. The pure Sr and Nd isotopic ratios were measured using a Thermo-Finnigan Triton thermal ionization mass spectrometer at Tianjin Institute of Geology and Mineral Resources. The ⁸⁷Rb/⁸⁶Sr and ¹⁴⁷Sm/¹⁴⁴Nd ratios were calculated based on Rb, Sr, Sm, and Nd contents determined by ICP-MS (CUGB). Mass fractionation corrections for Sr and Nd isotopic ratios were normalized to ⁸⁶Sr/⁸⁸Sr = 0.1194 and ¹⁴⁶Nd/¹⁴⁴Nd = 0.7219,

respectively. Rock standard BCR-2 was used to evaluate the separation and purification process of Rb, Sr, Sm, and Nd. Repeated analyses for the Nd and Sr standard samples (JNd_i and NBS987) yielded $^{143}\text{Nd}/^{144}\text{Nd} = 0.512120 \pm 11$ (2σ) and $^{87}\text{Sr}/^{86}\text{Sr} = 0.710250 \pm 11$ (2σ), respectively.

4.4. In situ zircon U-Pb dating analyses

Five samples including gabbro (T14-08, T14-25 and T15-38), serpentinized peridotite (T14-38) and island arc volcanic (T15-05) were chosen for in situ zircon U-Pb dating. Cathodoluminescence (CL) images were acquired to observe the internal structures of zircon grains, using a CL spectrometer (Garton Mono CL3+) equipped on a Quanta 200F environmental scanning electron microscope at scanning conditions of 15 kV/120 nA in the School of Physics, Peking University.

Measurements of U-Th-Pb isotopes for samples T14-08, T14-25 and T15-38 was conducted using a Cameca IMS-1280 SIMS in the Institute of Geology and Geophysics, Chinese Academy of Sciences in Beijing. Pb/U calibration was performed relative to zircon standard Plésovice (337 Ma, Sláma et al., 2008); U and Th concentrations were calibrated against zircon standard 91500 (Wiedenbeck et al., 1995). An in-house zircon standard Qinghu (159.5 ± 0.2 Ma, Li et al., 2013) was alternately analyzed as an unknown together with other unknown zircons in order to monitor the external uncertainties of SIMS U-Pb zircon dating calibrated against the Plésovice standard. The instrument description and analytical procedure is given in Li et al. (2009). Data reduction was carried out using the Isoplot/Ex v. 3.0 program (Ludwig, 2003).

Measurement of U-Th-Pb isotopes for samples T15-38 and T15-05 was carried out on an Agilent-7500a quadrupole inductively coupled plasma-mass spectrometry coupled with a New Wave SS UP193 laser sampler (LA-ICP-MS) at China University

of Geosciences, Beijing (CUGB). Laser spot size of 36 μm , laser energy density of 8.5 J/cm² and a repetition rate of 10 Hz were applied for analysis. National Institute of Standards and Technology 610 glass and zircon standard 91500 (Wiedenbeck et al., 1995) were used as external standards, Si as internal standard, and zircon standard Qinghu zircon (159.5 Ma) from China (Li et al., 2013) as the secondary standard. The software GLITTER (ver. 4.4, Macquarie University) was used to process the isotopic ratios and element concentrations of zircons. The common lead correction was done following Andersen (2002). Age calculations and plots of concordia diagrams were made using Isoplot/Ex v. 3.0 program (Ludwig, 2003). Analytical details are described in Song et al. (2010).

5. Results

5.1 Olivine and Cr-spinel in peridotite and boninite

Representative compositions for major element oxides, including olivine and spinel, are given in Table 1 and 2. Olivine in peridotite shows a narrow compositional variation of Fo (~91-92) with NiO content ranging from 0.30 to 0.44 wt. % (Fig. 4a). The Fo values are much higher than olivines from the present-day abyssal peridotite (Dick, 1989), but consistent with those from forearc peridotites (Fig. 4a and b; Ishii et al., 1992, Arai, 1994).

As a ubiquitous accessory phase in boninites and peridotites, Cr-spinel is a highly refractory and resistant mineral and has been considered as an effective petrogenetic indicator, capable of conveying information about magmatic features (Dick and Bullen, 1984; Arai, 1994, Kamenetsky, 2001). Cr-spinel in peridotite shows a homogeneous core and a narrow bright rim (Fig. 3f). The core has high Cr₂O₃ (48-55 wt. %), low Al₂O₃ (5.5-12.7 wt. %) and TiO₂ (0.01-0.55 wt. %) with Cr# ($100 \times \text{Cr} / (\text{Cr} + \text{Al})$) = 73-

87 (Fig. 4b and c). The rim has high Fe and low Cr, Al, and Mg owing to the chemical re-equilibrium or alteration at subsolidus conditions (Fig. 4c and d; Cao et al., 2016). For comparison, Cr-spinel in boninite is characterized by high Cr_2O_3 , and low Al_2O_3 , MgO and TiO_2 with high Cr# ($100 \times \text{Cr} / (\text{Cr} + \text{Al}) = 77\text{-}89$) and evolved $\text{Fe}^{2+} / (\text{Fe}^{2+} + \text{Mg})$ (0.97-0.99) (Fig. 4c). All spinel compositions in peridotites and boninites follow the Fe-Ti trend that is characterized by an increasing $\text{Fe}^{2+} / (\text{Fe}^{2+} + \text{Mg})$ ratio and Fe^{3+} content toward magnetite from core to rim (Fig. 4c and d).

5.2 Bulk rock geochemistry

Bulk rock major and trace element analysis for lavas and serpentinized peridotite samples from the ophiolite complexes and island arc assemblages are listed in Table 2. According to field occurrence and geochemical division (Fig. 5c-f), three groups of rocks can be distinguished: (1) pillow lavas in ophiolite complexes with MORB-like compositions, (2) the massive island arc volcanic complex, and (3) serpentinized peridotite with forearc signatures.

5.2.1 Pillow lavas from ophiolite complexes

Compositionally, the pillow lavas from the Guanzizhen and Wushan ophiolite complexes have sub-alkaline, tholeiitic compositions, similar to present-day normal and enriched MORB (Table 3). They plot in the basalt field in the TAS diagram of Wilson (1986) (Fig. 5a) and show tholeiitic trend in the $\text{FeO}_t / \text{MgO-SiO}_2$ diagram of Miyashiro (1975) (Fig. 5b) and AFM diagram of Pearce et al., (1977) (Fig. 5c). In the Hf-Th-Ta (Wood, 1980), Cr-Y and Ti-V diagrams (Fig. 5d-f), they mainly plot in the MORB fields.

Basalts from Guanzizhen ophiolite complex display flat REE patterns with slight depletion of LREE ($(\text{La/Sm})_N = 0.63\text{-}1.05$ and $(\text{La/Yb})_N = 0.79\text{-}1.29$) (Fig. 6a). The REE abundances of the basalt are $\sim 13\text{-}36 \times \text{C1}$, mostly higher than the N-MORB

($\sim 18 \times C1$) (Sun and McDonough, 1989). In Fig. 6b, all samples show patterns transitional from normal to enriched MORB with consistent HFSEs (Nb, Ta, Zr, Hf and Ti) relative to neighboring elements.

Data for basalts from the Wushan ophiolite complex are from Dong et al. (2007). Basalts from the Wushan ophiolite complex are characterized by slight enrichment of LREE ($(La/Sm)_N = 0.98\text{--}1.54$ and $(La/Yb)_N = 1.30\text{--}3.54$) (Chondrite-normalized, Sun and McDonough, 1989). The REE abundances of the basalt are $\sim 15\text{--}52 \times C1$, mostly higher than N-MORB and E-MORB ($\sim 18 \times C1$) (Sun and McDonough, 1989). In Fig. 6b, all samples show patterns of enriched MORB with consistent HFSEs (Nb, Ta, Zr, Hf and Ti) relative to neighboring elements.

5.2.2 Island arc volcanic complex

Massive lavas from the island arc complex plot in the basaltic-andesite to andesite field of the TAS diagram (Fig. 5a). They can be subdivided into two lithological types according to their chemical compositions: low-Mg calc-alkaline basaltic andesites and andesites ($MgO < 8$ wt. %) and high-Mg boninites ($MgO > 8$ wt. %). Low-Mg volcanics are characterized by relatively low contents of Cr (30–186 ppm), Ni (15–93 ppm), MgO (2.93–7.72 wt. %), but relatively high TiO_2 (0.41–1.05 wt. %) and Zr (34–101 ppm). All samples show a calc-alkaline trend (Fig. 5b and c); some display LREE depletion with $(La/Sm)_N$ ratio (0.4–0.5) and others show LREE enrichment with $(La/Sm)_N$ ratio (2.0–3.2) (Fig. 6e). All the low-Mg volcanics display patterns with negative Nb-Ta anomalies, varying negative Zr, Hf and Ti anomalies and enrichment of Rb, Ba and U (Fig. 6f). We refer to these calc-alkaline volcanics as two sub-groups, LREE-depleted and LREE-enriched, in the following descriptions.

The high-Mg boninite samples are characterized by high contents of MgO, Cr and Ni and low TiO₂ (< 0.5 wt. %), Zr (< 50 ppm). They plot in the boninite field in the Cr v Y and V v Ti/1000 diagrams of Figure 5e and f. These samples display slightly enriched LREE patterns ($(\text{La}/\text{Sm})_{\text{N}} = 0.68\text{-}2.09$, mostly > 1), but have lower ΣREE abundances than those MORB-like basalts in ophiolite complex and low-Mg calc-alkaline volcanics (Fig. 6g). They have notably negative HFSE (Nb, Ta, Zr, Hf, and Ti) anomalies, and enrichment of Cs, Rb, Ba, Th, U, and Pb (Fig. 6h).

5.2.3 Serpentinized peridotite

CIPW norm calculations using whole-rock major element compositions (Niu, 1997) show that serpentized peridotite is a cpx-poor harzburgite. The serpentized peridotite samples, except for the wehrlitic dike (T14-35), have high concentrations of MgO (42.6-46.1 wt. %, anhydrous basis) with low contents of TiO₂ (<0.1 wt. %), Al₂O₃ (0.10-1.21 wt. %) and CaO (0.01-0.27 wt. %). In Fig. 7, these samples are characterized by highly depleted REE profiles, with positive Eu anomalies ($\text{Eu}/\text{Eu}^*=0.63$ on average, except for T15-46). The HREE abundances of these samples are consistent with forearc peridotites from the Izu-Bonin-Mariana (IBM) arc and orogenic belts (Parkinson and Pearce, 1998; Song et al., 2009; Cao et al., 2016), but lower than the representative abyssal peridotite (Niu et al., 1997). The enrichment of peridotites in LREE commonly produces U-shaped REE patterns, showing the addition of relatively high amounts of slab-derived fluids to the mantle wedge.

5.3 Bulk rock Sr-Nd isotopic data

All the Sr-Nd isotopic data of basalts from ophiolite complexes and island arc volcanic complex in the TWAB are presented in Table 4 and illustrated in Figure 8. Lithological types include cumulate gabbro, pillow basalt, calc-alkaline volcanics,

boninite and serpentinized peridotite. The initial values of the gabbro-basalt and the island arc volcanic-boninite were calculated at 500Ma and 450 Ma, respectively. The samples of gabbro and basalt from the Guanzizhen and Wushan ophiolite complexes (Hou et al., 2006b and this study) display varying ϵ_{Nd} (t) values (+2.6 ~ +11.1) and I_{sr} values (0.703574-0.707453). Trends towards higher Sr isotope values at constant Nd isotope value may be attributed to the alteration by seawater or/and hydrothermal fluids. The positive ϵ_{Nd} (t) values range from those of modern plume-related OIB (Zindler, 1986; White and Duncan, 1996) to close to those of modern N-MORB (Zimmer et al., 1995). The island arc volcanics (LREE-depleted) have restricted ϵ_{Nd} (t) values (+6.0~+6.6) and high I_{sr} values (0.705817-0.706383). The boninite samples with evolved ϵ_{Nd} (t) and I_{sr} values plot within the island arc field, suggesting seawater alteration or/and contamination of slab-derived fluids/melts. The serpentinized peridotite samples have negative ϵ_{Nd} (t) values (-4.39 ~ 4.42) and high I_{sr} values (0.710859-0.712039), suggesting significant contamination by crust-derived fluids.

5.4 Zircon U-Pb geochronology

Three gabbro samples (T14-08, T14-25 and T15-38) from the Guanzizhen ophiolite complex, one island arc volcanic (TS15-05) and one serpentinized peridotite sample from the arc-volcanic complex (T14-38) were selected for SIMS and LA-ICPMS zircon U-Pb dating. The results are listed in Table 5.

Zircons from the gabbro samples are colorless and euhedral crystals with varying long axis lengths up to 50-150 μm and length/width ratios up to 1.2-2.5. CL images show variable luminescence with straight and wide oscillatory growth bands (Fig. 9). Zircons from sample T15-38 have various abundances of Th (33-434 ppm) and U (90-466 ppm) with relatively high Th/U ratios (0.35-0.93). Zircons from sample T14-25 have U (54-547 ppm) and Th (17-287 ppm) with Th/U ratios of 0.24-0.69. Zircons from

sample T14-08 have various abundances of Th (157-3157 ppm) and U (205-1814 ppm) with relatively high Th/U ratios (0.59-1.74). Twenty-five analyses of zircons from gabbro sample T15-38 yield apparent $^{206}\text{Pb}/^{238}\text{U}$ ages of 496-505 Ma, giving an weighted mean at 502 ± 2 Ma (MSWD = 0.21) (Fig. 10a). Twenty analyses of zircons from the gabbro sample T14-25 yield apparent $^{206}\text{Pb}/^{238}\text{U}$ ages of 493-511 Ma with a concordia age of 504 ± 2 Ma (MSWD = 1.1) (Fig. 10b), and twelve analyses from sample T14-08 yield apparent $^{206}\text{Pb}/^{238}\text{U}$ ages of 497-522 Ma with a concordia age of 512 ± 2 Ma (MSWD = 0.073) (Fig. 10c). The 502-512 Ma ages suggest the forming time of the ocean crust in the West Qinling is in Late Cambrian, similar to the Lajishan ophiolite complex in the South Qilian Accretionary Belt of the Qilian Orogen (Zhang et al., 2017).

Zircons from the serpentinized peridotite sample (14TS38) are colorless, rounded with length of shaft up to 50-100 μm . CL images show these zircons have patchy cores with blurred oscillatory zone and a thin dark luminescent rim (Fig. 9). The cores have various abundances of Th (74-337 ppm) and U (114-1079 ppm) with relatively high Th/U ratios (0.14-0.58) and yield discordant $^{207}\text{Pb}/^{206}\text{Pb}$ ages ranging from 1342-2522 Ma. The CL images and U-Pb results suggest that these zircon cores are probably either recycled from subduction zone or derived from surrounding rocks, rather than the peridotite itself. The zircon rims have low Th (10-21 ppm) and high U (593-1143 ppm) with extremely low Th/U ratios (0.009-0.025), suggesting a fluid-rich forming condition. Five analyses of the zircon rims form a concordia age of 452 ± 8 Ma (MSWD = 2.1) (Fig. 10d).

Zircons from the calc-alkaline basaltic-andesite (TS15-05) are euhedral and prismatic, showing oscillatory zoning of magmatic origin without any relict core (Fig. 9). Thirty-four analyses form a concordia age of 451 ± 1 Ma (MSWD = 3.5) (Fig. 10e).

This age, together with the metamorphic age from serpentинized peridotite sample, are interpreted as the formation time of an intra-oceanic arc.

6. Discussion and conclusions

6.1 Formation environment of the ophiolite complex: mantle plume-related?

Normal oceanic crust is not typically obducted and preserved as ophiolite complexes. Ophiolite complexes preserved within orogenic belts are generally those from SSZ-settings, or seamounts and oceanic plateau that stand above the seafloor and thus can be scraped off during subduction (Niu et al., 2003). Geochemical compositions of basalts in the upper part of ophiolite complexes can effectively record variations of spreading rate, proximity to plumes or trenches, mantle temperature, mantle fertility, and the availability of fluids (Dilek and Furnes, 2011; Song et al., 2015).

Nd-Pb isotopic compositions of mantle source in Tianshui-Wushan ophiolite complexes, as well as in those from Qilian Orogen, show mixture feature between DMM and EM II, similar to those in the Paleo-, Neo-Tethys and Indian Ocean, thus proposing that ancient oceanic mantle of these Early Paleozoic ophiolite complexes present the branch the of Paleo-Tethys (Hou et al., 2006a and b). Based on the elemental and isotopic compositions, previous investigations argued that the ophiolite complexes in the West Qinling Orogen either formed in island arc setting, or mid ocean ridge setting with enriched mantle source (Hou et al., 2006b) or initially expanded mid ocean ridge environment (Dong et al., 2007).

The marble slices on the top of ophiolite complex (Fig. 1c and 2d) are most likely a carbonate cap of a seamount, which provide the direct field evidence that the ophiolite complex might be the remnants of an oceanic plateau or seamounts. As shown in discrimination diagrams (Fig. 5), pillow lavas in the Guanzizhen and Wushan ophiolite

complexes show a tholeiitic trend and characteristics of enriched, subduction-unrelated MORB. However, the slightly high contents of K₂O and TiO₂ (1.65 wt. % on average) and evolved εNd (t)-Isr values (Fig. 10) of these lavas suggest that their mantle source is different from that of N-MORB. As Th is a mobile element in the SSZ setting and thus can effectively distinguish formation environments of ophiolite complexes (e.g. Wood, 1980; Regelous et al., 1997). All samples lie in the field of present oceanic plateau in the PM-normalized Nb/Th-Nb/La diagram (Fig. 11a), similar to Hawaiian basalts (Norman and Garcia, 1999) and the Lajishan-Yongjing ophiolite complex in the South Qilian Accretionary Belt of Qilian Orogen (Zhang et al., 2017). Figures. 11b-d show a compositional change from OIB to E-MORB and to N-MORB along the mantle array, from the Lajishan-Yongjing P-type ophiolite complex of the Qilian Orogen in the west, to the Wushan ophiolite complex in the middle and the Guanzizhen ophiolite complex in the east. Fig. 11c show that most lavas in these ophiolite complexes are originated from plume-related enriched mantle source (Zr/Nb ratio<10 and δNb >0; Zhu et al., 2008; Fitton et al., 1997). Zhang et al. (2017) suggested that the mantle source of ophiolite complexes in the South Qilian Accretionary Belt have been enriched by a mechanism related to a hot spot or mantle plume. Going from the Lajishan-Yongjing ophiolite complex, to the Wushan ophiolite complex through to Guanzizhen ophiolite complex, the reduced extent of mantle source enrichment may reflect a descending influence of mantle plume or hot spot activity from west to east. Thus, we propose that the Wushan-Guanzizhen ophiolite complexes are most likely the relics of an enriched oceanic crust with different intraplate characteristics located in different areas of the oceanic plateau.

6.2 Identification of an IBM-type intra-oceanic arc in the West Qinling Orogen

Early Paleozoic boninites have previously been reported from further east in the Qinling (Li et al., 2012, 2015), but not from the Wushan and Guanzizhen localities. Li et al. 2015 proposed a complex tectonic model where the former arc is split in two parts and the younger boninite-like lavas (ca. 474Ma) occurred at a back-arc basin spreading center. The problems are, at first, the older arc volcanic complex should be present on both sides of ophiolite complex if the former arc is split in two parts (Li et al., 2012, 2015), but it is not found to the south side of ophiolite complex. Second, the younger boninite-like lava sample (474 Ma: Li et al., 2012) is not a typical boninite but a metagabbro.

Our geochemical results indicate that the island arc complex of the TWAB formed in a forearc setting of an IBM-type intra-oceanic arc. This is because: (1) such boninite-related volcanic complexes, exhibiting a magmatic progression with continued mantle wedge depletion and the transition of slab-derived component from fluid mobile elements (e.g. Ba and U) to melt mobile elements (e.g. Nb, Ta, Th and LREE) (Fig. 12 a-d), are generally related to a young and warm forearc region (i.e. an immature forearc setting) (Crawford, 1989; Whattam and Stern, 2011); and (2) mineral (Cr-spinel and olivine) and bulk-rock compositions of the serpentinized peridotite suggest a forearc environment as discussed below.

6.3 Forearc peridotite: depletion and refertilization of the mantle wedge

The serpentinized peridotite massif in the TWAB shows characteristics of a refractory forearc mantle residue after a large extent of melt extraction based on the modal compositions, bulk-rock composition and mineral chemistry. Forearc peridotites, normally, do become extremely refractory (e.g. harzburgite/dunite) after two stages of partial melting in a mid-ocean ridge environment and supra-subduction zone environment, respectively (Parkinson and Pearce, 1998; Pearce et al., 2000; Uysal et

al., 2015). Lines of evidence for high-degree melting and the residual nature of the studied peridotite includes: (1) the very low whole rock CaO, Al₂O₃, TiO₂ and HREE contents (Pearce et al., 1992); (2) the low contents of TiO₂, Al₂O₃ and high Cr# in Cr-spinel, and the high Fo[#] values (~91-92) of olivine (Arai, 1994).

The partial melting event of refractory mantle can be modified by the refertilization of mantle wedge with influx of solidus-lowering aqueous fluids/melts prior to or during partial melting (e.g. Bédard, 1999; Garrido et al., 2006; Pagé et al., 2009). The enrichment of peridotites in LREE commonly produces U-shaped REE patterns (Dilek and Furnes, 2011; Uysal et al., 2015), showing the addition of large amounts of slab-derived fluids or melts to the mantle wedge (Fig. 7). Peridotite samples with high SiO₂ and FeO_T relative to fertile mantle peridotite (KR-4003: Herzberg, 2004), can be attributed to the addition of Fe³⁺ and SiO₂(Ol+SiO₂=Opx) from slab-derived hydrous fluids/melts and subsequent melt-rock reaction with elevated oxygen fugacity (Lee et al., 2003; Herzberg, 2004). The low $\epsilon_{\text{Nd}}(t)$ (-4.39~ -4.42) and high I_{sr} (0.710859-0.712039) values of serpentinized peridotite show possible contamination by slab-derived sediment melt or simple seafloor alteration. In addition, the very high Cr# of spinel (>70) is likely produced by a boninitic melt-rock reaction (Zhou et al., 1996; Cao et al., 2016).

The Ni/Yb versus Yb diagram is mainly used to reflect the degree of partial melting and the La/Yb versus Yb diagram is used to reflect the presence of fluxing material during open-system dynamic melting model (OSDM) and the fluxing ratios (Fig. 13; Uysal et al., 2015). In the La/Yb versus Yb diagram (Fig. 13a) and the Ni/Yb versus Yb diagram (Fig. 13b), we can explain the cpx-poor harzburgites with about 15-23% OSDM of the 10% depleted mantle with the fluxing rates ($\beta > 4.0\%$).

6.4 Geodynamics of subduction in the West Qinling Orogen

Two general mechanisms summarized by Stern (2010) are proposed to interpret subduction initiation process: spontaneous and induced nucleation of subduction zones. Spontaneous nucleation results from gravitational instability of oceanic lithosphere and is required to begin the modern regime of plate tectonics, i.e., the subduction initiation model from the IBM subduction system (e.g., Hall et al., 2003; Stern, 2004). In this model, the MORB-like lavas in either proto-forearc environment or back arc basin setting occur in close association to arc-like lavas with conformable boundaries (Whattam and Stern, 2011) and similar ages (Reagan et al., 2010). In contrast, induced nucleation of subduction is a response to continuing plate convergence following jamming of a subduction zone by buoyant crust, resulting in regional compression, uplift and underthrusting that may yield a new subduction zone (Stern 2004, 2010); this is equivalent to the “oceanic plateau model” proposed by Niu et al., (2003). Different from the tectonic model proposed by Li et al. (2012, 2015), we suggest that the ophiolite complexes and the island arc complex with different ages formed in different tectonic settings. As described above, enriched MORB in ophiolite complexes are interpreted to be products of mixing melts by an enriched source (mantle plume?) with normal mantle sources. Age data (534-500 Ma) of ophiolite complexes reveal that oceanic crust in this region formed in the Cambrian. In contrast, the island arc complex, incorporated closely with ophiolite complex, is interpreted to have formed in a forearc setting at ~460-440 Ma, much younger than the ophiolite complexes (Table 6. Fig. 10f).

The rock assemblages and age patterns of the TWAB in the West Qinling Orogen are essentially the same as the South Qilian Accretionary Belt of the Qilian Orogen (Zhang et al., 2017), and thus we infer a continuity between the two orogens (Fig. 1a) as described in the next section. As illustrated in Fig. 14, we propose that the MORB-like lavas with ages of 512-502 Ma, emplaced at the edge of the Lajishan-Yonjing oceanic

plateau (Zhang et al., 2017), represents the plume-related lithosphere remnants of the Qinling Ocean and obducted as an ophiolitic component in the TWAB when the buoyant plateau reached the subduction zone. The newly formed island arc complex was products of an intra-oceanic arc volcanic sequence in response to the collision between the Cambrian oceanic plateau and the pre-existing trench at ca. 460~440 Ma.

6.5 Evolution of the Proto-Tethyan Ocean and tectonic relations between the East Qinling Orogen and the Qilian Orogen

The “Proto-Tethyan Ocean”, separating the North China Craton (NCC) from eastern Gondwana, may actually be an eastern branch of the “Iapetus Ocean” which initiated in the Late Neoproterozoic-Early Cambrian (610-530Ma, Murphy et al., 2010). Previous studies have suggested that the Asian terranes (Hunia, East Kunlun, Qaidam, Qilian) (von Raumer et al., 2008) were located along the Cambrian Gondwana margin and accreted to the NCC in the Silurian because of the southward subduction of the Proto-Tethys Ocean. This process led to the opening of an eastern prolongation of the already existing Rheic Ocean during the Late Cambrian (von Raumer et al., 2008).

Recent studies suggested that the Qinling-Qilian-Kunlun Ocean was generated by breakup of Rodinia supercontinent in the late Neoproterozoic (~600-580 Ma), on the evidence of rift volcanics and ophiolite complexes (e.g., Song et al., 2013; Xu et al., 2015, 2016). Therefore, we believe that these oceans are interpreted as representing the “Proto-Tethyan Ocean” rather than the Rheic Ocean. Besides, these fragments, including the Central Qilian Block and Qaidam-Quanji Block, were separated from eastern Gondwana and surrounded by Qilian-Kunlun-Qinling Ocean. Different from the southward subduction model of Proto-Tethyan Ocean (von Raumer et al., 2008), we believe that they assembled northwards to the margin of the NCC by continuous subduction, initiated in ~ 520 Ma and terminated by closure of the Qilian Ocean at

~440-430 Ma (Song et al., 2013), while the Kunlun Ocean may have begun start to subduct towards the Qaidam block (Fig. 14).

Three major tectonic units, including the Qilian-Qaidam Orogen in the north, the Qaidam block in the middle and the East Kunlun Orogen in the south, lie to the west of the West Qinling Orogen (Fig. 1a). The Qilian-Qaidam Orogen consists of two accretionary belts and one continental-type ultra-high pressure metamorphic belt, including, from north to south, the North Qilian Accretionary Belt (NQAB), the South Qilian Accretionary Belt (SQAB) and the North Qaidam UHPM Belt (Song et al., 2013, 2014). Both the NQAB and East Kunlun Orogen are Andean-type active continental margins with the development of a back arc basin in the Early Paleozoic era, recording a subduction history of Qilian Ocean and Kunlun Ocean beneath the Alxa Block and Kunlun Terrane, respectively (Zhang et al., 2007; Xia et al., 2012; Song et al., 2006, 2013, 2017; Bian et al., 2004; Zhu et al., 2006; Mo et al., 2007; Meng et al., 2013, 2015; Qi et al., 2014; Hu et al., 2016). In contrast, the SQAB is composed of (1) P-type ophiolite complexes (525-500 Ma) with E-MORB, OIB and high-Mg komatiitic basalts and (2) island arc magmatic sequences (470-440 Ma) including intermediate-basic volcanic rock and boninite (Yang et al., 2002; Zhang et al., 2017). These P-type ophiolite complexes have been interpreted as fragments of an oceanic plateau of mantle plume-origin in the Qilian Ocean during the Cambrian (~525 Ma) (Zhang et al., 2017). While the arc-volcanic sequence, incorporated to the south side of the ophiolite complexes, is considered to have formed in an intra-oceanic forearc environment.

Therefore, the SQAB and TWAB have the same rock assemblages and age pattern, and thus can be considered as products of a uniform, newly-formed subduction zone in response to trench-jamming by an oceanic plateau collision. As a result, a new IBM-type intra-oceanic island arc was generated, with a boninite-bearing volcanic complex

and forearc peridotite in the south. This united accretionary belt extends at least ~600 km from Qilian Orogen in the west to the West Qinling Orogen, and further connects to the Shangdan Ocean of the Qinling Orogen (Dong and Santosh, 2016) in the east.

Acknowledgments

We thank X.H. Li, J. Li and H. Y. Zhang for helping with zircon U-Pb dating, W.G. Liu and W.P. Zhu for Sr-Nd isotopic analyses. We also thank for editors and reviewers for their time, efforts and constructive comments. This study was supported by the Major State Basic Research Development Program (2015CB856105) and National Natural Science Foundation of China (Grant Nos. 41572040, 41372060).

References

- Andersen, T., 2002. Correction of common lead in U-Pb analyses that do not report 204 Pb. Chemical Geology 192, 59-79.
- Arai, S., 1994. Characterization of spinel peridotites by olivine-spinel compositional relationships: Review and interpretation. Chemical Geology 113, 191-204.
- Barnes, S.J., Roeder, P.L., 2001. The Range of Spinel Compositions in Terrestrial Mafic and Ultramafic Rocks. J Petrology 42, 2279-2302.
- Bédard, J.H., 1999. Petrogenesis of Boninites from the Betts Cove Ophiolite, Newfoundland, Canada: Identification of Subducted Source Components. Clinical Microbiology Reviews 14, : 753-777.
- Bian, Q.T., Li, D.H., Pospelov, I., Yin, L.M., Li, H.S., Zhao, D.S., Chang, C.F., Luo, X.Q., Gao, S.L., Astrakhantsev, O., 2004. Age, geochemistry and tectonic setting of Buqingshan ophiolites, North Qinghai-Tibet Plateau, China. Journal of Asian Earth Sciences 23, 577-596.
- Brenan, J.M., Shaw, H.F., Ryerson, F.J., Phinney, D.L., 1995. Mineral-aqueous fluid partitioning of trace elements at 900°C and 2.0 GPa: Constraints on the trace element chemistry of mantle and deep crustal fluids. Geochim. Cosmochim. Acta 59, 3331-3350.

- Cao, Y., Song, S., Su, L., Jung, H., Niu, Y., 2016. Highly refractory peridotites in Songshugou, Qinling orogen: Insights into partial melting and melt/fluid–rock reactions in forearc mantle. *Lithos* 252–253, 234-254.
- Cawood, P.A., Kröner, A., Collins, W.J., Kusky, T.M., Mooney, W.D., Windley, B.F., 2009. Accretionary orogens through Earth history. Geological Society, London, Special Publications 318, 1-36.
- Crawford, A.J., Falloon, T. J., Green, D. H., 1989. Classification, petrogenesis and tectonic setting of boninites. In: Crawford, A.J. (Ed.), Boninites and Related Rocks. pp. 1-49, Unwin Hyman Ltd, London.
- Dewey, J.F., Bird, J.M., 1971. Origin and Emplacement of the Ophiolite Suite: Appalachian Ophiolites in Newfoundland. *Journal of Geophysical Research Atmospheres* 76, 3179-3206.
- Dick, H.J.B., 1989. Abyssal peridotites, very slow spreading ridges and ocean ridge magmatism. Geological Society London Special Publications 42, 71-105.
- Dick, H.J.B., Bullen, T., 1984. Chromian spinel as a petrogenetic indicator in abyssal and alpine-type peridotites and spatially associated lavas. *Contributions to Mineralogy and Petrology* 86, 54-76.
- Dilek, Y., Furnes, H., 2011. Ophiolite genesis and global tectonics: Geochemical and tectonic fingerprinting of ancient oceanic lithosphere. *Geological Society of America Bulletin* 123, 387-411.
- Dong, Y., Santosh, M., 2016. Tectonic architecture and multiple orogeny of the Qinling Orogenic Belt, Central China. *Gondwana Research* 29, 1-40.
- Dong, Y., Zhang, G., Neubauer, F., Liu, X., Genser, J., Hauzenberger, C., 2011a. Tectonic evolution of the Qinling orogen, China: Review and synthesis. *Journal of Asian Earth Sciences* 41, 213-237.
- Dong, Y., Zhang, G., Hauzenberger, C., Neubauer, F., Yang, Z., Liu, X., 2011b. Palaeozoic tectonics and evolutionary history of the Qinling orogen: Evidence from geochemistry and geochronology of ophiolite and related volcanic rocks. *Lithos* 122(1-2), 39-56.

- Dong, Y., Zhang, X., Liu, X., Li, W., Chen, Q., Zhang, G., Zhang, H., Yang, Z., Sun, S., Zhang, F., 2015. Propagation tectonics and multiple accretionary processes of the Qinling Orogen. *Journal of Asian Earth Sciences* 104, 84-98.
- Dong, Y.P., Yang, Z., Zhang, G.W., Zhao, X., Xu, J.G., Yao, A.P., 2008. Geochemistry of the Ophiolite in the Guanzizhen Area, West Qinling and its tectonic implications *Acta Geologica Sinica* 82, 1186-1194.
- Dong, Y.P., Zhang, G.W., Yang, Z., Zhao, X., Ma, H.Y., Yao, A.P., 2007. Geochemistry of the E-MORB type ophiolite and related volcanic rocks from the Wushan area, West Qinling. *Science China Earth Sciences* 50, 234-245.
- Elliott, T., Plank, T., Zindler, A., White, W., Bourdon, B., 1997. Element transport from slab to volcanic front at the Mariana arc. *Journal of Geophysical Research Atmospheres* 1021, 14991-15020.
- Fitton, J.G., Saunders, A.D., Norry, M.J., Hardarson, B.S., Taylor, R.N., 1997. Thermal and chemical structure of the Iceland plume. *Earth & Planetary Science Letters* 153, 197-208.
- Garrido, C.J., Bodinier, J., Burg, J., Zeilinger, G., Hussain, S.S., Dawood, H., Chaudhry, M.N., Gerville, F., 2006. Petrogenesis of Mafic Garnet Granulite in the Lower Crust of the Kohistan Paleo-arc Complex (Northern Pakistan): Implications for Intra-crustal Differentiation of Island Arcs and Generation of Continental Crust. *Journal of Petrology* 47.
- Hall, C.E., Gurnis, M., Sdrolias, M., Lavier, L.L., Muller, R.D., 2003. Catastrophic initiation of subduction following forced convergence across fracture zones. *Earth & Planetary Science Letters* 212, 15-30.
- He, S., H. Wang, X., Xu, H., Zhang, Ren, G., 2007. A LA-ICP-MS U-Pb Chronological Study of Zircons from Hongtubu Basic Volcanic Rocks and Its Geological Significance in the East Segment of North Qilian Orogenic Belt, *Advances in Earth Science*, 22(2), 143-151(in Chinese with English abstract).
- Herzberg, C., 2004. Geodynamic Information in Peridotite Petrology. *Journal of Petrology* 45, 2507-2530.

- Hou, Q.Y., Zhao, Z.D., Zhang, H.F., Zhang, B.R., Chen, Y.L., 2006a. Indian ocean-MORB-type isotopic signature of Yushigou ophiolite in north Qilian Mountains and its implications. *Science in China (Series D)* 49(6), 561-572.
- Hou, Q.Y., Zhao, Z.D., Zhang, H.F., Zhang, B.R., Zhang, L., Chen, Y.L., 2006b. Discussion on the tectonic affinity of ancient oceanic mantle in Western Qinling-Songpan continental tectonic node, China: From elemental and Sr-Nd-Pb isotopic evidences, *Acta Petrologica Sinica* 22(12): 2901-2909.
- Hu, Y., Niu, Y., Li, J., Ye, L., Kong, J., Chen, S., Zhang, Y., Zhang, G., 2016. Petrogenesis and tectonic significance of the Late Triassic mafic dikes and felsic volcanic rocks in the East Kunlun Orogenic Belt, Northern Tibet Plateau. *Lithos* 245, 205-222.
- Ishii, T., Robinson, P.T., Maekawa, H., Fiske, R., 1992. Petrological Studies of Peridotites from Diapiric Serpentinite Seamounts in the Izu-Ogasawara-Mariana Forearc, Leg 125. 125, 445-486.
- Kamenetsky, V.S., Crawford, A.J., Meffre, S., 2001. Factors Controlling Chemistry of Magmatic Spinel: an Empirical Study of Associated Olivine, Cr-spinel and Melt Inclusions from Primitive Rocks. *Journal of Petrology* 42, 655-671.
- Kostopoulos, D.K., Murton, B.J., 1992. Origin and distribution of components in boninite genesis: significance of the OIB component. *Geological Society of London* 25, 133-154.
- Lan, V.D., S.R, Arculus, R.J, Pearce, J.A, Murton, B.J, 1992. Petrography, mineral chemistry and phase relations of the basement boninite series of Site 786, Izu-Bonin forearc. *Rheumatology* 125, 171-201.
- Langmuir, C.H., Bézos, A., Escrig, S., Parman, S.W., 2006. Chemical systematics and hydrous melting of the mantle in back-arc basins. *Geophysical Monograph* 166, 87-146.
- Lee, C.T.A., Brandon, A.D., Norman, M., 2003. Vanadium in peridotites as a proxy for paleo- f O₂ during partial melting ☆ : prospects, limitations, and implications. *Geochim. Cosmochim. Acta* 67, 3045-3064.
- Li, W. 2008. Geochronology and Geochemistry of the Ophiolites and Island-arc type Igneous Rocks in the Western Qinling Orogen and the Eastern Kunlun Orogen: Implication for the Evolution of the Tethyan Ocean. University of Science and Technology of China, Hefei. pp. 1-154.

- Li, X.H., Liu, Y., Li, Q.L., Guo, C.H., Chamberlain, K.R., 2009. Correction to "Precise determination of Phanerozoic zircon Pb/Pb age by multicollector SIMS without external standardization". *Geochemistry Geophysics Geosystems* 10, 573-575.
- Li, X.H., Tang, G.Q., Bing, G., Yang, Y.H., Hou, K.J., Hu, Z.C., Li, Q.L., Liu, Y., Li, W.X., 2013. Qinghu zircon: A working reference for micro beam analysis of U-Pb age and Hf and O isotopes. *China Science Bulletin*. 58, 4647-4654.
- Li, Y., Yang, J., Dilek, Y., Zhang, J., Pei, X., Chen, S., Xu, X., Li, J., 2015. Crustal architecture of the Shangdan suture zone in the early Paleozoic Qinling orogenic belt, China: Record of subduction initiation and backarc basin development. *Gondwana Research* 27, 733-744.
- Li, Y., Yang, J.S., Pei, X.Z., Zhang, J., Chen, J.L., 2012. A model for multi-stage of the Early Palaeozoic Danfeng ophiolite in Qinling orogen belt: From arc to inter-arc basin. *Acta Petrologica Sinica* 28, 1896-1914.
- Liu, L., Liao, X.Y., Zhang, C.L., Chen, D.L., Gong, X.K., Kang, L., 2013. Multi metamorphic timings of HP-UHP rocks in the North Qinling and their geological implications. *Acta Petrologica Sinica* 29, 1634–1656 (in Chinese with English abstract).
- Liu, L., Liao, X., Wang, Y., Wang, C., Santosh, M., Yang, M., Zhang, C., Chen, D., 2016. Early Paleozoic tectonic evolution of the North Qinling Orogenic Belt in Central China: Insights on continental deep subduction and multiphase exhumation. *Earth-Science Reviews*, 58-81.
- Lu, S.N., Li, H.K., Chen, Z.H., Hao, G.J., Zhou, H.Y., Guo, J.J., Niu, G.H., Xiang, Z.Q., 2003. Meso-Neoproterozoic Geological Evolution of the Qinling and Its Response to Rodinia Event. Geological Publishing House, Beijing, pp. 1–194 (in Chinese with English abstract).
- Ludwig, K. R., 2003. User's Manual for Isoplot 3.00: A Geochronological Toolkit for Microsoft Excel, Spec. Publ., vol. 4, Berkeley Geochronology Center, and Berkeley, Calif.
- Mao, X., Zhang, J., Yu, S., Li, Y., Yu, X., Lu, Z., 2017. Early Paleozoic granulite-facies metamorphism and anatexis in the northern West Qinling orogen: Monazite and zircon U-Pb geochronological constraints, *Science China Earth Sciences*, 60, 943-957.
- Meng, F., Cui, M., Wu, X., Ren, Y., 2015. Heishan mafic-ultramafic rocks in the Qimantag area of Eastern Kunlun, NW China: Remnants of an early Paleozoic incipient island arc. *Gondwana Research* 27, 745–759.

- Meng, F., Zhang, J., Cui, M., 2013. Discovery of Early Paleozoic eclogite from the East Kunlun, Western China and its tectonic significance. *Gondwana Research* 23, 825-836.
- Meng, Q., Zhang, G., 1999. Timing of collision of the North and South China blocks: Controversy and reconciliation. *Geology* 27, 123-126.
- Meng, Q., Zhang, G., 2000. Geologic framework and tectonic evolution of the Qinling orogen, central China. *Tectonophysics* 323, 183-196.
- Miyashiro, A., 1975. Classification, Characteristics, and Origin of Ophiolites. *The Journal of Geology* 83, 249-281.
- Mo, X., Luo, Z., Deng, J., Yu, X., Liu, C., Yuan, W., Bi, X., 2007. Granitoids and Crustal Growth in the East- Kunlun Orogenic Belt. *Geological Journal of China Universities* 13, 403-414.
- Murphy, J.B., Keppie, J.D., Nance, R.D., Dostal, J., 2010. Comparative evolution of the Iapetus and Rheic Oceans: A North America perspective. *Gondwana Research* 17, 482-499.
- Niu, Y., 1997. Mantle Melting and Melt Extraction Processes beneath Ocean Ridges: Evidence from Abyssal Peridotites. *Journal of Petrology* 38, 1047-1074.
- Niu, Y., Langmuir, C.H., Kinzler, R.J., 1997. The origin of abyssal peridotites: a new perspective. *Earth & Planetary Science Letters* 152, 251-265.
- Niu, Y., O'Hara, M.J., Pearce, J.A., 2003. Initiation of Subduction Zones as a Consequence of Lateral Compositional Buoyancy Contrast within the Lithosphere: a Petrological Perspective. *Journal of Petrology* 44, 764-778.
- Norman, M.D., Garcia, M.O., 1999. Primitive magmas and source characteristics of the Hawaiian plume: petrology and geochemistry of shield picrites. *Earth & Planetary Science Letters* 168, 27-44.
- Pagé, P., Bédard, J.H., Tremblay, A., 2009. Geochemical variations in a depleted fore-arc mantle: The Ordovician Thetford Mines Ophiolite. *Lithos* 113, 21-47.
- Parkinson, I.J., Pearce, J.A., 1998. Peridotites from the Izu–Bonin–Mariana Forearc (ODP Leg 125): Evidence for Mantle Melting and Melt–Mantle Interaction in a Supra-Subduction Zone Setting. *Journal of Petrology* 39, 1577-1618.
- Pearce, J.A., Laan, V.D., S.R, Arculus, R.J, Murton, B.J, Ishii, Peate, 1992. Boninite and harzburgite from ODP Leg 125 (Bonin-Mariana forearc): a case study of magma genesis during the initial

- stages of subduction. *Proceedings of the Ocean Drilling Program Scientific Results* 125, 623-659.
- Pearce, J.A., 2008. Geochemical fingerprinting of oceanic basalts with applications to ophiolite classification and the search for Archean oceanic crust. *Lithos* 100, 14-48.
- Pearce, J.A., Barker, P.F., Edwards, S.J., Parkinson, I.J., Leat, P.T., 2000. Geochemistry and tectonic significance of peridotites from the South Sandwich arc–basin system, South Atlantic. *Contributions to Mineralogy and Petrology* 139, 36-53.
- Pearce, T.H., Gorman, B.E., Birkett, T.C., 1977. The relationship between major element chemistry and tectonic environment of basic and intermediate volcanic rocks. *Earth & Planetary Science Letters* 36, 121-132.
- Pei, X., Ding, S., Hu, B., Li, Y., Zhang, G., Guo, J., 2004. Definition of the Guanzizhen ophiolite in Tianshui area, western Qinling, and its geological significance, *Regional Geology of China*, 23(12), 1202-1208(in Chinese with English abstract).
- Pei, X., Li, Y., Lu, S., Chen, Z., Ding, S., Hu, B., Li, Z., 2005. Zircons U-Pb ages of the Guanzizhen intermediate-basic igneous complex in Tianshui area, West Qinling, and their geological significance, *Regional Geology of China*.
- Pei, X., Liu, H., Ding, S., Li, Z., Hu, B., Sun, R., Hou, Y., 2006. Geochemical characteristics and tectonic significance of the meta-volcanic rocks in the Liziyan Group from Tianshui area, western Qinling orogen, *Geotectonica Et Metallogenica*, 30(2), 193-205(in Chinese with English abstract).
- Pei, X., Ding, S., Li, Z., Liu, Z., Li, G., Li, R., Wei F., 2007a. LA-ICP-MS Zircon U-Pb Dating of the Gabbro from the Guanzizhen Ophiolite in the Northern Margin of the Western Qinling and Its Geological Significance, *Acta Geological Sinica*, 81(11), 1550-1561.
- Pei, X., Liu, Z., Ding, S., Li, Z., Li, G., Li, R., Wang, F., Li, F., 2007b. Zircon LA-ICP-MS U-Pb Dating of the Gabbro from the Baihua Igneous Complex in Tianshui Area, Eastern Gansu, and Its Geological Significance, *Advances in Earth Science*, 22(8), 818-827 (in Chinese with English abstract).

- Pei, X., Sun, R., Ding, S., Liu, H., Li, Z., Liu, Z., Meng, Y., 2007c. LA-ICP-MS zircon U-Pb dating of the Yanjiadian diorite in the eastern Qilian Mountains and its geological significance, *Geology in China*, 34(1), 8-16 (in Chinese with English abstract).
- Pei, X., Ding, S., Li, Z., Liu, Z., Li, R., Feng, J., Sun, Y., Zhang, Y., Zhang, X., Chen, G., 2009. Early Paleozoic Tianshui-Wushan tectonic zone of the northern margin of west Qinling and its tectonic evolution, *Acta Geological Sinica*, 83(11), 1547-1564.
- Puchtel, I.S., Hofmann, A.W., Mezger, K., Jochum, K.P., Shchipansky, A.A., Samsonov, A.V., 1998. Oceanic plateau model for continental crustal growth in the Archaean: A case study from the Kostomuksha greenstone belt, NW Baltic Shield. *Earth & Planetary Science Letters* 155, 57-74.
- Qi, S.S., Song, S.G., Shi, L.C., Cai, H.J., Hu, J.C., 2014. Discovery and its geological significance of Early Paleozoic edogite in Xiarihamu-Suhaitu area, western part of the East Kunlun. *Acta Petrologica Sinica* 30, 3345-3356.
- Raumer, J.F.V., Stampfli, G.M., 2008. The birth of the Rheic Ocean - Early Palaeozoic subsidence patterns and subsequent tectonic plate scenarios. *Tectonophysics* 461, 9-20.
- Reagan, M.K., Ishizuka, O., Stern, R.J., Kelley, K.A., Ohara, Y., Blichert-Toft, J., Bloomer, S.H., Cash, J., Fryer, P., Hanan, B.B., 2010. Fore-arc basalts and subduction initiation in the Izu-Bonin-Mariana system. *Geochemistry Geophysics Geosystems* 11, 427-428.
- Regelous, M., Collerson, K.D., Ewart, A., Wendt, J.I., 1997. Trace element transport rates in subduction zones: evidence from Th, Sr and Pb isotope data for Tonga-Kermadec arc lavas. *Earth & Planetary Science Letters* 150, 291-302.
- Sláma, J., Košler, J., Condon, D.J., Crowley, J.L., Gerdes, A., Hanchar, J.M., Horstwood, M.S.A., Morris, G.A., Nasdala, L., Norberg, N., 2008. Plešovice zircon - A new natural reference material for U-Pb and Hf isotopic microanalysis. *Chemical Geology* 249, 1-35.
- Song, S.G., Niu, Y.L., Su, L., Zhang, C., Zhang, L.F., 2014. Continental orogenesis from ocean subduction, continent collision/subduction, to orogen collapse, and orogen recycling: the example of the North Qaidam UHPM belt, NW China. *Earth-Science Reviews* 129, 59-84.
- Song, S., Niu, Y., Su, L., Xia, X., 2013. Tectonics of the North Qilian orogen, NW China. *Gondwana Research* 23, 1378-1401.

- Song, S., Su, L., Li, X., Niu, Y., Zhang, L., 2012. Grenville-age orogenesis in the Qaidam-Qilian block: The link between South China and Tarim. *Precambrian Research* 220-221, 9-22.
- Song, S., Niu, Y., Wei, C., Ji, J., Su, L., 2010. Metamorphism, anatexis, zircon ages and tectonic evolution of the Gongshan block in the northern Indochina continent—An eastern extension of the Lhasa Block. *Lithos* 120, 327-346.
- Song, S., Su, L., Niu, Y., Zhang, G., Zhang, L., 2009. Two types of peridotite in North Qaidam UHPM belt and their tectonic implications for oceanic and continental subduction: A review. *Journal of Asian Earth Sciences* 35, 285-297.
- Song, S.G., Wang, M.M., Xu, X., Wang, C., Niu, Y.L., Allen, M.B., Su, L., 2015. Ophiolites in the Xing'an-Inner Mongolia accretionary belt of the CAOB: Implications for two cycles of seafloor spreading and accretionary orogenic events. *Tectonics* 34, 2221-2248.
- Song, S.G., Zhang, L.F., Niu, Y.L., Su, L., Song, B.A., Liu, D.Y., 2006. Evolution from oceanic subduction to continental collision: a case study from the Northern Tibetan Plateau based on geochemical and geochronological data. *Journal of Petrology* 47, 435-455.
- Song, S.G., Yang, L.M., Zhang, Y.Q., Niu, Y.L., Wang, C., Su, L., Gao, Y.L., 2017. Qi-Qin Accretionary Belt in Central China Orogen: accretion by trench jam of oceanic plateau and formation of intra-oceanic arc in the Early Paleozoic Qin-Qi-Kun Ocean. *Science Bulletin* 62, 1035-1038.
- Stern, R.J., 2004. Subduction initiation: spontaneous and induced. *Earth & Planetary Science Letters* 226, 275-292.
- Stern, R.J., 2010. The anatomy and ontogeny of modern intra-oceanic arc systems. *Geological Society London Special Publications* 338, 7-34.
- Su, L., Song, S.G., Song, B., Zhou, D.W., Hao, J.R., 2004. The SHRIMP zircon U-Pb ages of the garnet pyroxenite and Fushui complex from Songshugou area and its constrain on the tectonic evolution of Qinling orogenic belt. *Chinese Science Bulletin* 49, 1209-1211 (in Chinese).
- Sun, S.S., McDonough, W.F., 1989. Chemical and isotopic systematics of oceanic basalts: implications for mantle composition and processes. *Geological Society London Special Publications* 42, 313-345.

- Takahashi, E., Uto, K., Schiling, J.G., 1987. Primary magma compositions and Mg/Fe ratios of their mantle residues along Mid Atlantic Ridge 29°N to 73°N. Technical Reports ISEI, pp. 1-4.
- Tseng, C.Y., Yang, H.J., Yang, H.Y., Liu, D., Wu, C., Cheng, C.K., Chen, C.H., Ker, C.M., 2009. Continuity of the North Qilian and North Qinling orogenic belts, Central Orogenic System of China: Evidence from newly discovered Paleozoic adakitic rocks. *Gondwana Research* 16, 285-293.
- Uysal, I., Ersoy, E.Y., Dilek, Y., Escayola, M., Sarıfakioğlu, E., Saka, S., Hirata, T., 2015. Depletion and refertilization of the Tethyan oceanic upper mantle as revealed by the early Jurassic Refahiye ophiolite, NE Anatolia—Turkey. *Gondwana Research* 27, 594-611.
- Wang, T., Wang, X.X., Tian, W., Zhang, C.L., Li, W.P., Li, S., 2009. North Qinling Paleozoic granite associations and their variation in space and time: implications for orogenic processes in the orogens of central China. *Science in China (Series D)* 52, 1359–1384.
- Wei, F., Pei, X., Li, R., Li, Z., Pei, L., Gao, J., Wang, Y., Liu, C., Wu, S., Chen, Y., 2012. LA-ICP-MS zircon U-Pb dating of Early Paleozoic Huangmenchuan granodiorite in Tianshui area of Gansu Province and its tectonic significance, *Geological Bulletin of China*, 31(9), 1496-1509 (in Chinese with English abstract).
- Whattam, S.A., Stern, R.J., 2011. The ‘subduction initiation rule’: a key for linking ophiolites, intra-oceanic forearcs, and subduction initiation. *Contributions to Mineralogy & Petrology* 162, 1031-1045.
- White, W.M., Duncan, R.A., 1996. Geochemistry and geochronology of the Society Islands: New evidence for deep mantle recycling.
- Wiedenbeck, M., Allé, P., Corfu, F., Griffin, W.L., Meier, M., Oberli, F., Quadt, A.V., Roddick, J.C., Spiegel, W., 1995. Three natural zircon standard for U-Th-Pb, Lu-Hf, trace element and REE analysis. *Geostandards & Geoanalytical Research* 19, 1-23.
- Wilson, M., 1986. A Chemical Classification of Volcanic Rocks Based on the Total Alkali-Silica Diagram. *Journal of Petrology* 27, 745-750.
- Wood, D.A., 1980. The application of a Th Hf Ta diagram to problems of tectonomagmatic classification and to establishing the nature of crustal contamination of basaltic lavas of the British Tertiary Volcanic Province. *Earth & Planetary Science Letters* 50, 11-30.

- Wu, Y., Zheng, Y., 2013. Tectonic evolution of a composite collision orogen: An overview on the Qinling–Tongbai–Hong'an–Dabie–Sulu orogenic belt in central China. *Gondwana Research* 23, 1402–1428.
- Xia, X., Song, S., Niu, Y., 2012. Tholeiite–Boninite terrane in the North Qilian suture zone: Implications for subduction initiation and back-arc basin development. *Chemical Geology* 328, 259–277.
- Xu, X., Song, S., Allen, M.B., Ernst, R.E., Niu, Y., Su, L., 2016. An 850–820 Ma LIP dismembered during breakup of the Rodinia supercontinent and destroyed by Early Paleozoic continental subduction in the northern Tibetan Plateau, NW China. *Precambrian Research* 282, 52–73.
- Xu, X., Song, S., Su, L., Li, Z., Niu, Y., Allen, M.B., 2015. The 600–580 Ma continental rift basalts in North Qilian Shan, northwest China: Links between the Qilian-Qaidam block and SE Australia, and the reconstruction of East Gondwana. *Precambrian Research* 257, 47–64.
- Yang, J., Liu, F., Wu, C., Xu, Z., Shi, R., Chen, S., Deloule, E., Wooden, J.L., 2003. Two Ultrahigh-Pressure Metamorphic Events Recognized in the Central Orogenic Belt of China: Evidence from the U-Pb Dating of Coesite-Bearing Zircons. *Acta Geologica Sinica* 47, 327–343.
- Yang, H., Zhang, H., Luo, B., Zhang, J., Xiong, Z., Guo, L., Pan, F., 2015. Early Paleozoic intrusive rocks from the eastern Qilian orogen, NE Tibetan Plateau: Petrogenesis and tectonic significance. *Lithos* 224–225, 13–31.
- Yang, H., Zhang, H., Luo, B., Gao, Z., Guo, L., Xu, W., 2016. Generation of peraluminous granitic magma in a post-collisional setting: A case study from the eastern Qilian orogen, NE Tibetan Plateau. *Gondwana Research* 36, 28–45.
- Yang, W., Q. Deng, and X. Wu 2002. Major characteristics of the Lajishan Orogenic Belt of the South Qilian Mountains and its geotectonic attribute. *Acta Geological Sinica*, 76(1), 110-117.
- Zhang, H.F., Zhang, B.R., Harries, N., Zhang, L., Chen, Y.L., Chen, N.S., Zhao, Z.D., 2006. U–Pb zircon SHRIMP ages, geochemical and Sr–Nd–Pb isotopic compositions of intrusive rocks from the Longshan–Tianshui area in the southeast corner of the Qilian orogenic belt, China: Constraints on petrogenesis and tectonic affinity. *Journal of Asian Earth Sciences*, 27(6): 751–764.

- Zhang, C.L., Liu, L., Wang, T., Wang, X.X., Li, L., Gong, Q.F., Li, X.F., 2013. Granitic magmatism related to early Paleozoic continental collision in North Qinling. *Chinese Science Bulletin* 58, 1–7.
- Zhang, J.X., Yang, J.S., Mattinson, C.G., Xu, Z.Q., Meng, F.C., Shi, R.D., 2005. Two contrasting eclogite cooling histories, North Qaidam HP/UHP terrane, western China: petrological and isotopic constraints. *Lithos* 84, 51–76.
- Zhang, J.X., Meng, F.C., Wan, Y.S., 2007. A cold Early Palaeozoic subduction zone in the North Qilian Mountains, NW China: petrological and U-Pb geochronological constraints. *Journal of Metamorphic Geology* 25, 285–304.
- Zhang, J.X., Mattinson, C.G., Meng, F.C., Yang, H.J., Wan, Y.S., 2009. U-Pb geochronology of paragneisses and metabasite in the Xitieshan area, north Qaidam Mountains, western China: constraints on the exhumation of HP/UHP metamorphic rocks. *Journal of Asian Earth Sciences* 35, 245–258.
- Zhang, J.X., Yu, S.Y., Meng, F.C., 2011. Ployphase Early Paleozoic metamorphism in the northern Qinling orogenic belt. *Acta Petrologica Sinica* 27, 1179–1190.
- Zhang, Y., Song, S., Yang, L., Su, L., Niu, Y., Allen, M.B., Xu, X., 2017. Basalts and picrites from a plume-type ophiolite in the South Qilian Accretionary Belt, Qilian Orogen: Accretion of a Cambrian Oceanic Plateau? *Lithos* 278–281, 97–110.
- Zhang, Z., Liu, D., Fu, G. 1994. Isotopic Geochronology of Metamorphic Strata in North Qinling, China, pp. 1-191, Geological Publishing House, Beijing.
- Zhou, M., Robinson, P.T., Malpas, J., Zijin, L.I., 1996. Podiform Chromitites in the Luobusa Ophiolite (Southern Tibet): Implications for Melt-Rock Interaction and Chromite Segregation in the Upper Mantle. *Journal of Petrology* 37, 3-21.
- Zhu, D.C., Mo, X.X., Wang, L.Q., Zhao, Z.D., Liao, Z.L., 2008. Hotspot-ridge interaction for the evolution of Neo-Tethys: Insights from the Late Jurassic-Early Cretaceous magmatism in southern Tibet. *Acta Petrologica Sinica* 24, 225-237.
- Zhu, Y., Lin, Q., Jia, C., Wang, G., 2006. SHRIMP zircon U-Pb age and significance of Early Paleozoic volcanic rocks in East Kunlun orogenic belt, Qinghai Province, China. *Science China Earth Sciences* 49, 88-96.

Zimmer, M., Kröner, A., Jochum, K.P., Reischmann, T., Todt, W., 1995. The Gabal Gerf complex: A Precambrian N-MORB ophiolite in the Nubian Shield, NE Africa. *Chemical Geology* 123, 29-51.

Zindler, A., And, Hart, S., 1986. Chemical Geodynamics. *Annual Review of Earth & Planetary Sciences* 14, 493-571.

ACCEPTED MANUSCRIPT

Figure captions

Fig. 1. (a) Sketch map of the Qinling-Qilian-Kunlun orogenic belt showing the spatial stretch of the Qi(lian)-Qin(ling) Accretionary belt. CAOB: Central Asian Orogenic belt; QB: Qaidam Block. (b) Geological map of the Tianshui-Wushan Accretionary Belt (simplified after Pei et al., 2009). (c) Cross-section of the Tianshui area.

Fig. 2. Field photos of the Wushan-Guanzizhen terrane. (a) Deformed pillow lavas; (b) Thin layers of metamorphic pelagic chert; (c) Deformed cumulate gabbro; (d) Marble slice; (e) Massive lavas.

Fig. 3. Microphotographs showing textures of samples from the TWAB. (a): Porphyritic texture and a clinopyroxene phenocryst in boninite (TS14-28); (b): Backscattered electron image of original Cr-spinel in boninite (TS14-28). (c): The olivine and pyroxene of peridotite have mostly metamorphosed to serpentine (TS15-54); (d): Backscattered electron image of original Cr-spinel in serpentinized peridotite (TS14-37).

Fig. 4. The compositions of olivine and spinel in boninites and peridotites. (a) NiO (wt. %) vs. Fo contents for olivine. The compositional fields of olivine in abyssal and forearc peridotite are from Dick (1989) and Ishii et al. (1992), respectively. Compositions of mantle olivine are also shown (Mantle Olivine Array) (Takahashi et al., 1987). (b) Cr# ($\text{Cr}/(\text{Cr} + \text{Al})$) for spinel vs. Fo contents for olivine. OSMA is the olivine–spinel mantle array as proposed by Arai (1994). (c) Cr# ($\text{Cr}/(\text{Cr} + \text{Al})$) vs. $\text{Fe}^{2+}/$

($\text{Fe}^{2+} + \text{Mg}$) for spinels. The compositional fields of spinel in mid-ocean ridge (MOR) peridotite, supra-subduction zone (SSZ) peridotite and boninite were from Dick and Bullen (1984), Ishii et al. (1992), and van der Lan et al. (1992), respectively. (d) Spinel Fe^{3+} -Cr-Al ternary diagram. The light blue shading regions represent 90% of the entire terrestrial spinel data points, respectively. The light yellow shading regions and heavy dashed line enclose 90% and 50% of the entire spinel data points from boninite, respectively (Barnes and Roger, 2001).

Fig. 5. Discrimination diagrams for lavas from the TWAB. (a) TAS diagram; (b) FeO/MgO - SiO_2 diagram; (c) AFM diagram; (d) Hf/3-Th-Ta diagram; (e) Cr-Y diagram; (f) Ti-V diagram.

Fig. 6. Chondrite-normalized REE pattern (a, c e and g) and PM normalized multi-elements pattern (b, d f and h) for three types of samples respectively. Values of primitive mantle, N-MORB and E-MORB are from Sun and McDonough, (1989).

Fig. 7. Primitive mantle-normalized REE patterns for serpentinized peridotite (modified after Uysal et al., 2015). Fields for Izu-Bonin-Mariana (IBM) fore arc peridotite are from Parkinson and Pearce. (1998) and abyssal peridotite are from Niu et al., (1997).

Fig. 8. Sr-Nd isotopic compositions of the various rocks from the WGAB. Average N-MORB values are from Zimmer et al. (1995). OIB and BSE values are from Zindler

(1986) and White and Duncan, (1996). Data of Guanzizhen-Wushan ophiolite are from Hou et al. (2006b).

Fig.9. Cathodoluminescence images of representative zircons for gabbro, serpentinized peridotite and island arc volcanic.

Fig.10. Concordia diagrams of zircon SIMS and LA-ICP-MS analyses for gabbro, serpentinized peridotite and island arc volcanic (a-e). (f) Distribution of zircon U-Pb ages from TWAB. Data are from Pei et al., 2005, 2007a, b and c; Li, 2008 and this study.

Fig.11. Discrimination diagrams for the mantle source enrichment of oceanic basalt from the TWAB and the adjacent Lajishan accretionary belt. (a) Primitive mantle-normalized $(\text{Nb}/\text{Th})_{\text{N}}$ vs. $(\text{Nb}/\text{La})_{\text{N}}$ diagram. Normalization values are from Sun and McDonough (1989). The field of recent oceanic plateau, MORB and island arc tholeiites are from Puchtel et al. (1998). (b) Nb/Yb versus Th/Yb diagram (Pearce, 2008). (c) Zr/Nb versus δNb diagram. The mantle plume and hotspot field with Zr/Nb ratio <10 and $\delta\text{Nb} > 0$; the depleted mantle field with Zr/Nb ratio >30 and $\delta\text{Nb} < 0$ (Zhu et al., 2008; Fitton et al., 1997); The values of N-MORB, E-MORB and OIB are from Sun and McDonough. (1989). (d) Ce versus Ce/Ta systematics (Kostopoulos and Murton, 1992). The oceanic basalt samples from different ophiolites: Lajishan-Yongjing ophiolite, the rock type include sub-alkaline basalts (E-MORB affinity), alkaline basalts (OIB features) and picrites (Zhang et al., 2017); Wushan ophiolite (Dong et al., 2007; Hou et al., 2006b); Guanzizhen ophiolite (Dong et al., 2008; this study).

Fig. 12. Diagrams for the island arc volcanic complex. (a) U/Th versus $(La/Sm)_N$ diagram. It appears most probable that uranium is enriched by addition of an oxidizing aqueous fluids, which is derived from the dehydration of minerals in the subduction slab (Brenan et al., 1995; Elliott et al., 1997). Fluid addition of uranium can increase U/Th ratios into the range observed in island arcs, on the contrary, melts addition can decrease U/Th ratios into the range because of the influx of thorium because U can become hexavalent and so may prefer partition into aqueous fluids relative to Th in more oxidizing conditions. (b) Ba/Nb versus $(La/Sm)_N$ (Langmuir et al., 2006). (c) Ce versus Ce/Ta diagram. Melts from unmodified depleted sources would have virtually unfractionated Ce/Ta ratios (i.e. 42 ± 5) and low Ce abundances (i.e. 0.2-2 ppm). Melts from depleted sources metasomatized by sediment melts would have both high Ce and Ce/Ta ratio values, whereas melts from depleted sources metamorphosed by mantle melts would have high Ce concentrations and unfractionated (i.e. MORB-like) to low (OIB-like) Ce/Ta ratios (Kostopoulos and Murton, 1992). SED: Sediment melts; SZF: Subduction Zone Fluids. (d) Nb/Yb versus Th/Yb diagram (Pearce, 2008).

Fig. 13. Melting models for the serpentinized peridotite (modified after Uysal et al., 2015 and reference therein). (a) La/Yb versus Yb (ppm) diagram showing the melting over an open-system dynamic melting model. (b) Ni/Yb ($\times 1000$) versus Yb (ppm) diagram showing the second-stage partial melting models. PM=Primitive mantle; (Φ) = critical melt porosity; (β) = mass flux rate; Flux material: SZC=subduction zone component.

Fig. 14. Schematic model for the tectono-magmatic evolution of the TWAB.

Table 1. Compositions of olivine in harzburgite from the Wushan-Tianshui terrane.

sa	T5																
Si	40	41	40	40	40	41	41	41	40	40	40	41	41	41	40	40	39
Ti	0.0	0.0	0.0	0.0	0.0	0.0	0.0	0.0	0.0	0.0	0.0	0.0	0.0	0.0	0.0	0.0	0.0
Al	0.0	0.0	0.0	0.0	0.0	0.0	0.0	0.0	0.0	0.0	0.0	0.0	0.0	0.0	0.0	0.0	0.0
Cr	0.0	0.0	0.0	0.0	0.0	0.0	0.0	0.0	0.0	0.0	0.0	0.0	0.0	0.0	0.0	0.0	0.0
Fe	8.8	8.4	8.1	8.0	8.2	8.3	8.6	7.6	7.7	7.8	8.4	8.4	8.9	8.7	8.6	8.8	
M	0.1	0.1	0.1	0.1	0.1	0.1	0.1	0.1	0.1	0.1	0.1	0.1	0.1	0.1	0.1	0.1	0.1
Ni	0.4	0.3	0.3	0.3	0.4	0.3	0.4	0.3	0.3	0.3	0.3	0.3	0.3	0.4	0.3	0.3	0.3
M	50.	51.	51.	50.	50.	50.	47.	50.	50.	50.	51.	51.	50.	49.	50.	50.	
Ca	0.0	0.0	0.0	0.0	0.0	0.0	0.0	0.0	0.0	0.0	0.0	0.0	0.0	0.0	0.0	0.0	0.0
Na	0.0	0.0	0.0	0.0	0.0	0.0	0.0	0.0	0.0	0.0	0.0	0.0	0.0	0.0	0.0	0.0	0.0
K ₂	0.0	0.0	0.0	0.0	0.0	0.0	0.0	0.0	0.0	0.0	0.0	0.0	0.0	0.0	0.0	0.0	0.0
To	10	10	10	99.	10	10	98.	10	10	10	10	10	10	10	10	10	99.
Calculation based on 4 Oxygen																	
Si	0.9	0.9	0.9	1.0	0.9	1.0	1.0	1.0	0.9	0.9	0.9	0.9	0.9	1.0	1.0	0.9	0.9
Ti	0.0	0.0	0.0	0.0	0.0	0.0	0.0	0.0	0.0	0.0	0.0	0.0	0.0	0.0	0.0	0.0	0.0
Al	0.0	0.0	0.0	0.0	0.0	0.0	0.0	0.0	0.0	0.0	0.0	0.0	0.0	0.0	0.0	0.0	0.0
Cr	0.0	0.0	0.0	0.0	0.0	0.0	0.0	0.0	0.0	0.0	0.0	0.0	0.0	0.0	0.0	0.0	0.0
Fe	0.1	0.1	0.1	0.1	0.1	0.1	0.1	0.1	0.1	0.1	0.1	0.1	0.1	0.1	0.1	0.1	0.1
M	0.0	0.0	0.0	0.0	0.0	0.0	0.0	0.0	0.0	0.0	0.0	0.0	0.0	0.0	0.0	0.0	0.0
Ni	0.0	0.0	0.0	0.0	0.0	0.0	0.0	0.0	0.0	0.0	0.0	0.0	0.0	0.0	0.0	0.0	0.0
M	1.8	1.8	1.8	1.8	1.8	1.8	1.7	1.8	1.8	1.8	1.8	1.8	1.8	1.8	1.8	1.8	1.8
Ca	0.0	0.0	0.0	0.0	0.0	0.0	0.0	0.0	0.0	0.0	0.0	0.0	0.0	0.0	0.0	0.0	0.0
Na	0.0	0.0	0.0	0.0	0.0	0.0	0.0	0.0	0.0	0.0	0.0	0.0	0.0	0.0	0.0	0.0	0.0
K	0.0	0.0	0.0	0.0	0.0	0.0	0.0	0.0	0.0	0.0	0.0	0.0	0.0	0.0	0.0	0.0	0.0
M	91	91	91	91	91	91	90	92	92	92	91	91	90	91	91	91	91

Table 1. Continued

Al	0.0	0.0	0.0	0.0	0.0	0.0	0.0	0.0	0.0	0.0	0.0	0.0	0.0	0.0	0.0	0.0
Cr	0.0	0.0	0.0	0.0	0.0	0.0	0.0	0.0	0.0	0.0	0.0	0.0	0.0	0.0	0.0	0.0
Fe	0.1	0.1	0.1	0.1	0.1	0.1	0.1	0.1	0.1	0.1	0.1	0.1	0.1	0.1	0.1	0.1
M	0.0	0.0	0.0	0.0	0.0	0.0	0.0	0.0	0.0	0.0	0.0	0.0	0.0	0.0	0.0	0.0
Ni	0.0	0.0	0.0	0.0	0.0	0.0	0.0	0.0	0.0	0.0	0.0	0.0	0.0	0.0	0.0	0.0
M	1.8	1.8	1.8	1.8	1.8	1.8	1.8	1.8	1.8	1.8	1.8	1.8	1.8	1.8	1.8	1.8
Ca	0.0	0.0	0.0	0.0	0.0	0.0	0.0	0.0	0.0	0.0	0.0	0.0	0.0	0.0	0.0	0.0
Na	0.0	0.0	0.0	0.0	0.0	0.0	0.0	0.0	0.0	0.0	0.0	0.0	0.0	0.0	0.0	0.0
K	0.0	0.0	0.0	0.0	0.0	0.0	0.0	0.0	0.0	0.0	0.0	0.0	0.0	0.0	0.0	0.0
M	91	91	91	90	91	91	90	91	90	91	91	91	91	91	91	91

Table 2. Compositions of spinel and chromite in harzburgite (TS34) and boninite (TS37, TS53, TS54) from the Wushan-Tianshui terrane.

Sa	TS3															
Si	0.0	0.0	0.0	0.0	0.0	0.0	0.0	0.0	0.0	0.0	0.0	0.0	0.0	0.0	0.0	0.0
Ti	0.4	0.2	0.4	0.4	0.4	0.1	0.1	0.2	0.5	0.3	0.5	0.4	0.4	0.0	0.0	0.5
Al ₂	8.5	9.8	8.7	10.	10.	10.	10.	11.	10.	12.	9.3	8.4	9.6	11.	11.	
Cr ₂	53.	49.	53.	51.	50.	52.	52.	51.	50.	47.	53.	53.	52.	50.	49.	
Fe	31.	33.	32.	32.	31.	30.	30.	31.	32.	32.	31.	31.	30.	29.	31.	
Mn	2.6	2.8	2.8	2.3	2.2	0.8	0.9	1.1	2.3	1.7	2.4	2.5	1.9	0.7	1.9	
Ni	0.0	0.0	0.0	0.1	0.0	0.0	0.0	0.0	0.1	0.1	0.1	0.0	0.0	0.0	0.0	0.0
Mg _#	1.9	1.6	1.7	2.7	2.9	5.2	5.4	4.9	2.9	4.0	2.4	1.9	3.3	5.5	3.5	
Ca	0.0	0.0	0.0	0.0	0.0	0.0	0.0	0.0	0.0	0.0	0.0	0.0	0.0	0.0	0.0	
Na	0.0	0.1	0.0	0.0	0.0	0.0	0.0	0.0	0.0	0.0	0.0	0.0	0.0	0.0	0.0	
K ₂	0.0	0.0	0.0	0.0	0.0	0.0	0.0	0.0	0.0	0.0	0.0	0.0	0.0	0.0	0.0	
Tot	98.	98.	99.	99.	98.	99.	99.	99.	99.	99.	100	98.	98.	98.	99.	
Si	0.0	0.0	0.0	0.0	0.0	0.0	0.0	0.0	0.0	0.0	0.0	0.0	0.0	0.0	0.0	0.0
Ti	0.0	0.0	0.0	0.0	0.0	0.0	0.0	0.0	0.0	0.0	0.0	0.0	0.0	0.0	0.0	0.0
Al	0.3	0.4	0.3	0.4	0.4	0.4	0.4	0.4	0.4	0.5	0.3	0.3	0.4	0.4	0.4	0.4
Cr	1.5	1.3	1.5	1.4	1.4	1.4	1.4	1.3	1.3	1.2	1.4	1.5	1.4	1.3	1.3	
Fe ²	0.8	0.8	0.8	0.7	0.7	0.7	0.7	0.7	0.7	0.7	0.8	0.8	0.7	0.6	0.7	
Fe ³	0.1	0.1	0.1	0.1	0.1	0.1	0.1	0.1	0.1	0.1	0.1	0.1	0.1	0.1	0.1	
Mn	0.0	0.0	0.0	0.0	0.0	0.0	0.0	0.0	0.0	0.0	0.0	0.0	0.0	0.0	0.0	
Ni	0.0	0.0	0.0	0.0	0.0	0.0	0.0	0.0	0.0	0.0	0.0	0.0	0.0	0.0	0.0	
Mg _#	0.1	0.0	0.0	0.1	0.1	0.2	0.2	0.2	0.1	0.2	0.1	0.1	0.1	0.2	0.1	
Ca	0.0	0.0	0.0	0.0	0.0	0.0	0.0	0.0	0.0	0.0	0.0	0.0	0.0	0.0	0.0	
Na	0.0	0.0	0.0	0.0	0.0	0.0	0.0	0.0	0.0	0.0	0.0	0.0	0.0	0.0	0.0	
K	0.0	0.0	0.0	0.0	0.0	0.0	0.0	0.0	0.0	0.0	0.0	0.0	0.0	0.0	0.0	
Mg _#	10.	7.9	8.6	13.	14.	23.	24.	22.	13.	18.	12.	9.9	16.	25.	16.	
Cr	80.	77.	80.	77.	76.	77.	77.	75.	75.	71.	79.	80.	78.	74.	73.	
Fe ²	0.8	0.9	0.9	0.8	0.8	0.7	0.7	0.7	0.8	0.7	0.8	0.8	0.8	0.7	0.8	
Fe ³	0.0	0.0	0.0	0.0	0.0	0.0	0.0	0.0	0.0	0.0	0.0	0.0	0.0	0.0	0.0	

Note: Mg# = Mg/ (Mg+ Fe²⁺); Cr# = Cr/ (Cr+ Al+ Fe³⁺); Fe²⁺# = Fe²⁺/ (Fe²⁺ + Mg); Fe3+# = Fe³⁺/(Fe³⁺ + Cr + Al)

Table 2. Continued

Sa	TS															
Si	0.0	0.0	0.0	0.0	0.0	0.0	0.0	0.0	0.0	0.0	0.0	0.0	0.0	0.0	0.0	0.0
Ti	0.0	0.0	0.0	0.0	0.0	0.0	0.0	0.0	0.0	0.0	0.0	0.0	0.0	0.0	0.0	0.0
Al	0.0	0.0	0.0	5.1	0.0	7.6	12.	11.	0.0	11.	0.2	11.	0.0	0.0	1.5	0.0
Cr	9.3	7.9	5.7	51.	9.1	52.	53.	52.	7.2	52.	38.	54.	20.	26.	48.	8.1
Fe	78.	79.	82.	29.	77.	26.	23.	22.	79.	24.	46.	22.	65.	60.	36.	80.
M	1.3	1.1	0.7	2.8	1.1	2.3	0.9	1.6	0.8	0.8	2.8	1.4	2.1	2.4	3.2	1.2
Ni	1.1	1.2	1.1	0.1	1.4	0.1	0.0	0.0	1.1	0.0	0.5	0.1	1.1	0.9	0.1	1.2
M	3.1	3.0	2.6	8.4	3.3	9.7	9.0	9.8	2.9	8.0	6.5	9.9	4.5	4.9	7.1	2.7
Ca	0.0	0.0	0.0	0.0	0.0	0.0	0.0	0.0	0.0	0.0	0.0	0.0	0.0	0.0	0.0	0.0
Na	0.0	0.0	0.0	0.0	0.0	0.0	0.0	0.0	0.0	0.0	0.0	0.0	0.0	0.0	0.0	0.0
K ₂	0.0	0.0	0.0	0.0	0.0	0.0	0.0	0.0	0.0	0.0	0.0	0.0	0.0	0.0	0.0	0.0
To	93.	92.	92.	97.	92.	99.	99.	98.	91.	98.	95.	99.	94.	94.	97.	93.

Si	0.0	0.0	0.0	0.0	0.0	0.0	0.0	0.0	0.0	0.0	0.0	0.0	0.0	0.0	0.0	0.0	0.0
Ti	0.0	0.0	0.0	0.0	0.0	0.0	0.0	0.0	0.0	0.0	0.0	0.0	0.0	0.0	0.0	0.0	0.0
Al	0.0	0.0	0.0	0.2	0.0	0.3	0.5	0.4	0.0	0.4	0.0	0.4	0.0	0.0	0.0	0.0	0.0
Cr	0.2	0.2	0.1	1.4	0.2	1.4	1.3	1.3	0.2	1.4	1.1	1.4	0.6	0.7	1.3	0.2	
Fe	0.7	0.7	0.7	0.4	0.7	0.4	0.5	0.4	0.7	0.5	0.5	0.4	0.6	0.6	0.5	0.7	
Fe	1.7	1.7	1.8	0.3	1.7	0.3	0.1	0.1	1.7	0.1	0.8	0.1	1.4	1.2	0.5	1.7	
M	0.0	0.0	0.0	0.0	0.0	0.0	0.0	0.0	0.0	0.0	0.0	0.0	0.0	0.0	0.1	0.0	
Ni	0.0	0.0	0.0	0.0	0.0	0.0	0.0	0.0	0.0	0.0	0.0	0.0	0.0	0.0	0.0	0.0	
M	0.1	0.1	0.1	0.4	0.1	0.4	0.4	0.4	0.1	0.4	0.3	0.4	0.2	0.2	0.3	0.1	
Ca	0.0	0.0	0.0	0.0	0.0	0.0	0.0	0.0	0.0	0.0	0.0	0.0	0.0	0.0	0.0	0.0	
Na	0.0	0.0	0.0	0.0	0.0	0.0	0.0	0.0	0.0	0.0	0.0	0.0	0.0	0.0	0.0	0.0	
K	0.0	0.0	0.0	0.0	0.0	0.0	0.0	0.0	0.0	0.0	0.0	0.0	0.0	0.0	0.0	0.0	
M	6.6	6.4	5.3	33.	7.1	39.	41.	43.	6.2	36.	20.	44.	10.	12.	25.	5.7	
Cr	99.	100	100	87.	100	82.	73.	75.	100	75.	98.	76.	99.	99.	95.	100	
Fe	0.8	0.8	0.8	0.5	0.8	0.4	0.5	0.4	0.8	0.5	0.6	0.4	0.7	0.7	0.5	0.8	
Fe	0.8	0.8	0.9	0.1	0.8	0.1	0.0	0.0	0.8	0.0	0.4	0.0	0.7	0.6	0.2	0.8	

Table 2. Continued

Sa	T5																
Si	0.1	0.0	0.0	0.0	0.0	0.0	0.0	0.0	0.0	0.0	0.0	0.0	0.0	0.0	0.1	0.0	
Ti	0.3	0.3	0.2	0.2	0.0	0.2	0.3	0.3	0.3	0.2	0.2	0.5	0.3	0.3	0.4	0.4	
Al ₂	5.8	5.6	5.6	5.7	1.8	5.9	5.5	0.0	6.2	6.0	1.6	5.7	5.9	6.3	6.5	7.9	7.7
Cr ₂	59.	59.	60.	60.	58.	60.	58.	25.	60.	60.	57.	58.	60.	60.	60.	59.	59.
Fe	27.	28.	27.	26.	34.	28.	28.	64.	26.	27.	34.	27.	27.	27.	26.	25.	25.
M	0.6	0.6	0.6	0.7	1.0	0.6	0.6	0.6	0.6	0.6	0.9	0.6	0.6	0.5	0.6	0.5	0.5
Ni	0.1	0.1	0.0	0.0	0.0	0.0	0.0	1.0	0.0	0.0	0.0	0.0	0.0	0.0	0.0	0.0	0.0
M	4.3	4.2	4.8	4.8	3.0	4.4	3.8	1.6	4.7	4.5	2.7	4.5	4.3	4.7	4.6	5.5	5.3
Ca	0.0	0.0	0.0	0.0	0.0	0.0	0.0	0.0	0.0	0.0	0.0	0.0	0.0	0.0	0.0	0.0	0.0
Na	0.0	0.0	0.0	0.0	0.0	0.0	0.0	0.0	0.0	0.0	0.0	0.1	0.0	0.0	0.0	0.0	0.0
K ₂	0.0	0.0	0.0	0.0	0.0	0.0	0.0	0.0	0.0	0.0	0.0	0.0	0.0	0.0	0.0	0.0	0.0
To	98.	98.	10	99.	98.	99.	97.	93.	99.	99.	97.	98.	98.	99.	99.	10	99.
Si	0.0	0.0	0.0	0.0	0.0	0.0	0.0	0.0	0.0	0.0	0.0	0.0	0.0	0.0	0.0	0.0	0.0
Ti	0.0	0.0	0.0	0.0	0.0	0.0	0.0	0.0	0.0	0.0	0.0	0.0	0.0	0.0	0.0	0.0	0.0
Al	0.2	0.2	0.2	0.2	0.0	0.2	0.2	0.0	0.2	0.2	0.0	0.2	0.2	0.2	0.2	0.3	0.3
Cr	1.6	1.6	1.6	1.6	1.6	1.6	1.6	0.7	1.6	1.6	1.6	1.6	1.6	1.6	1.6	1.6	1.6
Fe ²	0.7	0.7	0.7	0.7	0.8	0.7	0.7	0.8	0.7	0.7	0.8	0.7	0.7	0.7	0.7	0.7	0.7
Fe ³	0.0	0.0	0.0	0.0	0.2	0.0	0.0	1.2	0.0	0.0	0.2	0.0	0.0	0.0	0.0	0.0	0.0
M	0.0	0.0	0.0	0.0	0.0	0.0	0.0	0.0	0.0	0.0	0.0	0.0	0.0	0.0	0.0	0.0	0.0
Ni	0.0	0.0	0.0	0.0	0.0	0.0	0.0	0.0	0.0	0.0	0.0	0.0	0.0	0.0	0.0	0.0	0.0
M	0.2	0.2	0.2	0.2	0.1	0.2	0.2	0.0	0.2	0.2	0.1	0.2	0.2	0.2	0.2	0.2	0.2
Ca	0.0	0.0	0.0	0.0	0.0	0.0	0.0	0.0	0.0	0.0	0.0	0.0	0.0	0.0	0.0	0.0	0.0
Na	0.0	0.0	0.0	0.0	0.0	0.0	0.0	0.0	0.0	0.0	0.0	0.0	0.0	0.0	0.0	0.0	0.0
K	0.0	0.0	0.0	0.0	0.0	0.0	0.0	0.0	0.0	0.0	0.0	0.0	0.0	0.0	0.0	0.0	0.0
M	21.	21.	23.	24.	13.	21.	19.	4.3	24.	23.	12.	22.	22.	23.	23.	27.	26.
Cr	76.	77.	74.	74.	83.	76.	79.	90.	74.	75.	84.	75.	76.	75.	75.	71.	72.
Fe ²	0.7	0.7	0.7	0.7	0.8	0.7	0.7	0.9	0.7	0.7	0.8	0.7	0.7	0.7	0.7	0.7	0.7

Fe ³⁺	0.0	0.0	0.0	0.0	0.1	0.0	0.0	0.6	0.0	0.0	0.1	0.0	0.0	0.0	0.0	0.0	0.0
------------------	-----	-----	-----	-----	-----	-----	-----	-----	-----	-----	-----	-----	-----	-----	-----	-----	-----

Table 2. Continued

Sam	T53	T53	T54														
SiO ₂	0.04	0.05	0.03	0.04	0.00	0.05	0.00	0.05	0.00	0.07	0.09	0.00	0.07	0.09	0.00	0.07	0.00
TiO	0.35	0.26	0.38	0.32	0.22	0.26	0.25	0.25	0.33	0.11	0.31	0.36	0.39	0.48			
Al ₂	6.49	0.00	6.50	6.76	0.00	5.62	0.00	5.66	5.53	0.00	6.27	6.43	6.83	0.03			
Cr ₂	60.0	19.5	59.4	60.2	17.7	59.3	14.5	60.9	60.7	8.88	60.5	60.0	59.9	32.0			
FeO	26.8	69.5	27.7	27.5	71.4	29.6	72.4	27.3	26.9	80.1	27.1	27.8	27.0	58.6			
Mn	0.68	0.85	0.58	0.61	0.56	0.68	0.46	0.65	0.59	0.60	0.64	0.68	0.69	0.85			
NiO	0.00	0.73	0.02	0.01	0.88	0.00	0.74	0.00	0.00	0.89	0.06	0.01	0.04	0.42			
Mg	4.58	1.57	4.48	4.45	1.62	4.26	1.37	4.40	4.42	1.71	4.60	4.40	4.73	1.80			
CaO	0.03	0.00	0.00	0.05	0.01	0.00	0.00	0.02	0.06	0.03	0.03	0.02	0.03	0.00			
Na ₂	0.00	0.00	0.02	0.00	0.00	0.01	0.05	0.02	0.00	0.02	0.03	0.02	0.00	0.00			
K ₂ O	0.00	0.00	0.00	0.01	0.00	0.00	0.00	0.00	0.01	0.00	0.02	0.03	0.01	0.00			
Tota	99.0	92.5	99.2	100.	92.5	99.9	89.9	99.3	98.7	92.3	99.6	99.9	99.8	94.3			
Si	0.00	0.00	0.00	0.00	0.00	0.00	0.00	0.00	0.00	0.00	0.00	0.00	0.00	0.00			
Ti	0.01	0.01	0.01	0.01	0.01	0.01	0.01	0.01	0.01	0.00	0.01	0.01	0.01	0.01			
Al	0.27	0.00	0.27	0.28	0.00	0.23	0.00	0.24	0.23	0.00	0.26	0.26	0.28	0.00			
Cr	1.67	0.60	1.65	1.66	0.54	1.65	0.46	1.70	1.70	0.27	1.67	1.66	1.65	0.97			
Fe ²⁺	0.75	0.87	0.76	0.76	0.87	0.76	0.88	0.75	0.76	0.85	0.74	0.76	0.74	0.87			
Fe ³⁺	0.04	1.38	0.06	0.05	1.44	0.11	1.53	0.05	0.04	1.72	0.05	0.06	0.04	1.00			
Mn	0.02	0.03	0.02	0.02	0.02	0.02	0.02	0.02	0.02	0.02	0.02	0.02	0.02	0.03			
Ni	0.00	0.02	0.00	0.00	0.03	0.00	0.02	0.00	0.00	0.03	0.00	0.00	0.00	0.01			
Mg	0.24	0.09	0.23	0.23	0.09	0.22	0.08	0.23	0.23	0.10	0.24	0.23	0.25	0.10			
Ca	0.00	0.00	0.00	0.00	0.00	0.00	0.00	0.00	0.00	0.00	0.00	0.00	0.00	0.00			
Na	0.00	0.00	0.00	0.00	0.00	0.00	0.00	0.00	0.00	0.00	0.00	0.00	0.00	0.00			
K	0.00	0.00	0.00	0.00	0.00	0.00	0.00	0.00	0.00	0.00	0.00	0.00	0.00	0.00			
Mg#	23.3	3.87	22.3	22.3	3.88	20.3	3.26	22.2	22.6	3.67	23.2	21.9	23.7	5.19			
Cr#	75.7	90.5	76.3	76.6	90.2	77.4	91.5	76.4	76.3	89.6	75.5	76.7	75.2	89.4			
Fe ²⁺	0.76	0.91	0.76	0.77	0.90	0.77	0.92	0.76	0.76	0.90	0.76	0.77	0.75	0.89			
Fe ³⁺	0.02	0.70	0.03	0.02	0.73	0.05	0.77	0.03	0.02	0.86	0.03	0.03	0.02	0.51			

Table 3. Major and trace element analyses of various rocks from the Wushan-Tianshui terrane, West Qinling Orogen.

Sample Rock	T14-Serpentinized peridotite	T14-Gabbr	T14-Gabbr	T14-Gabbr	TS15-Gabbr	TS15-Gabbr	TS15-Gabbr	TS15-Gabbr	T14-Gabbr	T14-Gabbr	T15-38 Gabbr
Location	WS	WS	WS	WS	WS	WS	WS	WS	GZZ	GZZ	GZZ
Major element (wt. %)											
SiO ₂	40.36	46.04	40.73	40.21	42.28	43.8	44.14	40.64	47.92	58.73	54.94
TiO ₂	1.06	0.87	0.32	0.74	0.71	0.68	0.09	0.1	0.48	0.56	0.35
Al ₂ O ₃	0.04	0.07	0.01	0.04	0.01	0.01	0.01	0.01	16.37	13.45	17.22
Fe ₂ O ₃ T	7.16	9.21	4.3	5.68	7.3	7.69	6.68	7.43	13.46	8.46	9.83
MnO	0.17	12.32	0.07	0.06	0.23	0.01	0.23	0.15	0.21	0.21	0.14
MgO	37.03	22.68	40.09	38.69	37.82	38.02	36.79	39.92	6.77	4.00	4.34
CaO	0.02	0.05	0.02	0.02	0	0	0.01	0	10.49	9.34	7.45
Na ₂ O	0.19	0.25	0.2	0.2	0.01	0.01	0	0.01	1.66	0.99	3.68
K ₂ O	0.13	0.17	0.06	0.08	0.07	0.06	0.09	0.09	0.41	0.65	0.22
P ₂ O ₅	0.02	0.02	0.01	0.01	0.01	0.01	0	0.01	0.04	0.01	0.05
LOI	11.75	7.15	12.26	11.77	11.29	9.29	11.32	11.65	2.25	2.05	0.74
Trace element (ppm)											
Sc	2.28	89.42	8.05	43.78	10.30	8.73	2.17	2.18	46.66	38.60	35.32
V	17.46	118.86	27.18	38.42	41.16	11.34	53.70	69.58	412.2	210.0	294.20
Cr	5064	2100	3721	6828	3192	3036	4006	4436	115.76	29.40	30.02
Co	77.74	83.98	125.7	95.76	104.52	88.62	116.06	134.62	44.78	31.74	22.88
Ni	1555	257	2074	1773	2193	1948	1992	2234	42.22	16.97	17.80
Rb	0.272	0.506	0.790	0.537	0.330	0.369	0.074	0.103	12.59	20.28	4.57
Sr	5.704	96.70	0.589	0.054	14.923	2.240	13.482	9.654	166.7	242.2	235.60
Y	1.702	2.299	0.139	0.455	0.258	0.385	0.097	0.128	8.64	12.50	11.86
Zr	9.998	6.248	0.473	0.646	0.658	0.556	0.525	0.723	14.25	25.28	29.45
Nb	0.328	0.316	0.262	0.380	0.605	0.465	0.156	0.276	0.29	0.19	0.99
Cs	0.119	0.242	0.063	0.034	0.146	0.277	0.015	0.019	5.65	8.04	1.87
Ba	10.17	28.58	2.489	2.444	3.042	0.477	1.006	1.123	98.88	200.8	46.08
La	1.718	1.255	0.064	0.069	0.420	0.391	0.075	0.106	1.102	2.338	1.750
Ce	3.640	2.870	0.142	0.160	0.805	0.852	0.155	0.224	3.468	5.972	4.680
Pr	0.497	0.376	0.018	0.022	0.083	0.099	0.019	0.026	0.537	0.838	0.670
Nd	2.002	1.551	0.068	0.104	0.275	0.379	0.085	0.109	2.706	4.024	3.200
Sm	0.457	0.405	0.020	0.045	0.051	0.105	0.017	0.025	0.854	1.264	1.030
Eu	0.098	0.145	0.002	0.006	0.041	0.033	0.004	0.005	0.414	0.552	0.380
Gd	0.422	0.432	0.023	0.063	0.045	0.090	0.016	0.021	1.098	1.724	1.340
Tb	0.060	0.075	0.003	0.011	0.007	0.013	0.003	0.004	0.206	0.317	0.230
Dy	0.337	0.448	0.023	0.076	0.043	0.072	0.015	0.020	1.394	2.086	1.710
Ho	0.068	0.092	0.006	0.019	0.009	0.013	0.003	0.004	0.326	0.478	0.380
Er	0.186	0.253	0.019	0.051	0.027	0.038	0.010	0.014	1.001	1.400	1.240
Tm	0.027	0.038	0.003	0.006	0.004	0.005	0.001	0.003	0.162	0.213	0.190
Yb	0.177	0.241	0.020	0.039	0.033	0.036	0.011	0.014	1.131	1.406	1.350
Lu	0.026	0.036	0.003	0.005	0.006	0.006	0.002	0.003	0.184	0.221	0.210
Hf	0.238	0.149	0.014	0.022	0.018	0.015	0.013	0.017	0.374	0.649	0.820
Ta	0.019	0.019	0.017	0.054	0.058	0.033	0.012	0.022	0.015	0.022	0.100
Pb	0.826	12.00	0.241	0.326	0.744	0.493	0.088	0.216	1.732	1.667	4.740
Th	1.307	0.886	0.061	0.039	0.038	0.034	0.034	0.037	0.122	0.484	0.480

U	0.455	0.257	0.188	0.012	0.252	0.370	0.028	0.039	0.103	0.089	0.190
---	-------	-------	-------	-------	-------	-------	-------	-------	-------	-------	-------

Table 3. Continued.

Sample	T14-PB	T14-WS	T14-PB	T14-WS	T14-PB	T14-WS	T14-PB	T14-WS	16TS-PB	16TS-WS	16TS-PB
Rock	PB	WS	PB	WS	PB	WS	PB	WS	PB	WS	PB
Location											
Major element (wt.%)											
SiO ₂	50.77	51.99	50.76	51.82	51.47	47.97	50.00	48.66	55.02	52.87	51.55
TiO ₂	1.56	1.58	1.81	1.82	1.41	1.54	2.00	1.30	1.08	1.14	1.20
Al ₂ O ₃	12.56	13.76	12.78	12.52	13.42	14.13	13.27	14.06	12.35	11.91	12.27
Fe ₂ O ₃ T	12.34	11.89	12.02	12.08	11.51	13.95	13.60	11.67	10.96	12.71	13.65
MnO	0.22	0.25	0.23	0.22	0.19	0.19	0.19	0.23	0.15	0.17	0.19
MgO	7.70	6.07	7.07	6.63	7.42	9.17	7.79	7.99	6.96	7.51	7.10
CaO	10.20	8.72	11.56	11.69	9.45	9.02	7.93	12.68	7.45	8.12	8.85
Na ₂ O	3.20	4.26	2.03	1.62	4.07	3.35	3.87	2.34	4.40	3.90	3.56
K ₂ O	0.16	0.20	0.15	0.16	0.10	0.15	0.16	0.24	0.07	0.07	0.09
P ₂ O ₅	0.09	0.10	0.11	0.10	0.07	0.08	0.12	0.06	0.08	0.08	0.09
LOI	0.98	0.76	1.32	1.04	0.58	0.84	1.15	0.94	0.68	0.67	0.91
Trace elements (ppm)											
Sc	55.18	52.12	50.94	50.12	52.10	62.64	56.86	58.60	45.34	48.52	48.16
V	431.4	401.2	374.2	375.4	388.2	427.6	499.4	391.4	317.20	311.40	340.60
Cr	279.6	115.8	163.7	154.8	275.2	307.8	142.1	333.6	349.60	355.60	390.40
Co	52.88	55.08	52.80	47.66	51.18	66.80	52.20	47.48	51.20	57.28	57.30
Ni	129.4	82.42	70.00	67.74	98.76	113.1	81.32	103.3	97.82	116.26	105.28
Rb	1.85	3.08	1.96	3.75	1.26	1.83	1.12	6.04	0.49	0.35	0.44
Sr	120.3	157.0	154.3	161.9	138.5	146.5	106.7	278.2	52.80	48.86	64.50
Y	35.78	34.86	39.15	38.07	27.84	31.25	39.06	26.73	20.98	22.10	22.78
Zr	92.34	84.00	110.4	111.4	74.78	82.48	110.6	69.17	63.42	68.98	68.82
Nb	4.11	4.32	5.26	5.72	3.36	4.04	7.54	2.89	2.87	3.17	3.37
Cs	0.89	1.16	2.82	5.07	0.32	0.45	0.30	1.72	0.09	0.04	0.03
Ba	22.66	55.68	35.92	48.36	51.08	25.96	74.46	208.0	21.24	19.99	22.42
La	4.16	3.85	5.71	5.86	4.13	3.96	4.99	4.19	1.93	1.47	2.18
Ce	12.02	10.70	16.23	15.94	11.16	11.49	13.72	10.50	5.46	4.76	6.12
Pr	1.96	1.75	2.58	2.53	1.77	1.92	2.30	1.83	1.07	0.98	1.13
Nd	10.13	9.19	13.05	12.71	9.00	9.92	11.79	9.01	5.82	5.63	6.10
Sm	3.53	3.40	4.22	4.14	2.96	3.33	3.97	2.93	2.15	2.20	2.23
Eu	1.27	1.32	1.64	1.48	1.08	1.18	1.36	1.19	0.52	0.51	0.56
Gd	4.93	4.87	5.70	5.55	4.05	4.58	5.44	3.86	2.73	2.88	2.87
Tb	0.93	0.93	1.04	1.02	0.74	0.86	1.02	0.71	0.51	0.54	0.52
Dy	6.11	6.03	6.67	6.58	4.81	5.53	6.71	4.61	3.46	3.68	3.73
Ho	1.37	1.34	1.47	1.45	1.07	1.23	1.49	1.02	0.75	0.80	0.81
Er	3.97	3.78	4.17	4.16	3.04	3.49	4.30	2.90	2.14	2.29	2.34
Tm	0.59	0.55	0.61	0.61	0.45	0.52	0.64	0.43	0.32	0.34	0.35
Yb	3.80	3.44	3.89	3.87	2.89	3.31	4.12	2.72	1.97	2.11	2.16
Lu	0.59	0.51	0.59	0.59	0.44	0.50	0.63	0.41	0.30	0.32	0.33
Hf	2.36	2.26	2.71	2.85	1.91	2.11	2.78	1.75	1.53	1.67	1.68
Ta	0.25	0.28	0.46	0.41	0.20	0.25	0.55	0.18	0.19	0.18	0.23
Pb	1.29	3.48	2.94	2.80	5.00	5.30	1.60	2.60	0.92	0.74	0.85

Th	0.42	0.44	0.53	0.55	0.39	0.42	0.55	0.34	0.24	0.25	0.26	0.20
U	0.16	0.87	0.18	0.18	0.13	0.12	0.74	0.15	0.08	0.07	0.07	0.09

Table 3. Continued.

Sample	16TS-PB-GZZ											
Rockty Locatio												
SiO ₂	51.22	51.39	50.50	49.44	49.52	49.96	49.50	50.86	50.31	51.12	50.05	52.35
TiO ₂	1.59	1.45	1.60	1.52	2.52	2.57	2.47	2.45	2.05	1.83	1.88	1.03
Al ₂ O ₃	12.81	13.61	13.59	14.04	12.62	12.08	12.30	11.52	12.42	11.97	12.43	14.54
Fe ₂ O ₃ T	15.88	12.61	13.29	13.34	17.16	17.79	18.18	17.52	15.94	15.29	15.89	10.98
MnO	0.21	0.21	0.21	0.22	0.20	0.22	0.22	0.21	0.27	0.28	0.28	0.16
MgO	5.49	6.24	6.14	6.53	4.91	5.30	5.02	4.92	6.02	6.28	6.34	6.88
CaO	7.83	9.79	10.15	10.45	6.68	6.39	7.09	7.02	8.59	8.68	8.65	8.39
Na ₂ O	3.21	2.38	2.35	2.47	3.90	3.91	3.08	2.95	3.05	2.93	3.02	4.17
K ₂ O	0.16	0.27	0.30	0.29	0.21	0.17	0.18	0.16	0.20	0.16	0.20	0.14
P ₂ O ₅	0.15	0.14	0.16	0.15	0.27	0.27	0.27	0.27	0.21	0.18	0.20	0.09
LOI	0.92	1.08	1.06	1.16	1.65	0.92	1.34	1.41	0.55	0.69	0.73	0.77
Major element (wt.%)												
Sc	49.48	46.70	46.30	47.04	46.86	47.32	43.86	44.32	44.98	43.26	44.32	42.04
V	568.60	476.40	512.60	493.40	732.08	736.00	669.40	698.00	556.60	543.80	583.40	366.00
Cr	60.08	235.20	198.54	249.60	39.88	41.16	36.10	36.96	78.24	96.92	88.16	173.90
Co	45.94	42.52	44.88	43.52	45.75	49.32	52.04	47.30	48.64	51.20	52.24	43.10
Ni	49.72	87.12	84.80	89.56	47.48	47.40	43.54	40.58	49.28	55.38	56.14	62.18
Rb	0.95	3.81	5.97	4.29	3.45	2.74	1.75	1.48	1.15	0.90	1.90	1.05
Sr	74.96	127.98	119.30	127.36	143.77	128.36	174.12	176.14	170.36	157.08	153.40	293.80
Y	35.58	32.98	35.56	33.88	56.11	56.60	52.02	53.36	39.86	37.36	41.04	21.66
Zr	96.88	92.64	112.92	100.92	188.64	192.96	177.46	184.84	130.38	125.78	134.04	53.44
Nb	4.43	4.62	5.10	4.85	8.92	8.99	7.86	9.70	6.64	5.91	6.18	3.12
Cs	0.24	0.17	0.31	0.19	2.65	1.53	1.56	1.21	0.25	0.23	0.30	0.26
Ba	30.92	33.18	47.52	34.18	61.85	50.22	50.42	50.00	42.62	28.30	36.62	29.14
La	4.39	4.65	5.33	4.81	9.52	8.68	7.98	8.28	6.28	5.75	6.56	3.14
Ce	10.62	11.55	12.99	11.97	22.54	22.12	20.26	21.04	15.90	14.43	16.01	7.60
Pr	1.87	1.92	2.12	1.97	3.61	3.57	3.27	3.39	2.58	2.35	2.55	1.27
Nd	9.64	9.77	10.71	10.07	17.98	17.86	16.39	16.99	12.96	11.81	12.77	6.48
Sm	3.37	3.30	3.57	3.40	5.84	5.86	5.42	5.60	4.27	3.91	4.17	2.16
Eu	1.18	1.17	1.23	1.21	1.93	1.94	1.79	1.85	1.45	1.36	1.46	0.79
Gd	4.36	4.24	4.57	4.39	7.34	7.31	6.74	7.01	5.27	4.86	5.24	2.75
Tb	0.81	0.79	0.84	0.81	1.33	1.33	1.22	1.27	0.97	0.88	0.95	0.51
Dy	5.61	5.36	5.76	5.54	8.98	8.96	8.28	8.58	6.49	5.96	6.45	3.49
Ho	1.24	1.17	1.27	1.22	1.97	1.96	1.81	1.87	1.41	1.29	1.41	0.76
Er	3.63	3.39	3.64	3.50	5.64	5.65	5.21	5.38	4.01	3.70	4.06	2.17
Tm	0.55	0.51	0.55	0.53	0.85	0.85	0.78	0.81	0.60	0.55	0.60	0.32
Yb	3.48	3.19	3.43	3.32	5.29	5.30	4.89	5.09	3.78	3.42	3.75	2.00
Lu	0.54	0.49	0.52	0.51	0.81	0.81	0.74	0.78	0.57	0.51	0.57	0.31

Hf	2.51	2.45	2.80	2.39	4.59	4.68	4.26	4.52	3.19	3.00	3.19	1.41
Ta	0.26	0.28	0.31	0.30	0.57	0.55	0.48	0.71	0.41	0.34	0.37	0.20
Pb	1.90	1.27	1.46	1.24	2.54	2.48	1.39	1.44	2.05	1.94	1.64	1.85
Th	0.30	0.37	0.42	0.39	0.67	0.67	0.61	0.65	0.49	0.42	0.45	0.21
U	0.11	0.13	0.16	0.14	0.32	0.23	0.31	0.35	0.23	0.19	0.20	0.11

Table 3. Continued.

Sample	16TS-PB	T14-AV	T14-AV	T14-AV								
Rocktyp	GZZ	GZZ	GZZ	GZZ								
Location												
Major element (wt.%)												
SiO ₂	51.36	51.18	50.10	51.43	53.14	51.22	53.18	53.41	51.87	56.12	53.99	53.43
TiO ₂	1.69	0.90	1.21	1.17	1.16	1.17	0.94	0.92	1.09	0.85	0.86	0.75
Al ₂ O ₃	13.12	14.52	14.78	13.98	11.97	14.00	12.16	12.32	13.35	11.78	11.92	12.30
Fe ₂ O ₃ T	14.63	13.11	12.62	12.58	12.44	12.60	14.60	14.38	11.48	11.52	12.60	11.56
MnO	0.18	0.17	0.17	0.17	0.17	0.18	0.20	0.19	0.20	0.17	0.18	0.18
MgO	5.92	6.90	8.10	8.17	7.76	8.02	5.77	5.70	8.02	6.20	7.00	7.59
CaO	7.42	10.35	7.70	7.41	7.90	7.56	7.93	7.79	8.84	7.20	7.44	8.07
Na ₂ O	4.60	1.28	4.52	4.00	3.91	4.13	3.72	3.67	3.89	4.51	4.26	4.27
K ₂ O	0.15	0.15	0.10	0.10	0.09	0.10	0.09	0.09	0.10	0.11	0.11	0.15
P ₂ O ₅	0.19	0.06	0.09	0.09	0.09	0.09	0.09	0.09	0.08	0.05	0.06	0.03
LOI	0.27	1.09	0.58	0.54	0.50	0.60	0.46	0.54	0.60	0.47	0.64	0.73
Trace elements (ppm)												
Sc	49.74	48.54	50.38	51.18	44.80	47.46	47.38	48.10	55.12	55.88	64.52	54.16
V	500.80	361.60	416.20	402.60	382.80	402.80	434.20	443.00	441.40	397.20	468.20	383.60
Cr	135.32	255.60	320.00	322.20	305.00	291.80	53.46	54.78	314.00	68.62	74.96	186.90
Co	49.62	56.96	59.36	60.22	55.18	51.90	54.70	56.44	59.36	55.58	65.08	51.98
Ni	69.86	93.28	105.54	106.60	91.88	99.18	54.82	58.32	105.18	77.24	85.56	92.84
Rb	1.61	2.54	0.58	0.61	0.43	1.04	0.66	0.84	0.83	1.30	0.81	3.05
Sr	137.84	97.86	93.44	96.10	81.94	91.04	52.06	53.72	115.70	60.32	95.06	119.40
Y	37.10	21.16	23.80	23.52	22.22	24.20	27.80	27.96	24.12	31.51	33.75	25.71
Zr	112.68	39.44	69.82	67.00	64.00	71.40	47.79	45.77	63.80	49.43	57.75	43.80
Nb	5.71	1.41	3.49	3.40	3.23	3.73	2.13	2.14	3.19	1.17	1.41	1.17
Cs	0.14	1.79	0.10	0.12	0.07	0.18	0.16	0.23	0.34	0.35	0.25	1.14
Ba	55.28	101.26	53.94	49.42	46.98	50.08	18.18	19.83	24.88	17.84	21.80	48.08
La	5.37	1.55	3.12	3.14	3.07	3.23	2.04	2.21	3.12	1.76	1.69	1.33
Ce	14.25	3.95	8.40	8.46	8.07	8.65	5.35	5.75	8.23	5.50	5.76	4.15
Pr	2.30	0.72	1.40	1.41	1.34	1.47	0.91	0.96	1.34	1.00	1.06	0.75
Nd	11.58	3.94	7.18	7.22	6.93	7.67	4.98	5.16	6.87	5.65	6.06	4.35
Sm	3.82	1.58	2.45	2.45	2.34	2.61	1.96	2.00	2.42	2.28	2.47	1.85
Eu	1.12	0.57	0.91	0.87	0.84	1.01	0.71	0.74	0.81	0.81	0.89	0.70
Gd	4.77	2.24	3.09	3.06	2.90	3.41	2.84	2.86	3.02	3.61	3.88	2.92
Tb	0.86	0.44	0.56	0.56	0.53	0.62	0.56	0.56	0.73	0.78	0.59	
Dy	5.81	3.15	3.77	3.74	3.55	4.28	4.00	4.00	3.75	5.08	5.41	4.10
Ho	1.27	0.73	0.82	0.81	0.77	0.93	0.92	0.92	0.82	1.19	1.27	0.96
Er	3.65	2.18	2.32	2.31	2.18	2.65	2.75	2.76	2.32	3.54	3.77	2.88

Tm	0.53	0.33	0.34	0.34	0.32	0.40	0.42	0.42	0.34	0.54	0.58	0.44
Yb	3.28	2.16	2.14	2.11	1.97	2.50	2.74	2.72	2.12	3.56	3.85	2.88
Lu	0.50	0.34	0.32	0.32	0.30	0.39	0.42	0.42	0.32	0.56	0.60	0.45
Hf	2.70	1.07	1.71	1.66	1.58	2.05	1.13	1.09	1.59	1.40	1.59	1.27
Ta	0.30	0.13	0.21	0.22	0.18	0.23	0.13	0.14	0.18	0.08	0.09	0.09
Pb	0.88	2.14	2.58	0.96	0.96	2.82	1.61	1.99	9.60	3.43	1.58	6.79
Th	0.38	0.10	0.25	0.27	0.23	0.32	0.17	0.18	0.22	0.18	0.19	0.13
U	0.48	0.06	0.09	0.08	0.07	0.12	0.06	0.06	0.13	0.11	0.19	0.05

Table 3. Continued.

Sample	T14-AV	T14-AV	T14-Bo	T14-Bo	T14-Bo	T14-Bo	T14-Bo	16TS-Bo	16TS-Bo	16TS-Bo	16TS-Bo	16TS-Bo
Rockty	GZZ	GZZ	GZZ	GZZ	GZZ							
Locatio												
Major element (wt.%)												
SiO ₂	63.35	57.09	56.64	51.39	53.06	53.65	52.08	56.55	51.80	49.27	54.05	53.13
TiO ₂	0.71	0.65	0.48	0.29	0.29	0.29	0.30	0.36	0.42	0.44	0.35	0.37
Al ₂ O ₃	9.08	11.28	12.66	11.25	10.56	9.54	11.51	12.61	9.68	11.00	9.45	15.33
Fe ₂ O ₃ T	10.00	10.02	7.74	10.13	8.25	8.66	9.99	8.21	10.84	11.59	10.33	9.57
MnO	0.14	0.16	0.15	0.18	0.15	0.14	0.23	0.14	0.22	0.23	0.19	0.13
MgO	4.95	7.03	7.86	9.35	12.74	14.10	10.82	8.02	12.03	13.43	13.03	9.07
CaO	6.67	7.63	8.46	13.09	10.89	9.65	10.98	8.03	12.60	12.15	9.80	6.07
Na ₂ O	3.15	4.39	4.13	0.67	1.65	1.48	1.76	4.23	0.56	0.73	0.72	4.81
K ₂ O	0.15	0.06	0.13	0.62	0.14	0.18	0.57	0.19	0.19	0.16	0.33	0.09
P ₂ O ₅	0.04	0.04	0.05	0.02	0.03	0.02	0.02	0.04	0.06	0.06	0.04	0.05
LOI	0.58	0.64	0.70	2.19	1.43	1.48	0.95	0.64	0.89	0.89	1.22	0.84
Trace elements (ppm)												
Sc	44.38	48.58	43.76	41.50	46.28	39.58	50.52	55.64	33.67	39.88	37.18	44.20
V	339.6	354.6	323.8	202.4	228.8	197.8	297.4	314.2	228.83	270.20	211.80	307.00
Cr	54.18	123.9	547.2	2068	1173	1087	1264	1127	1327	1694	1580	785.2
Co	50.32	49.82	43.62	68.06	65.04	67.64	58.30	59.08	65.98	70.00	62.30	55.94
Ni	62.92	80.98	177.1	457.4	367.2	469.2	269.8	279.4	301.10	328.40	292.00	207.00
Rb	0.51	0.53	1.88	50.16	3.53	5.66	7.27	2.70	2.61	1.43	5.08	0.79
Sr	56.60	105.4	164.2	189.7	109.4	75.70	100.5	116.7	102.44	87.16	116.92	165.10
Y	23.63	22.27	17.98	11.59	11.43	10.35	12.00	14.00	12.41	12.05	9.33	11.98
Zr	40.04	34.10	46.84	26.40	15.26	15.25	24.66	32.96	31.35	28.78	23.58	32.22
Nb	0.60	0.31	0.72	0.91	0.48	2.40	0.28	0.39	1.02	1.08	1.05	0.74
Cs	0.08	0.27	0.57	13.09	1.97	0.95	0.53	0.42	3.55	1.11	1.83	0.22
Ba	44.36	13.08	64.26	135.2	31.04	47.62	91.28	63.40	54.01	19.76	87.66	23.58
La	1.27	1.03	7.84	1.04	0.81	0.93	1.07	3.64	2.60	2.21	2.45	3.69
Ce	3.74	3.42	18.49	2.62	2.16	2.38	3.05	9.27	5.72	4.75	4.81	8.79
Pr	0.75	0.65	2.57	0.44	0.35	0.37	0.55	1.31	0.80	0.68	0.64	1.27
Nd	4.29	3.79	11.67	2.33	1.88	1.90	2.98	6.25	3.70	3.24	2.89	5.76
Sm	1.79	1.60	2.91	0.93	0.77	0.71	1.03	1.81	1.15	1.04	0.90	1.59
Eu	0.61	0.46	0.99	0.32	0.32	0.31	0.44	0.62	0.45	0.37	0.34	0.50
Gd	2.76	2.58	3.03	1.41	1.22	1.12	1.46	2.04	1.41	1.34	1.11	1.62
Tb	0.56	0.52	0.48	0.28	0.26	0.23	0.28	0.34	0.26	0.25	0.21	0.27

Dy	3.86	3.61	2.98	1.89	1.81	1.60	1.88	2.23	1.85	1.78	1.43	1.78	2.14	1.82
Ho	0.90	0.85	0.67	0.44	0.43	0.38	0.44	0.51	0.43	0.41	0.32	0.40	0.48	0.41
Er	2.67	2.50	1.95	1.32	1.30	1.17	1.32	1.53	1.29	1.24	0.96	1.20	1.42	1.23
Tm	0.41	0.38	0.29	0.20	0.20	0.18	0.20	0.24	0.20	0.19	0.15	0.18	0.22	0.20
Yb	2.77	2.46	1.96	1.35	1.33	1.21	1.36	1.57	1.36	1.28	0.98	1.17	1.42	1.28
Lu	0.43	0.38	0.31	0.21	0.21	0.19	0.22	0.25	0.22	0.20	0.16	0.18	0.22	0.20
Hf	1.10	0.95	1.22	0.75	0.39	0.43	0.65	0.86	0.81	0.74	0.59	0.82	0.96	0.86
Ta	0.04	0.03	0.06	0.06	0.07	0.18	0.02	0.05	0.10	0.08	0.10	0.05	0.09	0.07
Pb	0.64	0.99	5.42	28.24	1.97	1.24	1.92	3.28	2.04	1.51	1.38	2.08	2.24	1.68
Th	0.13	0.09	1.72	0.33	0.08	0.11	0.44	1.28	0.40	0.37	0.31	0.85	1.05	0.84
U	0.16	0.05	0.36	0.29	0.03	0.04	0.19	0.43	0.22	0.15	0.14	0.25	0.31	0.24

Table 3. Continued.

Sampl	16TS-	16TS-	16TS-	16TS-	16TS-	16TS-	TS15-	TS15-	TS15-	TS15-	TS15-	16TS-	16TS-	16TS-
Rockt	Bo	Bo	Bo	Bo	Bo	Bo	AV							
Locati	GZZ	GZZ	GZZ	LZY	WS	WS	WS							
Major element (wt.%)														
SiO ₂	52.99	51.00	52.31	52.18	50.33	51.23	54.82	60.47	53.34	57.76	54.31	59.22	58.46	62.50
TiO ₂	0.27	0.29	0.32	0.55	0.56	0.54	0.885	0.715	1.001	0.939	0.492	0.48	0.43	0.40
Al ₂ O ₃	11.49	12.06	12.04	14.63	14.99	14.97	16.95	13.96	19.97	15.80	15.61	15.77	16.90	15.26
Fe ₂ O ₃	10.64	11.52	10.94	9.40	9.47	9.33	7.636	5.753	7.591	7.949	6.043	8.29	8.04	6.87
MnO	0.13	0.14	0.14	0.14	0.18	0.17	0.088	0.071	0.066	0.094	0.132	0.15	0.13	0.12
MgO	12.55	13.29	12.47	9.50	9.80	8.49	4.457	3.891	4.778	3.787	2.692	3.65	3.35	3.02
CaO	7.87	7.72	7.40	7.96	9.47	10.31	4.362	4.708	2.433	5.064	7.476	5.38	5.72	4.66
Na ₂ O	2.43	1.63	2.24	4.27	4.15	3.63	3.152	3.262	5.437	2.868	4.510	4.44	4.54	4.47
K ₂ O	0.08	0.19	0.19	0.13	0.16	0.16	2.246	1.437	1.143	1.399	1.022	0.54	0.70	0.50
P ₂ O ₅	0.03	0.03	0.04	0.09	0.09	0.09	0.207	0.170	0.258	0.211	0.154	0.07	0.07	0.07
LOI	0.75	1.73	1.26	0.75	0.82	0.90	4.052	4.535	3.085	2.595	6.564	0.95	0.84	1.18
Trace elements (ppm)														
Sc	37.36	41.27	41.04	48.30	44.50	44.70	18.27	20.00	16.77	16.20	18.17	33.28	31.46	28.70
V	215.2	213.3	230.2	329.4	325.6	309.2	216.9	219.6	202.9	229.4	130.4	232.6	261.4	207.6
Cr	1911	2583	1989	782.2	772.0	864.2	73.30	87.14	74.28	67.40	29.71	117.9	90.92	82.24
Co	67.66	78.10	69.14	60.88	58.14	63.96	28.68	30.20	26.94	26.44	16.85	26.26	25.18	22.38
Ni	413.6	524.2	378.6	250.4	256.6	267.0	44.13	48.04	39.31	47.94	14.90	45.26	46.10	43.62
Rb	1.31	5.59	5.06	1.62	1.91	2.39	48.49	42.88	27.40	36.26	41.30	8.75	11.49	8.20
Sr	160.5	125.5	157.0	158.1	135.9	156.9	238.5	517.2	228.0	757.4	427.4	82.60	93.52	83.08
Y	6.96	7.64	9.36	15.10	15.50	15.86	12.24	12.23	9.94	12.52	12.15	16.08	16.13	14.05
Zr	21.16	22.18	24.70	41.99	41.25	41.17	96.59	94.50	101.5	94.84	63.31	66.92	65.38	57.87
Nb	1.10	1.02	1.05	1.00	1.02	0.92	6.01	5.94	6.45	7.17	5.95	1.80	3.25	1.55
Cs	1.37	7.41	3.75	1.76	0.49	0.52	1.49	1.31	2.59	1.91	2.09	1.02	1.14	0.87
Ba	13.48	16.44	18.28	54.32	72.02	96.70	783.5	613.8	448.9	546.4	354.9	83.14	107.4	86.14
La	1.12	1.27	1.32	5.46	6.07	8.64	13.28	12.82	13.43	16.08	10.98	8.07	7.68	5.83
Ce	2.63	2.99	3.14	13.26	14.42	19.35	29.96	29.56	30.40	34.28	20.54	17.05	16.04	13.20
Pr	0.38	0.43	0.46	2.05	2.11	2.63	3.80	3.81	3.86	4.32	2.51	2.13	1.97	1.66
Nd	1.79	2.01	2.23	9.57	9.55	11.52	15.85	16.03	15.84	18.05	10.10	8.78	8.19	6.92
Sm	0.62	0.66	0.77	2.54	2.42	2.67	3.27	3.38	3.19	3.71	2.13	2.30	2.19	1.91

Eu	0.22	0.24	0.21	0.71	0.71	0.77	1.11	1.17	1.00	1.13	0.76	0.79	0.79	0.61
Gd	0.82	0.86	1.05	2.34	2.28	2.44	2.87	2.97	2.63	3.25	2.13	2.29	2.24	1.96
Tb	0.15	0.16	0.20	0.37	0.36	0.37	0.38	0.38	0.33	0.41	0.30	0.37	0.36	0.33
Dy	1.07	1.12	1.41	2.37	2.31	2.37	2.16	2.16	1.83	2.26	1.87	2.39	2.41	2.12
Ho	0.24	0.25	0.32	0.51	0.50	0.52	0.40	0.40	0.33	0.41	0.39	0.53	0.52	0.47
Er	0.70	0.77	0.94	1.47	1.45	1.47	1.14	1.13	0.94	1.12	1.26	1.55	1.56	1.38
Tm	0.11	0.12	0.15	0.22	0.22	0.21	0.15	0.15	0.13	0.15	0.20	0.24	0.24	0.21
Yb	0.68	0.77	0.94	1.41	1.41	1.33	0.98	0.98	0.87	0.96	1.42	1.55	1.55	1.37
Lu	0.11	0.12	0.15	0.22	0.22	0.20	0.14	0.14	0.13	0.14	0.22	0.24	0.24	0.21
Hf	0.54	0.55	0.61	1.06	1.05	1.03	2.27	2.25	2.40	2.26	1.58	1.66	1.63	1.41
Ta	0.09	0.06	0.06	0.06	0.08	0.05	0.33	0.34	0.49	0.66	0.35	0.10	0.42	0.10
Pb	0.95	1.00	1.08	3.02	2.77	2.06	2.77	5.67	5.90	11.71	6.33	3.06	3.24	3.19
Th	0.23	0.24	0.27	1.04	0.99	1.00	1.90	1.62	2.17	2.51	2.56	1.78	1.69	1.51
U	0.12	0.13	0.14	0.19	0.19	0.10	0.55	0.45	0.51	0.69	0.49	0.43	0.41	0.36

Abbreviations: PB = Pillow basalt, AV = arc volcanics, Bo = boninite, WS = Wushan, GZZ = Guanzizhen, LZY = Liziyuan

Table 4. Whole-rock Sr-Nd isotopic data for the Wushan-Guanzizhen terrane

	Rb(ppm)	Sr(p pm)	87Rb /86Sr	87Sr/ 86Sr	Isr	Sm (ppm)	Nd (pp m)	147Sm /144Nd	143Nd/ 144Nd	initial Nd	$\epsilon\text{Nd}(0)$	$\epsilon\text{Nd}(T)$
MORB-like lavas												
T1 4-10	1.85	120 .34	0.043 3	0.70 67	0.7 063 9	3.53	10.1 3	0.221	0.5128 78	0.51 2154	4.7	3.1
T1 4-12	1.96	154 .36	0.035 8	0.70 4114	0.7 038 6	4.22	13.0 5	0.2049	0.5129 8	0.51 2309	6.7	6.2
T1 4-13	3.75	161 .92	0.065 5	0.70 3994	0.7 035 3	4.14	12.7 1	0.2065	0.5132 4	0.51 2564	11. 7	11. 1
T1 4-18	1.26	138 .56	0.025 6	0.70 54	0.7 052 2	2.96	9	0.2083	0.5128 56	0.51 2174	4.3	3.5
T1 4-19	1.83	146 .54	0.035 4	0.70 568	0.7 054 3	3.33	9.92	0.2131	0.5128 6	0.51 2162	4.3	3.3
T1 4-33	6.04	278 .2	0.061 3	0.70 648	0.7 060 4	2.93	9.01	0.206	0.5127 92	0.51 2117	3	2.4
Gabbro												
T1 4-08	12.5 9	166 .78	0.213 2	0.70 7012	0.7 054 9	0.85	2.71	0.2003	0.5127 91	0.51 2201	3	2.8
T1 4-15	20.2 8	242 .2	0.236 5	0.70 8969	0.7 072 8	1.26	4.02	0.1992	0.5127 76	0.51 2189	2.7	2.5
Boninite												
T1 4-16	50.1 6	189 .76	0.746 6	0.71 578	0.7 109 9	0.93	2.33	0.2532	0.513	0.51 2254	7.1	3.8
T1 4-22	3.53	109 .48	0.091	0.70 6439	0.7 058 6	0.77	1.88	0.2599	-	-	-	-
T1 4-23	5.66	75. 7	0.211 1	0.70 6637	0.7 052 8	0.71	1.9	0.2371	0.5130 43	0.51 2344	7.9	5.6
T1 4-27	7.27	100 .58	0.204 2	0.70 6721	0.7 054 1	1.03	2.98	0.2199	0.5128 71	0.51 2223	4.5	3.2
T1 4-14	1.88	164 .22	0.032 3	0.70 5178	0.7 049 7	2.91	11.6 7	0.1584	0.5127 68	0.51 2301	2.5	4.7

T1 4- 28	2.7	116 .74	0.065 2	0.70 5874	0.7 054 6	1.81	6.25	0.1834	0.5127 41	0.51 2201	2	2.8
Island arc volcanic (tholeiitic)												
T1 4- 20	1.3	60. 32	0.060 6	0.70 6772	0.7 063 8	2.28	5.65	0.2558	0.5131 41	0.51 2387	9.8	6.4
T1 4- 24	3.05	119 .4	0.072 2	0.70 6679	0.7 062 2	1.85	4.35	0.2697	0.5131 93	0.51 2398	10. 8	6.6
T1 4- 21	0.81	95. 06	0.024 1	0.70 6046	0.7 058 9	2.47	6.06	0.2583	0.5131 5	0.51 2388	10	6.4
T1 4- 30	0.51	56. 6	0.025 6	0.70 6381	0.7 062 2	1.79	4.29	0.2644	0.5131 47	0.51 2368	9.9	6
T1 4- 31	0.53	105 .46	0.014 3	0.70 5909	0.7 058 2	1.6	3.79	0.2684	0.5131 75	0.51 2384	10. 5	6.4
Serpentinized peridotite												
T1 4- 34	0.27	5.7	0.134 7	0.71 1722	0.7 107 6	0.46	2	0.1448	0.5122 6	0.51 1833	- 7.4	- 4.4
T1 4- 35	0.51	96. 7	0.014 8	0.71 2134	0.7 120 3	0.4	1.55	0.1656	0.5123 2	0.51 1832	- 6.2	- 4.4
T1 4- 37	0.79	0.5 9	3.790 1	0.71 1422	0.6 844 2	0.02	0.07	0.1906	-	-	-	-

Note: (1) $I_{Sr} = ^{87}Sr/^{86}Sr - ^{87}Rb/^{86}Sr \times (e\lambda T - 1)$, where $\lambda Rb = 1.42 \times 10^{-11} \text{ year}^{-1}$; (2) $\epsilon Nd(T) = \{(^{143}Nd/^{144}Nd - ^{147}Sm/^{144}Nd \times (e\lambda T - 1)) / (^{143}Nd/^{144}Nd) CHUR(0) - (^{147}Sm/^{144}Nd) CHUR(0) \times (e\lambda T - 1)\} \times 10,000$, where $\lambda Sm = 6.54 \times 10^{-12} \text{ year}^{-1}$; $(^{143}Nd/^{144}Nd) CHUR(0) = 0.512638$; $(^{147}Sm/^{144}Nd) CHUR(0) = 0.1967$; (3) $T = 500 \text{ Ma}$ and 450 Ma , respectively.

Table 5. Zircon U-Pb data by SIMS and LA-ICP-MS for the Wushan-Tianshui terrane.

LA-ICPMS	$^{207}\text{Pb}/^{206}\text{Pb}$	1 σ	$^{207}\text{Pb}/^{235}\text{U}$	1 σ	$^{206}\text{Pb}/^{238}\text{U}$	1 σ	$^{207}\text{Pb}/^{206}\text{Pb}$	1 σ	$^{207}\text{Pb}/^{235}\text{U}$	1 σ	$^{206}\text{Pb}/^{238}\text{U}$	1 σ	U	Th	P _b	T h/U
T15-05-01	0.0569	0.0014	0.5691	0.0133	0.025	0.0082	487	32	457	9	451	5	141	77	11	0.54
T15-05-02	0.0546	0.0014	0.5504	0.0132	0.032	0.0079	394	34	445	9	455	5	219	105	18	0.48
T15-05-03	0.0591	0.0026	0.5944	0.0254	0.023	0.0087	569	72	474	16	454	5	113	57	9	0.51
T15-05-04	0.0565	0.0013	0.5473	0.0118	0.00703	0.0071	471	30	443	8	438	4	274	236	23	0.86
T15-05-05	0.0548	0.0016	0.5443	0.0152	0.021	0.0079	402	43	441	10	449	5	220	261	21	1.18
T15-05-06	0.0562	0.0017	0.5633	0.016	0.027	0.0083	460	42	454	10	452	5	146	87	12	0.59
T15-05-07	0.0577	0.0024	0.574	0.0229	0.022	0.0088	518	66	461	15	449	5	101	55	8	0.54
T15-05-08	0.0561	0.0021	0.5563	0.0196	0.02	0.0089	454	56	449	13	448	5	119	79	10	0.66
T15-05-09	0.0564	0.0025	0.5622	0.0239	0.023	0.009	467	72	453	16	450	5	111	59	9	0.53
T15-05-10	0.0569	0.0020	0.567	0.0192	0.023	0.0084	486	54	456	12	450	5	178	172	16	0.97
T15-05-11	0.0556	0.0017	0.5531	0.0161	0.022	0.0082	435	44	447	11	449	5	199	147	17	0.74
T15-05-12	0.0567	0.0028	0.5668	0.0277	0.025	0.0091	479	86	456	18	451	5	101	70	9	0.7
T15-05-13	0.0577	0.0020	0.6155	0.0208	0.0274	0.0087	518	54	487	13	480	5	134	62	11	0.46
T15-05-14	0.0568	0.0014	0.5709	0.0129	0.029	0.0076	485	32	459	8	453	5	261	272	24	1.04
T15-05-15	0.0569	0.0012	0.5726	0.0115	0.029	0.0075	489	26	460	7	454	5	342	218	29	0.64
T15-05-16	0.0567	0.0022	0.5689	0.0217	0.028	0.0089	479	62	457	14	453	5	93	56	8	0.61

T15-05-17	0.0584	0.0013	0.5581	0.0121	0.0694	0.00071	543	30	450	8	432	4	295	384	28	1.3
T15-05-18	0.0569	0.0013	0.5681	0.0120	0.0724	0.00074	486	29	457	8	451	4	300	278	27	0.93
T15-05-19	0.0567	0.0019	0.568	0.018	0.0726	0.00082	481	50	457	12	452	5	163	108	14	0.66
T15-05-20	0.0573	0.0029	0.5786	0.0288	0.0732	0.00099	503	86	464	19	456	6	102	58	8	0.57
T15-05-21	0.0561	0.0020	0.5627	0.0191	0.0728	0.00099	455	53	453	12	453	5	84	55	7	0.66
T15-05-22	0.0554	0.0028	0.5503	0.0272	0.072	0.00097	430	86	445	18	448	6	68	48	6	0.7
T15-05-23	0.0541	0.0037	0.5427	0.0361	0.0727	0.00104	376	125	440	24	452	6	61	33	5	0.55
T15-05-24	0.0578	0.0043	0.5736	0.0416	0.072	0.00121	521	130	460	27	448	7	64	39	5	0.61
T15-05-25	0.0552	0.0030	0.5548	0.0293	0.0729	0.00095	419	95	448	19	454	6	107	74	9	0.7
T15-05-26	0.0558	0.0034	0.5561	0.0331	0.0722	0.00103	446	108	449	22	450	6	69	39	6	0.56
T15-05-27	0.0554	0.0037	0.5554	0.037	0.0727	0.00105	427	124	449	24	453	6	64	41	5	0.64
T15-05-28	0.0565	0.0023	0.5646	0.0227	0.0724	0.00092	473	66	454	15	451	6	91	51	7	0.56
T15-05-29	0.0560	0.0030	0.5597	0.029	0.0724	0.00105	454	89	451	19	451	6	71	46	6	0.65
T15-05-30	0.0557	0.0019	0.5596	0.0183	0.0728	0.00088	440	51	451	12	453	5	112	87	10	0.78
T15-05-31	0.0553	0.0029	0.5524	0.028	0.0724	0.00096	425	90	447	18	451	6	66	57	6	0.86
T15-05-32	0.0562	0.0021	0.5573	0.0205	0.0719	0.00086	460	60	450	13	448	5	116	56	9	0.49
T15-05-33	0.0575	0.0023	0.5713	0.0223	0.072	0.00092	511	63	459	14	448	6	104	65	9	0.62
T15-05-34	0.0565	0.0017	0.5623	0.0164	0.0722	0.00081	472	44	453	11	449	5	124	75	10	0.6

TS15-38-01	0.0588	0.012	0.6562	0.0123	0.0809	0.0081	560	24	512	8	501	5	174	78	16	0.45
TS15-38-02	0.0606	0.008	0.6792	0.0081	0.0813	0.007	625	12	526	5	504	4	466	434	49	0.93
TS15-38-03	0.0583	0.009	0.6523	0.0084	0.0812	0.0072	539	14	510	5	503	4	262	136	25	0.52
TS15-38-04	0.057	0.02	0.6316	0.0216	0.0804	0.0082	492	81	497	13	498	5	130	55	12	0.43
TS15-38-05	0.0593	0.02	0.6607	0.0214	0.0808	0.0091	577	51	515	13	501	5	102	50	10	0.49
TS15-38-06	0.058	0.012	0.6472	0.0124	0.081	0.0077	528	26	507	8	502	5	212	122	20	0.58
TS15-38-07	0.0602	0.024	0.6726	0.0258	0.081	0.0105	612	60	522	16	502	6	90	33	8	0.36
TS15-38-08	0.0601	0.017	0.6696	0.0174	0.0808	0.0085	608	38	520	11	501	5	120	54	11	0.45
TS15-38-09	0.0566	0.02	0.6246	0.0216	0.0808	0.0078	477	81	493	14	496	5	401	321	41	0.8
TS15-38-10	0.0591	0.016	0.6593	0.0167	0.0809	0.0085	570	37	514	10	502	5	115	48	11	0.42
TS15-38-11	0.0565	0.02	0.6346	0.0217	0.0814	0.0096	472	55	499	14	505	6	115	41	10	0.35
TS15-38-12	0.057	0.011	0.6411	0.0112	0.0814	0.0077	492	22	502	7	504	5	272	165	26	0.61
TS15-38-13	0.0591	0.01	0.6597	0.011	0.081	0.0074	570	18	514	6	502	4	392	288	39	0.74
TS15-38-14	0.0587	0.011	0.6573	0.0117	0.0812	0.0078	556	22	513	7	503	5	327	203	32	0.62
TS15-38-15	0.0578	0.013	0.6439	0.013	0.0808	0.008	522	27	505	8	501	5	249	96	23	0.39
TS15-38-16	0.0576	0.018	0.6432	0.0196	0.081	0.0093	514	47	504	12	502	6	136	52	12	0.38
TS15-38-17	0.0586	0.012	0.6565	0.0123	0.0812	0.008	554	24	512	8	503	5	321	216	32	0.67
TS15-38-18	0.0584	0.014	0.6516	0.0143	0.081	0.008	543	31	509	9	502	5	255	143	27	0.56

TS15-38-19	0.0583	0.019	0.6545	0.0201	0.0814	0.0009	541	48	511	12	505	5	169	69	16	0.41
TS15-38-20	0.0561	0.012	0.6288	0.0123	0.0814	0.00078	454	27	495	8	504	5	357	300	36	0.84
TS15-38-21	0.0573	0.014	0.6379	0.0144	0.0808	0.00082	502	32	501	9	501	5	281	187	27	0.67
TS15-38-22	0.0573	0.013	0.6407	0.014	0.0811	0.00084	504	30	503	9	502	5	348	278	35	0.8
TS15-38-23	0.0572	0.021	0.6323	0.0221	0.0802	0.00084	498	82	498	14	497	5	293	152	28	0.52
TS15-38-24	0.0606	0.012	0.6807	0.0121	0.0814	0.00078	626	22	527	7	505	5	286	193	28	0.67
TS15-38-25	0.0569	0.017	0.6356	0.0185	0.0811	0.00078	486	69	500	11	503	5	445	257	43	0.58

By SIMS

T14-25-01	0.0585	0.49	0.6326	1.62	0.0796	1.51	516.2	12.5	497.7	6.4	493.7	7.2	371	132	33	0.36
T14-25-02	0.0585	0.72	0.625	1.72	0.0797	1.51	486.4	18.2	493.8	6.8	494.4	7.2	283	164	25	0.58
T14-25-03	0.0599	0.94	0.6309	2.17	0.0801	1.57	495.4	32.6	496.6	8.6	496.9	7.5	188	91	17	0.48
T14-25-04	0.0594	1.49	0.621	2.48	0.0803	1.55	456.3	42.3	490.5	9.7	497.8	7.4	145	70	13	0.49
T14-25-05	0.0585	0.77	0.624	1.88	0.0803	1.6	467	21.4	492.4	7.3	497.8	7.7	175	52	16	0.3
T14-25-06	0.0591	1.63	0.6172	2.59	0.0804	1.56	439.6	45.5	488.1	10.1	498.5	7.5	54	175	5	0.31
T14-25-07	0.0595	0.90	0.6625	1.78	0.0807	1.53	586.7	19.5	516.2	72	500.4	74	155	43	14	0.28
T14-25-08	0.0608	1.41	0.6333	2.43	0.0808	1.64	484.8	39	498.1	96	501	79	100	52	9	0.52
T14-25-09	0.0583	0.54	0.6374	1.65	0.0809	1.52	496.7	14.1	500.7	65	501.5	73	317	76	29	0.24
T14-25-10	0.0586	0.76	0.6395	1.8	0.0811	1.52	499.2	21.1	502.2	72	502.6	74	408	281	37	0.69

T14-25-11	0.0612	2.26	0.6433	3.1	0.0813	1.7	506.5	5.1	504.3	1.2.4	503.9	8.2	77	33	7	0.43
T14-25-12	0.0609	0.86	0.6569	1.87	0.0815	1.54	547.4	23	512.7	7.6	505	7.5	146	52	13	0.36
T14-25-13	0.0582	0.82	0.6396	1.82	0.0815	1.52	487.1	21.9	502	7.2	505.3	7.4	164	70	15	0.43
T14-25-14	0.0586	0.59	0.6498	1.67	0.0817	1.55	518.3	13.8	508.3	6.7	506.1	7.5	547	182	50	0.33
T14-25-15	0.0588	0.75	0.6492	1.72	0.0817	1.52	516.4	17.8	508	6.9	506.1	7.4	207	60	19	0.29
T14-25-16	0.0599	1.26	0.6552	2.09	0.082	1.54	528.5	30.7	511.7	8.4	507.9	7.5	83	28	8	0.33
T14-25-17	0.0588	0.61	0.6572	1.7	0.0823	1.52	526.2	16.4	512.9	6.9	509.9	7.5	176	50	16	0.28
T14-25-18	0.0582	0.79	0.6451	1.85	0.0825	1.53	480.4	22.9	505.5	7.4	511	7.5	104	49	9	0.47
T14-25-19	0.0586	0.99	0.6563	1.91	0.0832	1.53	498.7	25.2	512.4	7.7	515.4	7.6	151	46	14	0.3
T14-25-20	0.0579	0.53	0.6551	1.69	0.0834	1.56	490.8	14.1	511.6	6.8	516.3	7.7	246	87	23	0.36
T14-08-01	0.0602	0.78	0.664	1.94	0.0834	1.5	519	26.8	517.1	7.9	516.7	7.5	1814	3157	168	1.74
T14-08-02	0.0592	0.65	0.6605	1.8	0.0837	1.53	501.5	21	514.9	7.3	517.9	7.6	205	157	19	0.77
T14-08-03	0.0592	0.62	0.6548	1.67	0.0824	1.51	515	15.5	511.4	6.7	510.6	7.4	241	243	22	1.01
T14-08-04	0.0581	0.51	0.6261	1.65	0.0802	1.5	477.7	15.3	493.7	6.5	497.1	7.2	385	253	34	0.66
T14-08-05	0.0584	0.61	0.6549	1.67	0.0829	1.53	502	14.8	511.5	6.7	513.6	7.6	348	204	32	0.59
T14-08-06	0.0584	0.84	0.6501	1.82	0.0823	1.58	501.6	19.8	508.5	7.3	510.1	7.8	253	214	23	0.85
T14-08-07	0.0584	0.47	0.6601	1.69	0.0833	1.51	510.1	16.5	514.7	6.8	515.7	7.5	491	562	46	1.14
T14-08-08	0.0581	0.53	0.6479	1.61	0.0819	1.51	505	12.4	507.2	6.5	507.7	7.4	501	353	46	0.7

T14-08-09	0.0585	0.31	0.6733	1.61	0.0844	1.57	523.2	7.5	522.7	6.6	522.6	7.9	1297	1513	1.22	1.17
T14-08-10	0.0583	0.39	0.6478	1.57	0.0814	1.51	519.7	9.4	507.1	6.3	504.3	7.3	662	477	60	0.72
T14-08-11	0.0579	0.33	0.6768	1.54	0.0848	1.5	525.7	7.2	524.8	6.3	524.6	7.6	766	928	72	1.21
T14-08-12	0.0581	0.35	0.6542	1.58	0.0824	1.53	514.8	8.3	511.1	6.4	510.2	7.5	810	990	74	1.22
T14-38-01-rim	0.0556	0.72	0.5482	1.67	0.0715	1.5	438.1	1.61	443.8	6	444.9	6.5	273	337	28	1.24
T14-38-02-rim	0.0625	0.88	0.5612	1.92	0.0727	1.5	451.2	2.63	452.3	7	452.6	6.6	1143	10	88	0.01
T14-38-03-rim	0.0572	0.64	0.549	1.67	0.0705	1.52	471.6	1.5	444.3	6	439.1	6.5	621	12	46	0.02
T14-38-04-rim	0.057	0.67	0.5793	1.65	0.0741	1.5	481	1.5	464	6.2	460.6	6.7	593	12	47	0.02
T14-38-05-rim	0.0653	0.4	0.5885	1.81	0.073	1.5	548.3	2.1.9	469.9	6.8	454	6.6	859	21	67	0.02
T14-38-06-core	0.0872	0.41	2.327	1.57	0.1959	1.5	1341.6	8.6	1220.6	1.1.2	1153.2	1.5.9	332	131	79	0.39
T14-38-07-core	0.0887	0.35	2.6402	1.55	0.2162	1.51	1394.5	6.7	1311.9	1.1.5	1262.4	1.7.4	375	148	98	0.39
T14-38-08-core	0.0966	0.48	2.4853	1.6	0.1901	1.51	1524.5	1.0.2	1267.8	1.1.7	1121.9	1.5.5	212	74	51	0.35
T14-38-09-core	0.0986	0.64	2.6665	1.74	0.1998	1.61	1563.3	1.2.6	1319.2	1.3	1174.2	1.7.3	623	114	143	0.18
T14-38-10-core	0.0994	0.55	2.9027	1.85	0.2132	1.76	1600.5	1.0.7	1382.6	1.4.1	1245.9	20	922	129	224	0.14
T14-38-11-core	0.1015	0.3	2.7516	1.54	0.2006	1.5	1614.2	6.8	1342.5	1.1.6	1178.7	1.6.2	883	229	210	0.26
T14-38-12-core	0.1037	0.46	3.6082	1.6	0.2582	1.5	1648.9	1.0.2	1551.3	1.2.8	1480.7	1.9.9	114	154	45	1.35
T14-38-13-core	0.1018	0.98	3.5732	1.8	0.2552	1.51	1652.9	1.8.1	1543.6	1.4.4	1465.1	1.9.8	253	104	79	0.41
T14-38-14-core	0.1018	0.44	3.9168	1.61	0.2795	1.55	1654.3	8.3	1617.1	1.3.1	1588.7	2.1.8	188	925	65	0.49
T14-38-15-core	0.1021	0.36	2.8655	1.58	0.2037	1.53	1661	6.7	1372.9	1.1.9	1195.3	1.6.7	234	995	59	0.42

T14-38- 16-core	0.104 1	0.4 9	4.07 79	1.8 1	0.28 48	1.7 4	1694. 1	9. 1	1649 .9	1 4. 8	1615 .5	2 4. 9	11 6	27	3 8	0. 23
T14-38- 17-core	0.106 7	0.7 3	3.65 44	1.7 7	0.24 86	1.6 1	1742. 1	1 3. 3	1561 .5	1 4. 2	1431 .4	2 0. 7	51 3	82	1 4. 7	0. 16
T14-38- 18-core	0.150 2	0.3 2	6.28 26	1.5 6	0.30 49	1.5 2	2339. 7	5. 5	2016 .7	1 3. 7	1715 .5	2 3	10 79	33 7	4 0. 7	0. 31
T14-38- 19-core	0.166 8	0.3 5	7.59 01	1.7	0.33 07	1.6 7	2522. 2	5. 9	2183 .7	1 5. 4	1841 .9	2 6. 8	36 0	20 7	1 6. 5	0. 57

Highlight

This Belt consists of Cambrian ophiolites and Ordovician island-arc complex.

Ophiolites likely represent remnants of an oceanic plateau or seamounts.

The island arc complex has affinity to IBM-type oceanic arc, formed in ~460-440 Ma.

This belt links the East Qinling Orogen to the east and Qilian Orogen to the west.

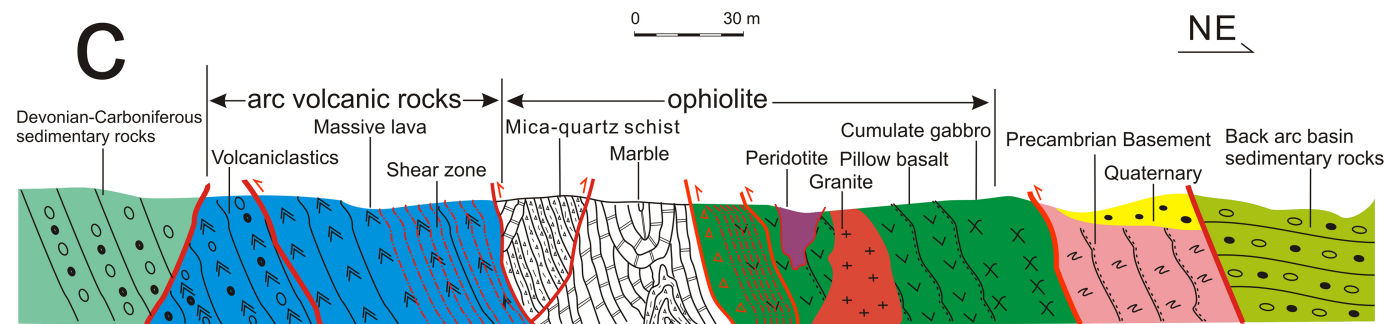
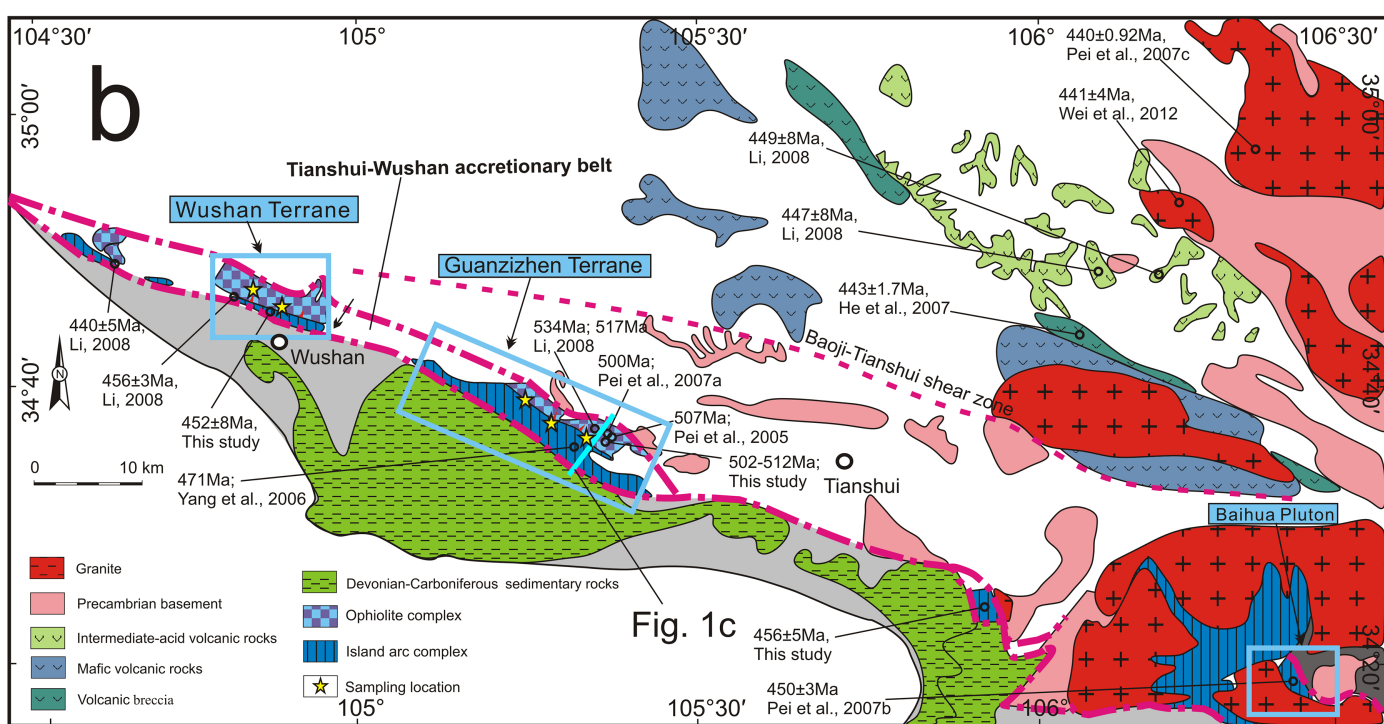
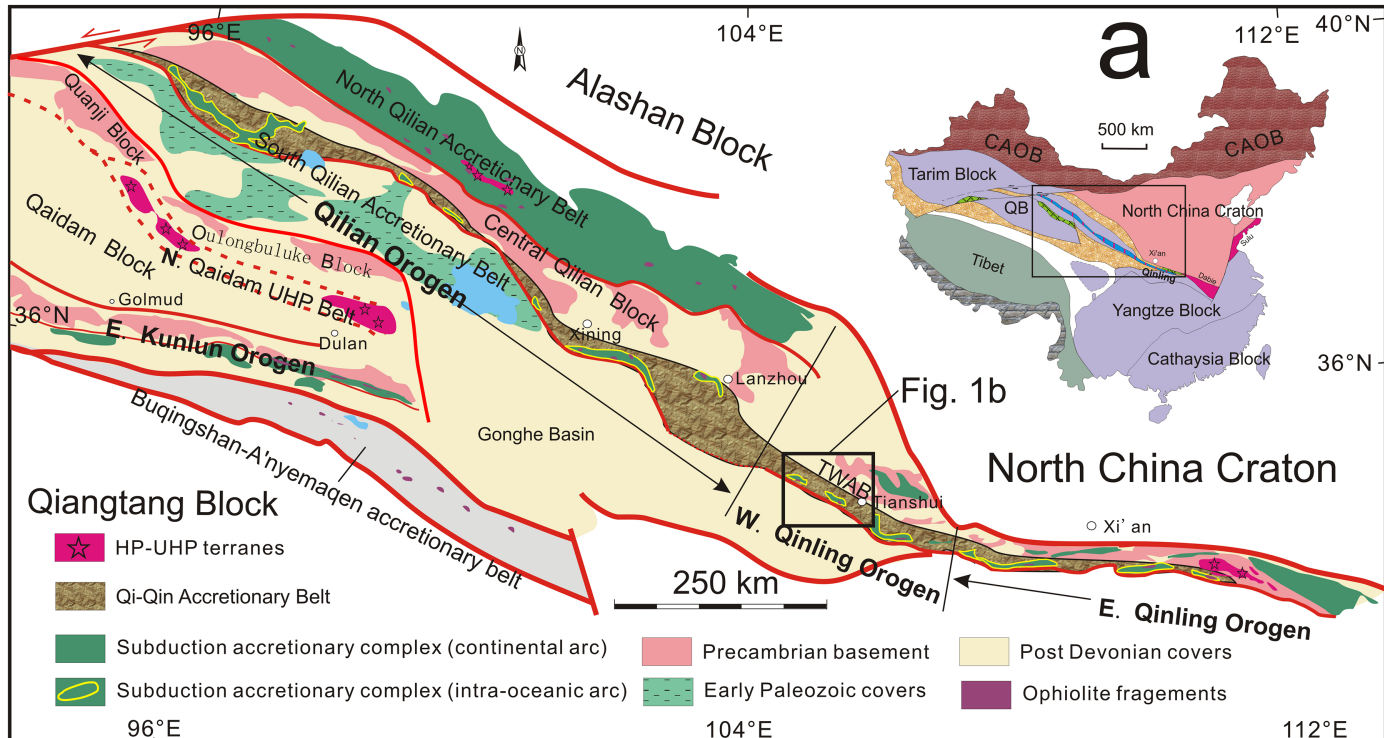


Figure 1

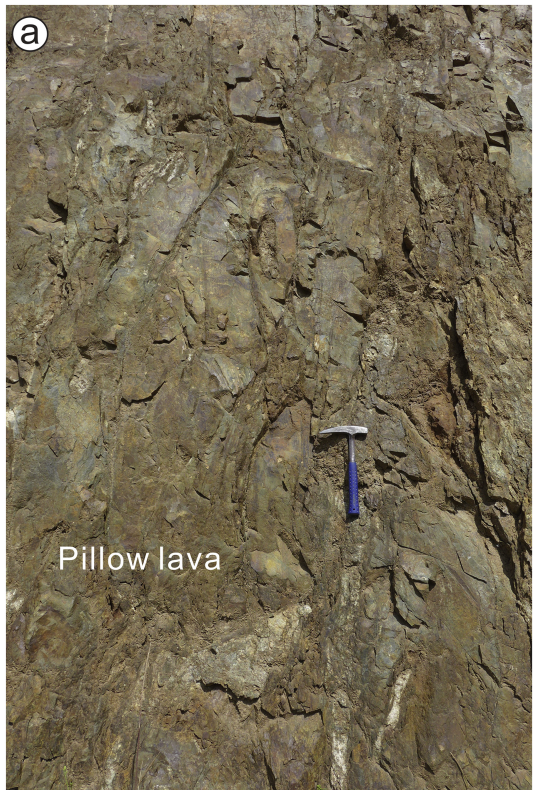


Figure 2

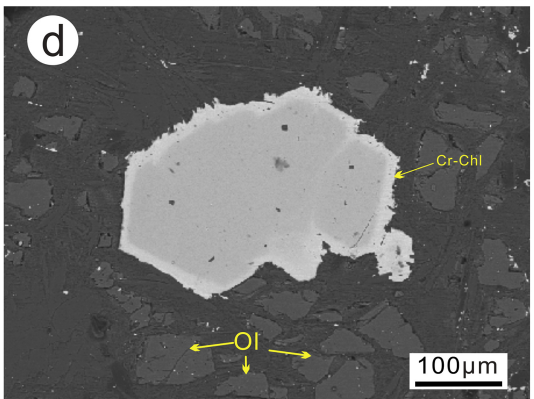
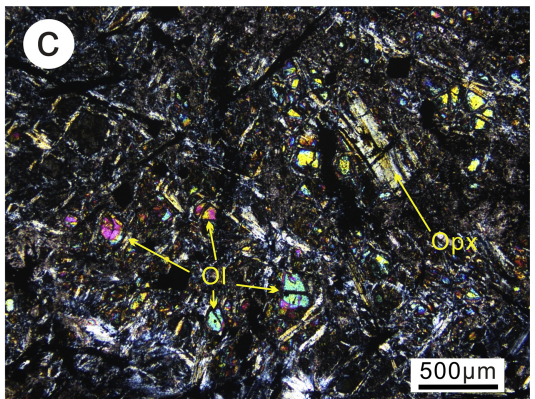
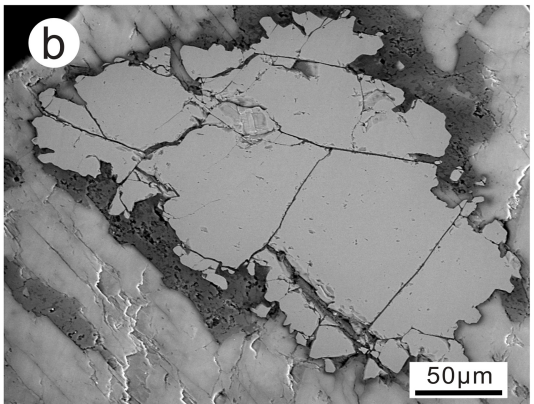
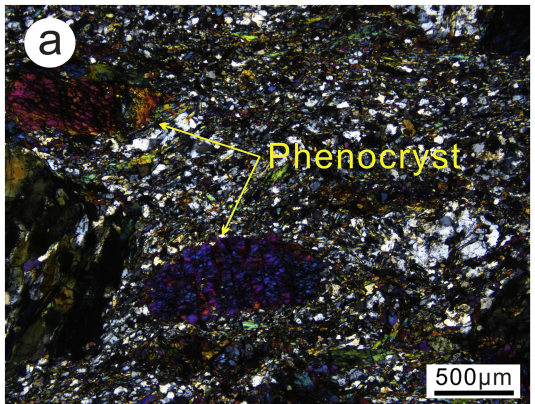


Figure 3

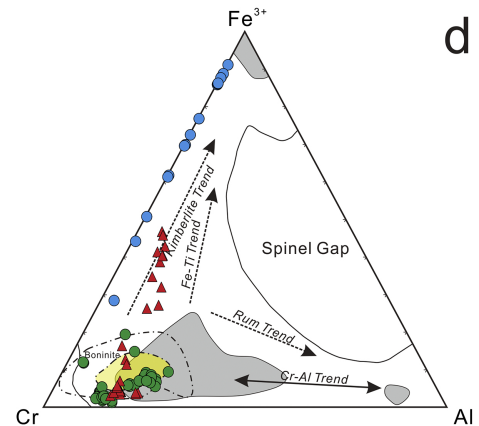
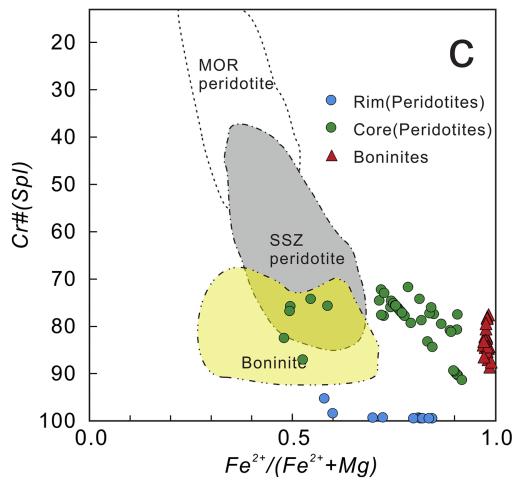
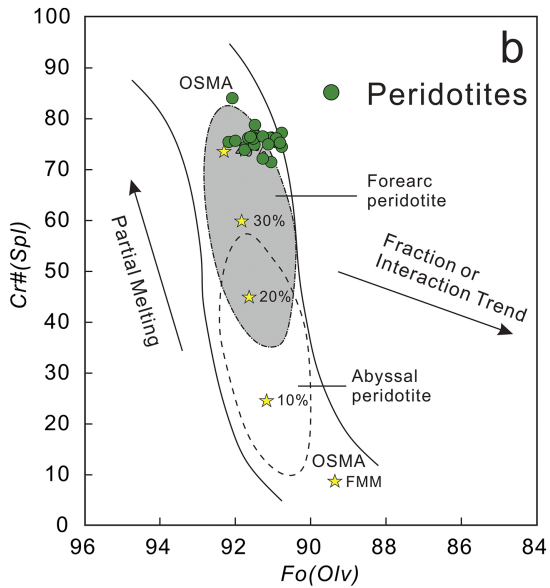
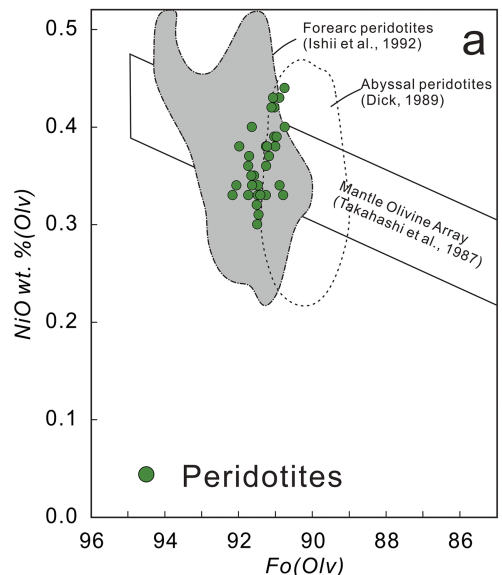


Figure 4

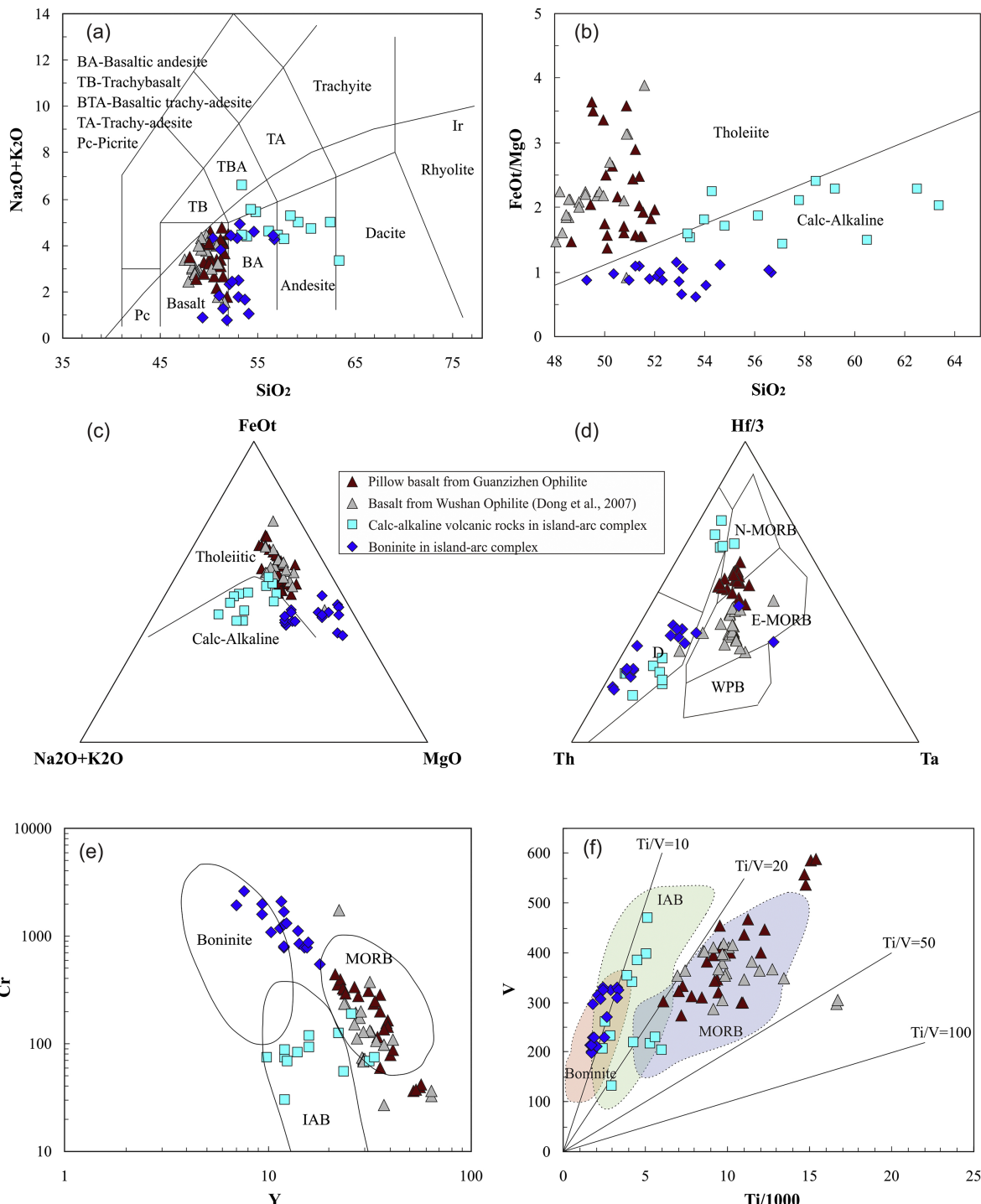


Figure 5

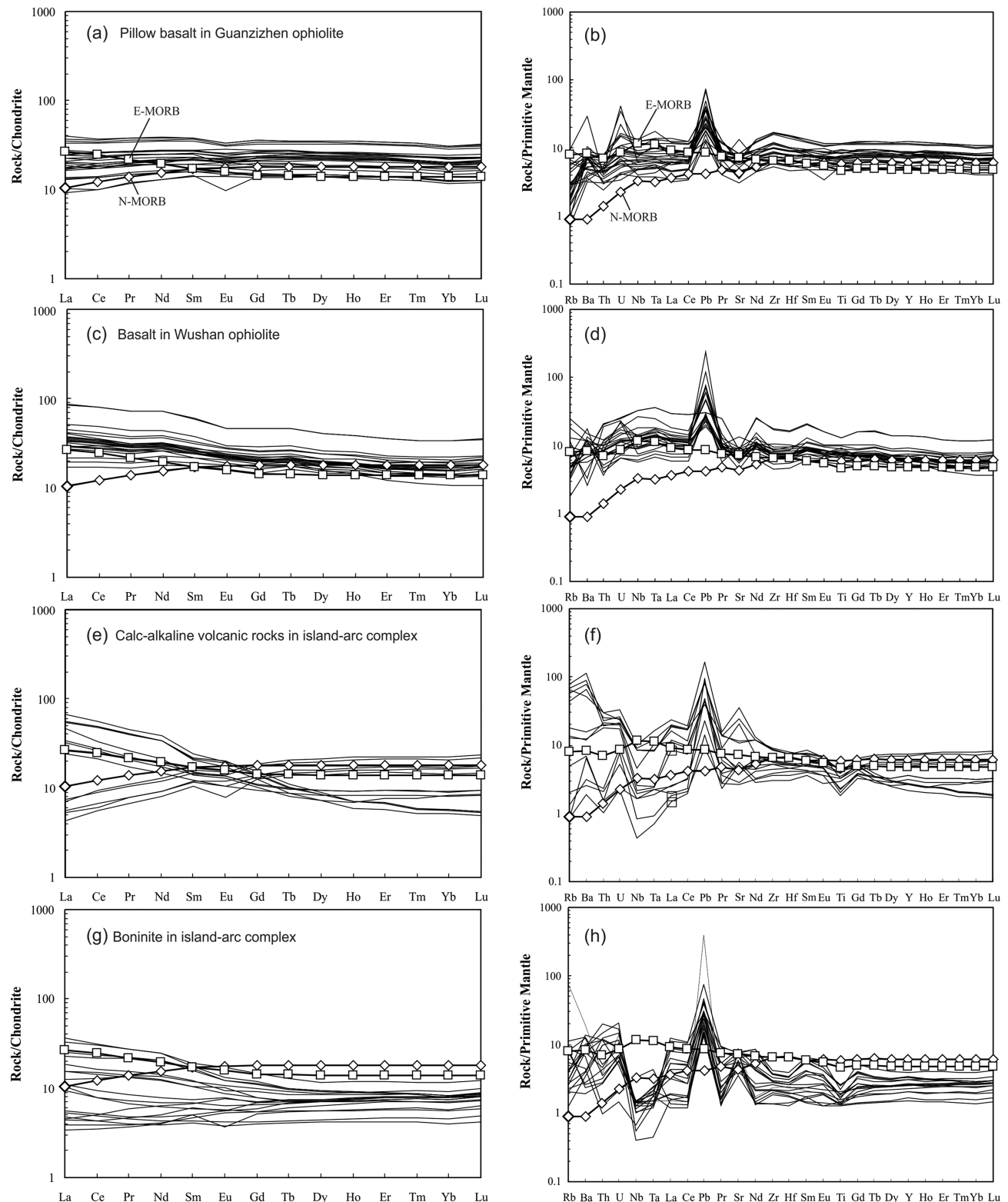


Figure 6

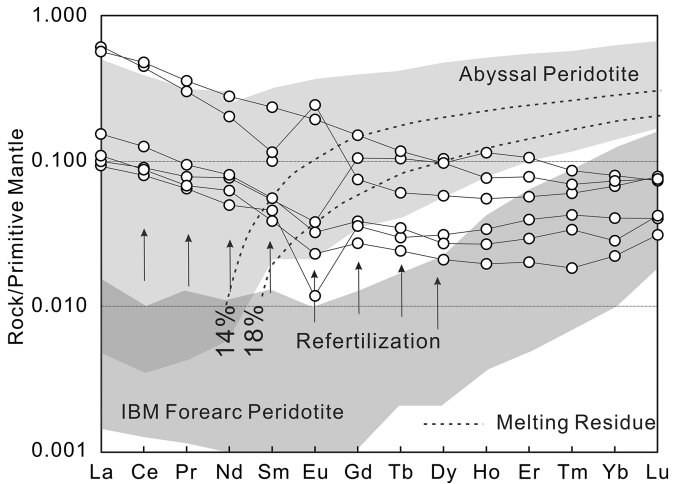


Figure 7

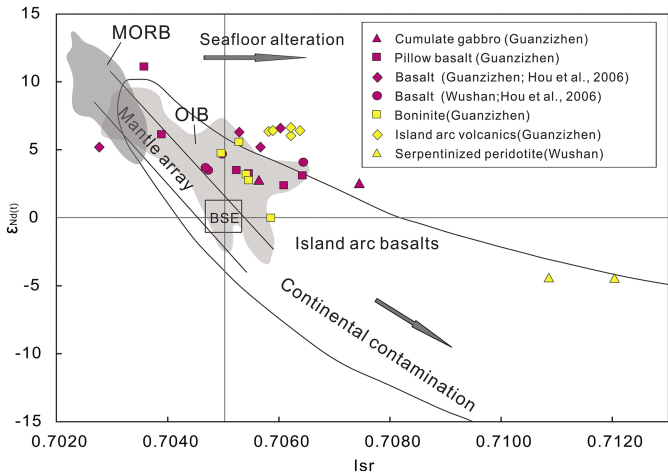
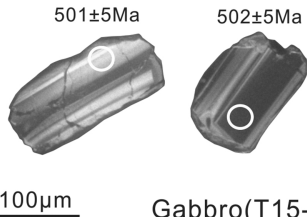


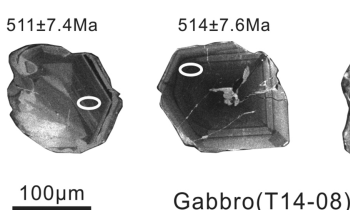
Figure 8



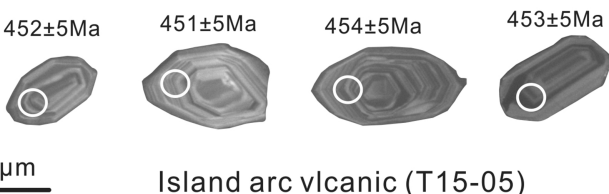
Gabbro(T15-38)



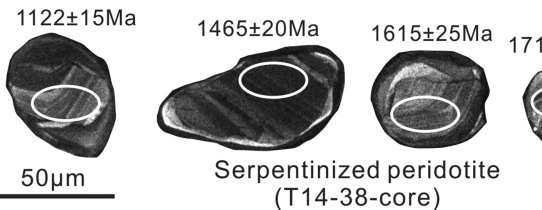
Gabbro(T14-25)



Gabbro(T14-08)



Island arc volcanic (T15-05)



Serpentinized peridotite
(T14-38-core)



Serpentinized peridotite
(T14-38-rim)

Figure 9

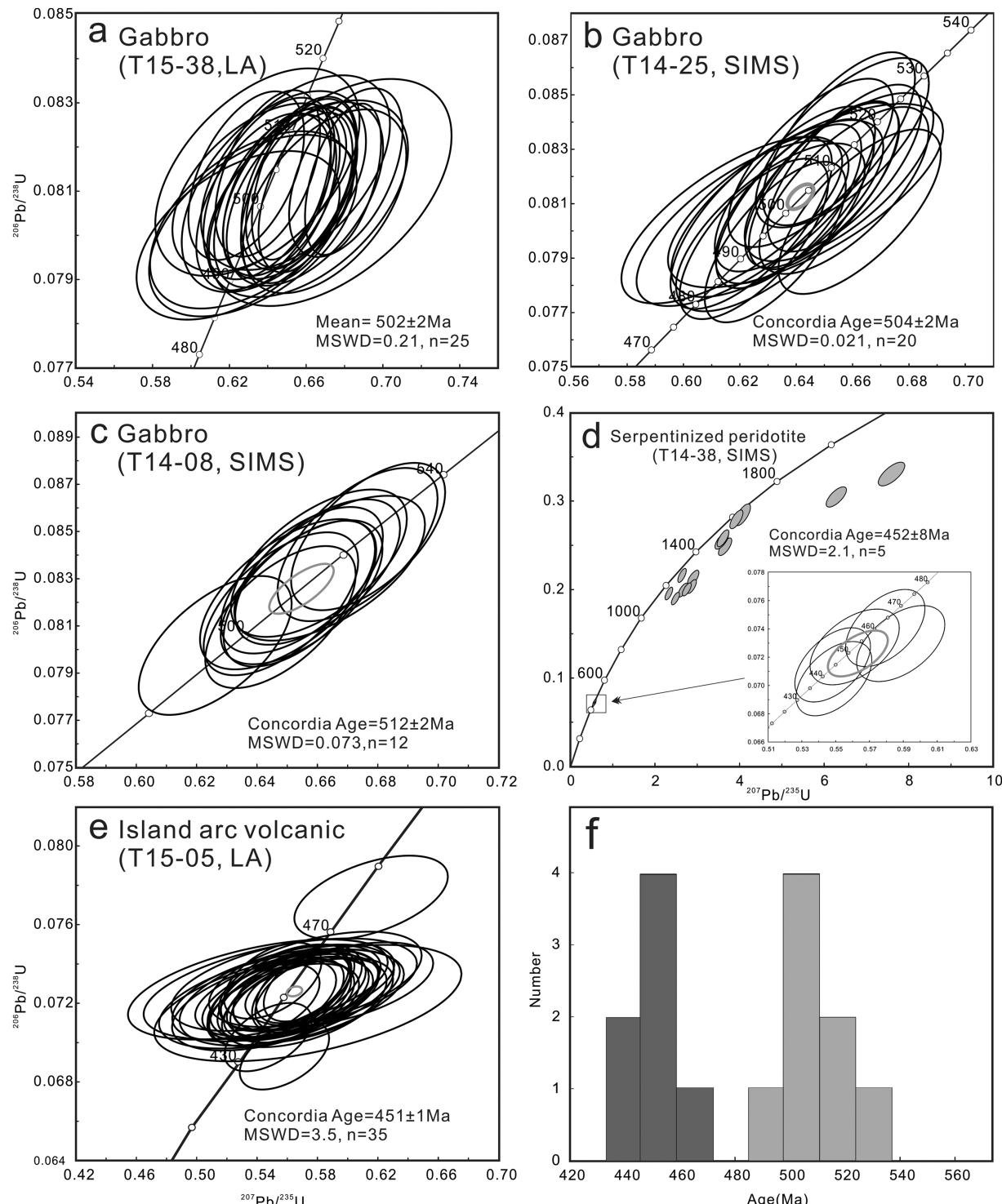


Figure 10

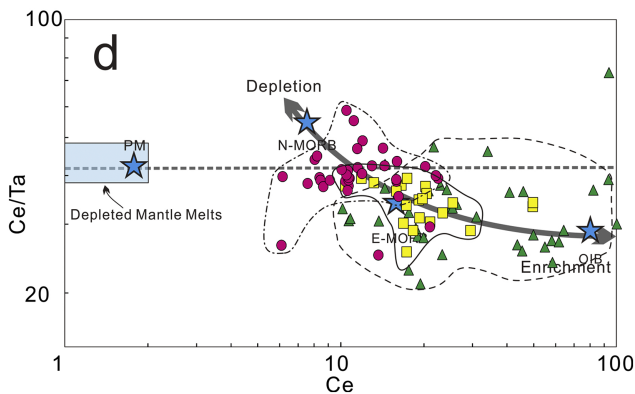
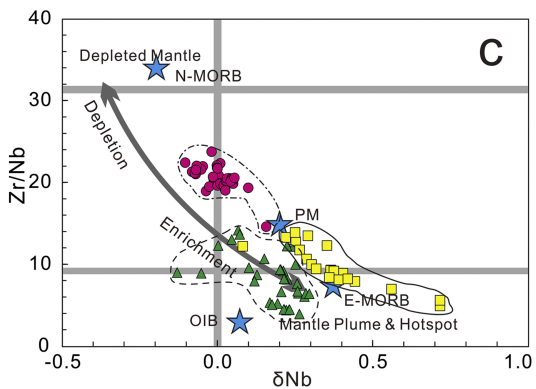
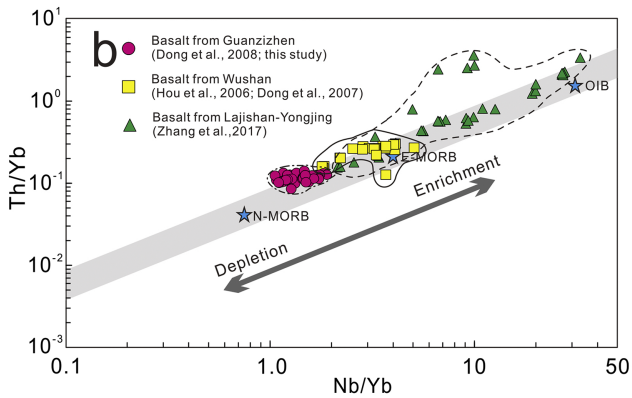
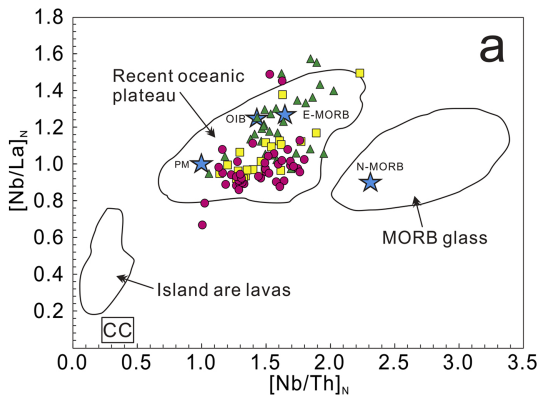


Figure 11

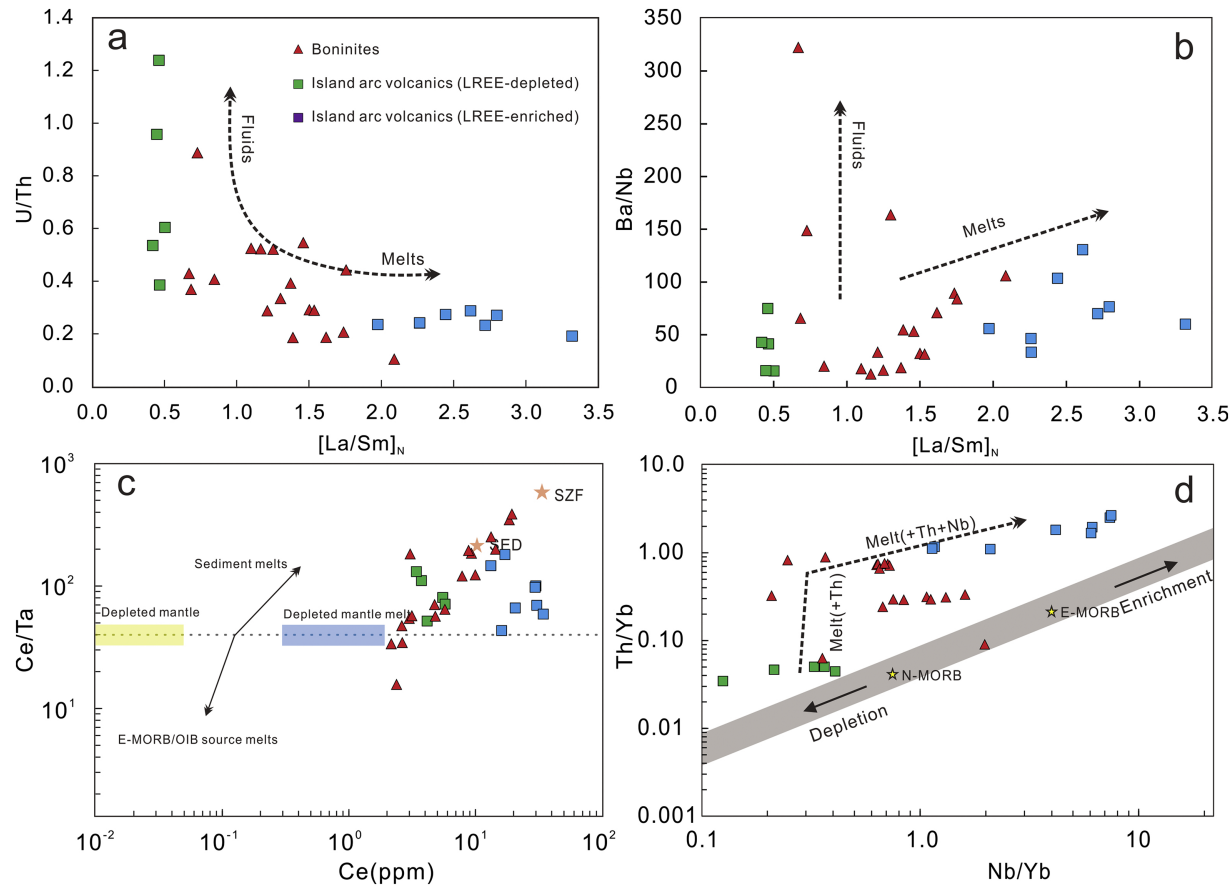


Figure 12

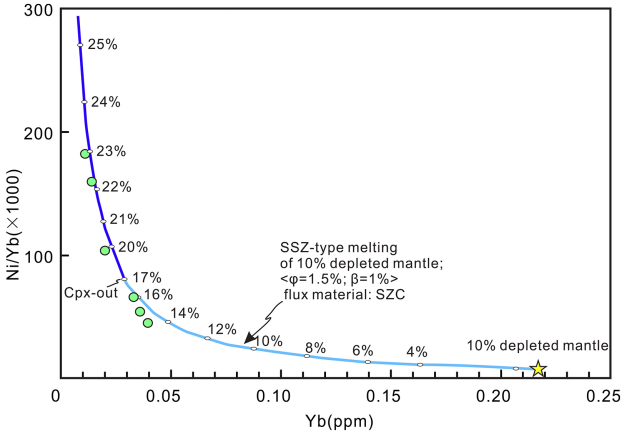
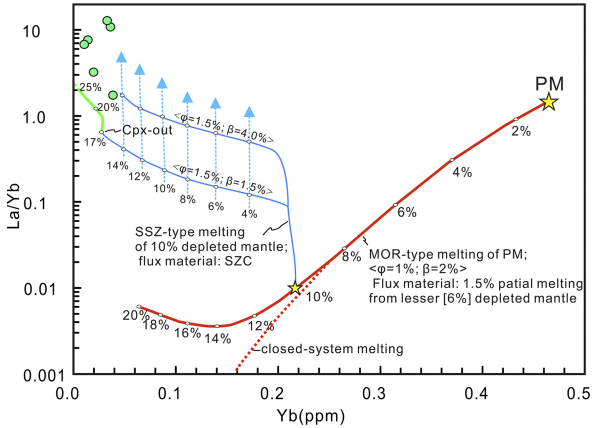
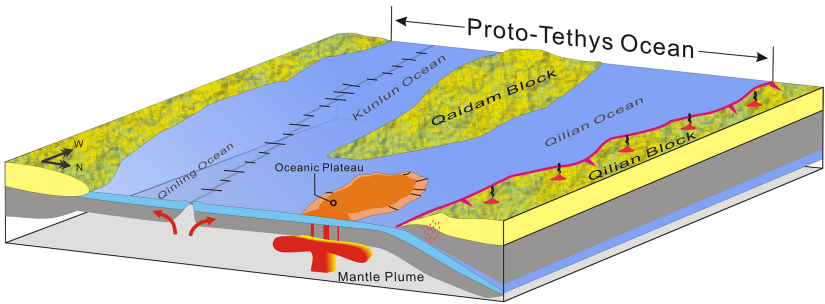
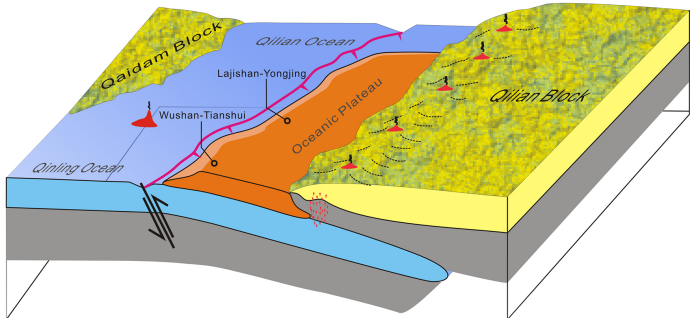


Figure 13

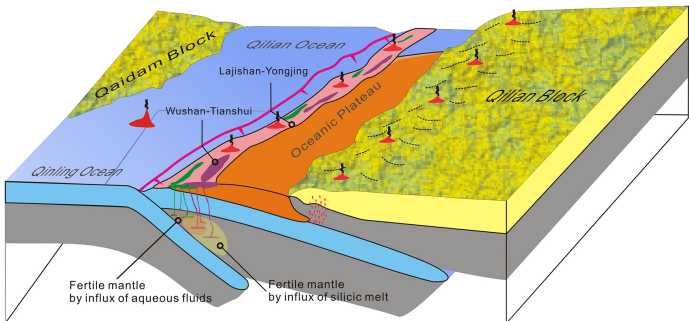
(1) Formation of oceanic plateau~525-500Ma



(2) Collision between oceanic plateau and continental margin at ~470Ma

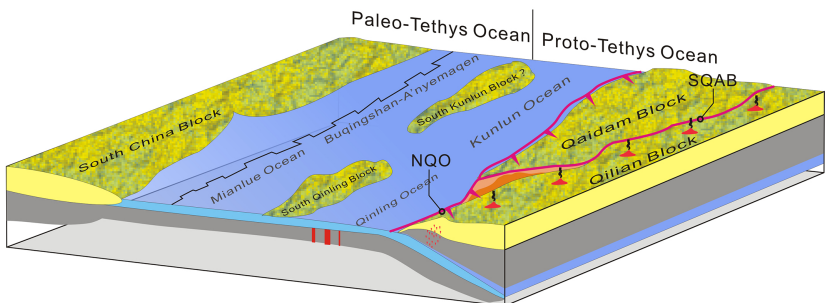


(3) Subduction zone retreatment and the formation of volcanic arc ~460-440Ma



■ Stage1: Island arc volcanics (LREE-depleted) ■ Stage2: Boninites ■ Stage 3: Island arc volcanics (LREE-enriched)

(4) Closure of Qilian ocean ~440-430Ma



NQO: North Qinling Orogen

EKO: East Kunlun Orogen

SQAB: South Qilian Accretionary Belt

Figure 14